Mix, A.C., Tiedemann, R., Blum, P., et al., 2003
Proceedings of the Ocean Drilling Program, Initial Reports Volume 202

5. Site 1234[1]

Shipboard Scientific Party[2]

INTRODUCTION

Site 1234 (proposed Site SEPAC-13B) is located at 36°13.153′S, 73°40.902′W on a relatively flat bench in the middle of the continental slope, at 1015 m water depth, ~60 km shoreward of the Peru-Chile Trench and ~65 km offshore (Fig. F1). Basement is likely continental crust. The continental shelf here is ~60 km wide. Predrilling surveys (970312 *Revelle,* Mix et al., 1998; SO161-5 *Sonne,* Wiedecke-Hombach et al., 2002), indicate mostly hemipelagic sedimentation at the site. The uppermost part of the seismic profile shows flat-lying reflectors with deformed but continuous layers farther below, possibly reflecting the original relief of the acoustic basement (Fig. F2). Disrupted reflectors only occur at the base of the seismic profile. This site was chosen to take advantage of the high sedimentation rates to reconstruct continental climate and oceanography on millennial to centennial timescales for the late Quaternary. Canyons to the north and south of the site appear to channel most turbidity currents away from this shallow basin.

Site 1234 is ~7 km southwest of Site 1235 but is located at greater depth (Fig. F1). These two sites are expected to be influenced by similar surface water conditions so that major differences in physical, chemical, and paleontological properties can be attributed to depth-related effects.

The regional surface circulation at Site 1234 is marked by the northward-flowing Peru-Chile Current (PCC) and the e Coastal Current (CC), which are separated by the poleward-flowing Peru-Chile Counter Current (PCCC) (Strub et al., 1998) (Fig. F3A). The PCC and the CC transport cold, nutrient-enriched subpolar water masses northward, whereas of the CC is significantly affected by admixture of low-salinity waters from the Chile fjord region (Fig. F3B). The PCCC stretches from 100 to 300 km offshore and transports subtropical surface water to the south. Beneath these surface currents, at a depth of 100–400 m, the poleward-

F1. Three-dimensional bathymetry images of Sites 1234 and 1235, p. 18.

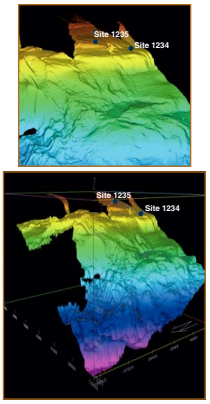

F2. Seismic profile at Site 1234, p. 19.

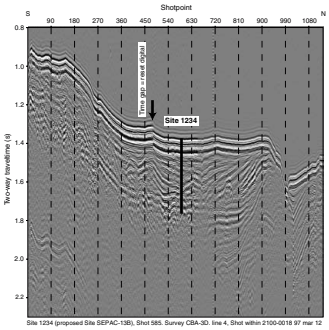

F3. Sites 1232–1235 and oceanographic features off southern and central Chile, p. 20.

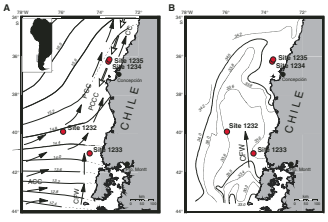

[1]Examples of how to reference the whole or part of this volume. [2]Shipboard Scientific Party addresses.

Ms 202IR-105

flowing Gunther Undercurrent transports relatively low-oxygen and high-salinity water masses southward along the shelf edge. These nutrient-rich water masses provide the source of nearshore upwelled waters (Fonseca, 1989). At Site 1234, seasonal upwelling favors high biogenic productivity during the southern summer as long as wind directions from south to south-southwest dominate. During winter, dominant wind directions from the north significantly reduce coastal upwelling (Strub et al., 1998).

Deeper currents include the northward-flowing Antarctic Intermediate Water (AAIW) at a depth between 400 and 1000 m. This water mass is relatively high in oxygen and low in salinity and overlies the southward-flowing nutrient-rich Pacific Central Water (PCW). We expect that benthic proxies at Site 1234 will reflect temporal and vertical changes of these water masses because Site 1234 is positioned in the modern transition zone between AAIW and PCW (Fig. **F4**).

The continental climate of southern Chile constitutes a transition zone between summer-dry Mediterranean climates to the north and heavy year-round rainfall to the south of Site 1234, due to the influence of westerly winds. Interannual rainfall in this region of Chile is thought to reflect the influence of El Niño Southern Oscillation (ENSO) events emanating from the tropics (Hebbeln et al., 2000; Dettinger et al., 2001). Modern sediments on the southern Chile continental slope are primarily provided by rivers (Lamy et al., 2002). Thus we expect variations in terrigenous sediment composition and mineralogy at Site 1234 to reflect changes in the latitudinal position of the westerly winds through time.

Primary goals of this site were to

1. Assess the late Quaternary history of biological production in a coastal upwelling center near Concepción, Chile, which is sensitive to regional winds, with millennial- to centennial-scale resolution;
2. Assess the late Quaternary history of terrigenous sedimentation off central Chile, indicative of continental climate variability;
3. Assess variations in the boundary between oxygen-rich AAIW and oxygen-depleted PCW using tracers of paleo-oxygen and paleonutrients; and
4. Assess late Quaternary variations in paleomagnetic intensities in the southeast Pacific as a stratigraphic tool for comparison with similar data from the Northern Hemisphere.

F4. North-south cross section of water masses, p. 21.

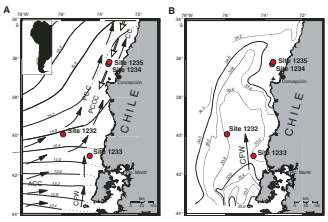

OPERATIONS

The 288-nmi voyage to Site 1234 (proposed Site SEPAC-13B) was accomplished in 26.0 hr at an average speed of 11.1 kt. During the early morning hr of 15 April 2002, the captain reduced speed because of heavy fog and the presence of fishing boats in the area. At 0600 hr, the vessel slowed as it approached the location. The 3.5-kHz precision depth recorder (PDR) was used as a final check of the site characteristics, by comparison to precruise survey data. The vessel was on station by 0650 hr on 15 April, and a beacon was deployed.

Hole 1234A

Hole 1234A was initiated at 1010 hr on 15 April with a shot from 1018.8 meters below rig floor (mbrf). The seafloor depth inferred from the recovery of mudline Core 1H was 1026.6 mbrf, 3.8 m shallower than the corrected PDR depth. Advance piston corer (APC) coring deepened the hole until Core 11H failed to achieve a full stroke at 100.3 meters below seafloor (mbsf). The recovery for the piston-cored interval was 101.1 m, representing an average recovery of 101% (Table T1). Most cores were affected by expanding gas during recovery, resulting in gas voids and growing cores on the catwalk. Holes were drilled into the core liners to relieve some of the gas pressure before cores were processed on the catwalk. Cores were oriented starting with Core 4H. Downhole temperature measurements were taken with the advanced piston corer temperature (APCT) tool (Table T1). Coring continued with the extended core barrel (XCB) system to the target depth of 205.2 mbsf. XCB coring penetrated 104.9 m and recovered 87.94 m. The total results for Hole 1234A were 205.2 m cored and 189.02 m recovered (recovery = 92%) (Table T1). The bit was pulled free of the seafloor at 0145 hr on 16 April.

T1. Operations summary, Site 1234, p. 46.

Hole 1234B

The vessel was moved 10 m east. Prior to coring, a bottom water temperature measurement was taken with the bit at 1019 mbrf, which, combined with the downhole temperature measurements in Hole 1234A, established a temperature gradient of ~4.2°C/100 m for this site. To obtain the desired stratigraphic overlap with the first hole, the bit was then positioned at 1025 mbrf and Hole 1234B was initiated at 0319 hr. The seafloor depth was 1025.4 mbrf based on the mudline recovered in Core 1H. Piston coring advanced to refusal at 93.8 mbsf. The cores were oriented starting with Core 3H. Of the 93.8 m cored, 97.1 m was recovered. The hole was deepened to 182.4 mbsf with the XCB before coring was completed. The interval from 132.3 to 134.3 mbsf (2 m) was drilled to maintain a stratigraphic overlap with the XCB portion of the first hole. The XCB cored 86.6 m with an average recovery of 84% (Table T1). The results of APC and XCB operations in this hole were 180.4 m cored with an average recovery of 94% (Table T1). The bit was pulled free of the seafloor at 1515 hr on 12 April.

Hole 1234C

The vessel was offset 10 m east of Hole 1234B. The bit was positioned at a depth of 1027 mbrf in an effort to target remaining coring gaps. Hole 1234C was initiated with the APC at 1548 hr on 16 April. Piston coring advanced to the target depth of 79.1 mbsf. The interval from 39.6 to 41.1 mbsf was drilled. A total of 76.0 m was cored and 76.4 m was recovered (recovery = 101%) (Table T1). The cores were oriented starting with Core 3H. With the completion of this hole, operations at Site 1234 were concluded.

Because the next site was located at ~500 m water depth and only 7 mi east of the present location, it was decided that we would offset the vessel in dynamic positioning mode with the drill string partially deployed and the bit at a depth of 375 mbrf. After the hydrophones were retracted and the beacon was retrieved, the vessel left location at 2300 hr on 16 April.

COMPOSITE SECTION

We built a composite depth scale (0.00–240.39 meters composite depth [mcd]) (Table T2) and a splice (as defined in "Composite Section," p. 4, in the "Explanatory Notes" chapter) that ranges from the top of Core 202-1234A-1H to the bottom of Section 202-1234B-9H-7 (0.00–94.44 mcd) (Table T3). Below Core 202-1234B-9H, we appended cores based on the assumption that the cumulative offset growth factor (see "Composite Section," p. 4, in the "Explanatory Notes" chapter) for cores below the splice was the same as in the splice. The depth offsets of cores from Hole 1234B were then adjusted for optimum correlation of magnetic susceptibility with those from Hole 1234A.

The mcd scale and the splice are based on the stratigraphic correlation of whole-core OSU Fast Track magnetic susceptibility data (OSUS-MS) collected at 5-cm depth intervals using 1-s integration times. OSUS-MS data for Holes 1234A, 1234B, and 1234C and the primary splice constructed from them are presented on the primary mcd scale in Figure F5 and in Tables T4, T5, and T6. The splice tie points (Table T3) were used to construct representative spliced records for reflectance (L*), multisensor track magnetic susceptibility (MST-MS), gamma ray attenuation (GRA) bulk density, and natural gamma radiation (NGR) data (Fig. F6). Magnetic susceptibility was the most useful tool for stratigraphic correlation.

We assumed that the uppermost sediment in Core 202-1234A-1H was the sediment/water interface (the "mudline"). A mudline was also recovered in Core 202-1234B-1H, and this helped to confirm the fidelity of the top of the recovered section. Core 202-1234A-1H, the "anchor" in the composite depth scale, is the only core with depths that are the same on the mbsf and mcd scales. From this anchor, we worked downhole, correlating records on a core-by-core basis. Comparison of the mcd and mbsf depth scales (Fig. F7) shows that the mcd scale is, on average, 18% longer than the mbsf scale. Core 202-1234B-1H was assigned a negative offset of –0.19 m because the best correlation with Core 202-1234A-1H, made on the broad susceptibility maximum at ~2.5 mcd, shifts Core 202-1234B-1H up 19 cm relative to Core 202-1234A-1H. Such small differences may occur in cores that contain the mudline, which typically consists of very soupy sediment. They are most likely a result of the behavior of the sediment in response to drilling.

Continuous recovery of the sediment section at Site 1234 could not be demonstrated based on shipboard data below Cores 202-1234A-9H and 202-1234B-9H (Fig. F5D). Although cores below 94 mcd could not be tied directly to the cores within the spliced interval, most could be correlated with one or more cores in the other hole (Fig. F5D, F5E, F5F, F5G). These correlations resulted in "floating splices." First, cores with tops at depths greater than 94 mcd (starting with Cores 202-1234A-10H and 202-1234B-10H) were all assigned a depth offset based on the assumption that mcd = 1.18 (mbsf) (i.e., that the growth factor is constant). Then, cores from Hole 1234B were correlated where possible (six out of ten cases) with cores from Hole 1234A. The cumulative offsets of cores from Hole 1234B that could not be correlated were left unaltered.

To facilitate the calculation of mass accumulation rates (MARs), we provide corrected meters composite depth (cmcd) in Tables T2 and in Table T3 for depths within the splice. The mcd growth factor for the

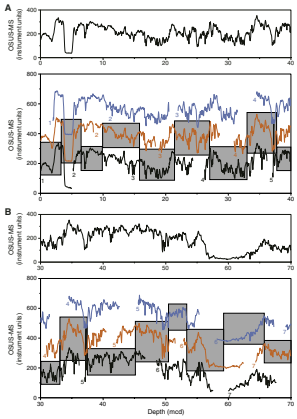

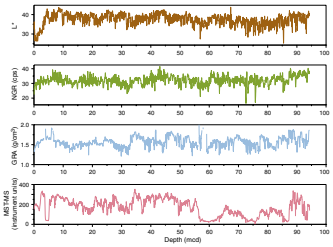

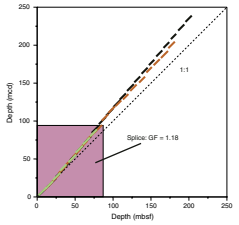

spliced interval at Site 1234 is 1.18. This growth factor was assumed to apply to the interval below the splice.

LITHOSTRATIGRAPHY

A 203.7-m-thick sequence (238.9 mcd) of hemipelagic sediments from the late Quaternary was recovered at Site 1234. A single lithostratigraphic unit is primarily defined based on visual core description and smear slide examination (Table T7; Fig. F8). The major lithology of this unit consists of homogeneous dark olive-gray to dark gray diatom nannofossil silty clay and clay, with subtle and gradational color changes. Siliciclastic components are dominated by clay minerals and feldspar. Minor components primarily include quartz, amphibole, pyroxene, mica, and opaque minerals. Authigenic calcite and pyrite are present throughout the sequence. The biogenic fraction is dominated by calcareous nannofossils and diatoms. The ratio of siliciclastic vs. biogenic components generally increases downhole.

Thin silt-rich layers and volcanic ash layers are present as minor lithologies. Magnetic susceptibility is highly variable and reaches high values of up to 600 instrument units. Bulk density shows little downhole trend at Site 1234. As at Site 1233, sediments at Site 1234 are consistent with a hemipelagic upper continental slope setting characterized by high fluvial sediment input from the Chilean Coastal Range and the Andes. Thin silt layers may represent distal turbidites. Some intervals appear to be significantly affected by diagenesis, particularly in the lower half of the recovered sequence.

T7. Lithologic Unit I, p. 52

F8. Lithostratigraphic summary, p. 28.

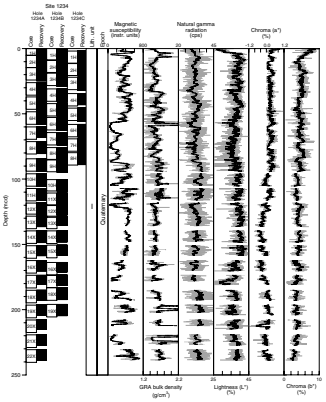

Description of Lithologic Unit

Unit I

Intervals: Cores 202-1234A-1H through 22X; Cores 202-1234B-1H through 19X; and Cores 202-1234C-1H through 8H
Depths: Hole 1234A: 0.0–203.7 mbsf (0.0–238.9 mcd); Hole 1234B: 0.0–181.4 mbsf (0.0–204.7 mcd); and Hole 1234C: 1.6–78.8 mbsf (2.0–88.9 mcd)
Age: late Quaternary (<0.26 Ma) (see "Biostratigraphy," p. 8)

The major lithologies of Unit I are diatom nannofossil and diatom- or nannofossil-bearing silty clay and clay with little visual variability and few sedimentary structures. The sediment color within Unit I typically ranges from dark olive gray to dark gray. Most color changes are subtle and gradational, indicating small compositional variations within the dominant lithology. Black spots and dispersed mottling originating from disseminated monosulfides are common on the surface of newly split cores. These features fade within 1 to 2 hr after splitting and may introduce noise to the color reflectance data, depending on the time elapsed between splitting and color measurement. Bioturbation is rarely visible within the major lithology, probably as a result of the homogeneous lithology. Macroscopic shell fragments are common, primarily randomly oriented, and partly concentrated in patches.

Clay and feldspar (primarily plagioclase) are the predominant siliciclastic components in the sediments (Fig. F9). Quartz is generally present in minor amounts except for two intervals at ~40 and ~80 mcd. Above these maxima, the quartz/feldspar ratio gradually increases and

F9. Siliciclastic, biogenic, and authigenic components vs. MS, p. 29.

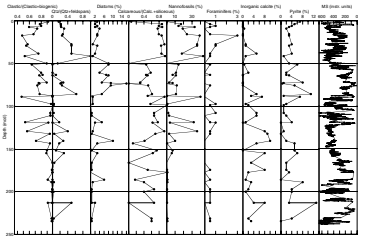

drops abruptly below. Further, primarily silt-sized siliciclastic components within the major lithology include amphiboles, pyroxenes, glauconite, opaque minerals, and volcanic glass, which are present in variable amounts throughout the sequence.

The ratio of siliciclastic vs. biogenic components generally increases downhole (Fig. F9). Biogenic components primarily consist of calcareous nannofossils and diatoms. Nannofossils are the dominant biogenic component and reach up to >30% the upper ~40 mcd, generally decrease downhole until ~160 mcd, and are absent below that depth (Fig. F9). Foraminifers are present in very minor amounts (mostly ≤1%) throughout the sequence. Diatoms are more abundant and present in variable amounts of generally a few percent except for the interval from ~50 to 90 mcd, where up to ~10% is reached. Other siliceous microfossils are present in minor amounts and include ubiquitous sponge spicules and, in some intervals, radiolarians and silicoflagellates.

Authigenic components include relatively abundant pyrite reaching up to ~10% and monosulfidic minerals. Inorganic calcite is present in significant amounts of more than ~5% in the lower half of the sequence and mirrors the decrease in calcareous microfossils. Intervals of increased inorganic calcite contents between ~130 and 140 mcd, 150 and 180 mcd, and 210 and 220 mcd are characterized by higher bulk density and reduced porosity and water content.

Notable minor lithologies within Unit I include silt-rich layers, dark clay layers, and volcanic ash layers. The silt-rich layers (<1 cm thick) are primarily clayey silt composed of clay minerals, feldspar, and opaque minerals. Many of the layers are discontinuous, soupy, or disturbed (e.g., Core 202-1234A-10H). Thin (~1–5 cm) layers of very dark olive-gray clay are also occasionally present (Fig. F10). These layers contain significant amounts of glauconite and opaque minerals and little or no biogenic material. They are often discontinuous, likely as a result of bioturbation. Similar sediment is sometimes present within mottled intervals or as burrow fill.

Eight layers of volcanic ash were recovered in Unit I (Table T8). These ash layers dominantly consist of clear volcanic glass with rare accessory minerals, including andesine or labradorite plagioclases (Table T8). Three ash layers found in Hole 1234A are brown and have diffuse boundaries (e.g., interval 202-1234A-3H-5, 115–122 cm). One ash layer in Hole 1234A (Fig. F11) and two in Holes 1234B and 1234C occur as white patches (e.g., interval 202-1234C-6H-3, 47–53 cm). The others found in Holes 1234B and 1234C are brown and have sharp lower boundaries and diffuse upper boundaries.

The sediments at Site 1234 were slightly to moderately disturbed by the coring process, primarily as a result of gas expansion (methane and hydrogen sulfide) (see "Geochemistry," p. 12). Coring disturbance features are expressed as porous, soupy sediment, occasional larger gas voids, and numerous small fissures. In some cases (e.g., Sections 202-1234A-17X-4 and 17X-5) sediments were ejected from the liner and had to be reinserted.

Magnetic susceptibility is highly variable, especially in intervals with higher than average values. Intervals of low magnetic susceptibility exhibit less variability (~120–180 mcd and ~210–220 mcd) (Fig. F8). Lack of magnetic minerals in these intervals is presumably due to reductive diagenesis (see "Paleomagnetism," p. 10).

GRA bulk density and moisture and density bulk density measurements parallel one another with a variable offset of ~0.1 to 0.3 g/cm³, but they are poorly correlated (Fig. F12). Although GRA bulk density

F10. Dark green layer, p. 30.

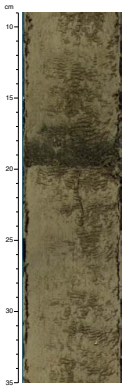

T8. Depth intervals, thickness, and associated minerals of volcanic ash layers, p. 53.

F11. Brownish white ash layer interbedded in sediments, p. 31.

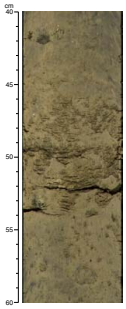

F12. MAD and GRA bulk densities, p. 32.

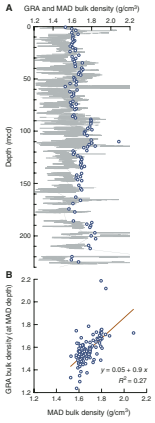

may be strongly affected by coring disturbance, neither type of density measurement shows discernable downhole trends toward higher values that are usually ascribed to compaction. Instead, bulk densities seem highly variable, presumably due to time-dependent diagenesis that can change the physical properties of the sediment locally through textural changes and cementation. Porosity and water content are also variable (Fig. **F13**), most likely because of localized incipient lithification (i.e., cementation and dehydration).

In the a*-b* color space, all color measurements at Site 1234 plot in the "yellow" domain (Fig. **F14**). However, sediment colors are more chromatic than at previous sites, and they exhibit a weak bimodal distribution with one trend characteristic to brownish sediments (a* > 0) and the other typical to more greenish sediments (a* < 0). The lightness (L*) (Fig. **F8**) appears to be low where high total organic carbon (TOC) and high NGR sediments are encountered, but this correlation is not confirmed by a simple regression. Assuming a two-component chromatic system, preliminary predictive relationships between reflectance, carbonate, and TOC via a multiple linear regression are weaker than at Site 1233 (i.e., r^2 = ~0.5 for carbonate, and r^2 = ~0.7 for TOC).

Interpretation and Depositional History

Sediments at Site 1234 are primarily composed of fine-grained siliciclastics consistent with undisturbed hemipelagic sedimentation, except for occasional thin silt-rich layers that may represent distal turbidites. Pathways of major turbidity currents in the region are known to be confined to large submarine canyons (Thornburg and Kulm, 1987). The calcareous biogenic components diminish and their preservation decreases (see **"Biostratigraphy,"** p. 8) in the lower half of the recovered sequence, suggesting increasing diagenesis downhole.

Nannofossil biostratigraphy indicates that the cored sequence is younger than 260 ka, suggesting that sedimentation rates are very high at Site 1234. As at Site 1233, these above-average sedimentation rates are most likely the result of high rainfall in the Chilean hinterland. Onshore from Site 1234, the largest Chilean river (Bío-Bío) primarily drains easily erodible source rocks from the Andes. Smaller rivers supply additional material from the Coastal Range. Changes in the ratio of quartz vs. feldspar in the younger part of the sequence (Fig. **F9**) may indicate changes in the relative contribution of lithologically different source rocks from these source regions.

Based on preliminary shipboard paleomagnetic evidence (see **"Paleomagnetism,"** p. 10), the Laschamp Excursion (~41 ka) is located at a depth of ~23 mcd at Site 1234 compared to ~70 mcd at Site 1233 (see **"Age Model and Mass Accumulation Rates,"** p. 16, in the "Site 1233" chapter), suggesting comparatively lower sedimentation rates at Site 1234 during marine isotope Stages 1 to early 3, which may be consistent with northward decreasing rainfall and correspondingly less fluvial sediment supply in central Chile. The basal age of <260 ka suggests higher sedimentation rates at Site 1234 prior to the Laschamp Excursion, whereas sedimentation rates were significantly lower at Site 1233 (see **"Age Model and Mass Accumulation Rates,"** p. 16, in the "Site 1233" chapter). This may indicate that changes in transport pathways of terrigenous material and syndepositional sediment focusing might also have influenced siliciclastic sedimentation at both sites.

Site 1234 is located within the highly productive upwelling area off Concepción. For such a setting, contents of biogenic components ap-

F13. Moisture and density, p. 33.

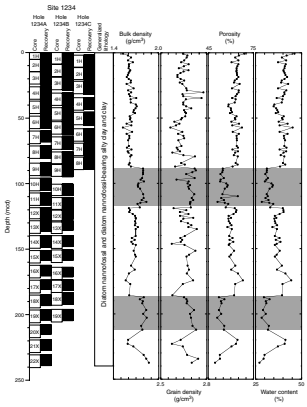

F14. Color measurements, p. 34.

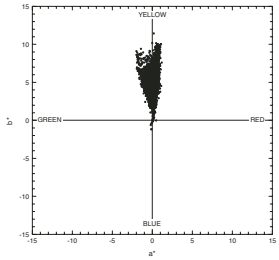

pear comparatively low as a result of the overwhelming dilution by siliciclastics. Biogenic components are primarily dominated by calcareous nannofossils, except for the interval from ~40 to 90 mcd, where diatoms reach equal amounts. This shift may be related to a change in the extension of the Concepción upwelling cell.

The presence of authigenic monosulfides, pyrite, and inorganic calcite in the sediments at Site 1234 reflects diagenetic processes associated with degradation of organic matter. The increased abundance of authigenic calcite and the disappearance of calcareous nannofossils downhole (Fig. F9) imply an increase of diagenesis in the lower part of the sections, resulting from the dissolution and recrystallization of primary biogenic calcite (see "Geochemistry," p. 12).

Ash layers observed at Site 1234 are mainly composed of clear volcanic glass shards with minor amounts of andesine or labradorite plagioclases and trace amounts of quartz, mica, amphiboles, and pyroxenes, suggesting a nearby source of intermediate-composition volcanism, such as the Andes. Bioturbation may have resulted in mixed and/or homogenized sediments of volcanic ash and the major lithology suggested by the ubiquitous presence of volcanic glass outside the distinct ash layers. Two ash layers recognized from approximately equivalent depth intervals in Holes 1234B and 1234C (Table T8) provide a useful interhole correlation. These two ash layers were not found in Hole 1234A because of coring gaps. Lack of interhole correlation between the other ash layers found in Hole 1234A may be caused by dispersion of the layers by bioturbation.

BIOSTRATIGRAPHY

Calcareous nannofossils, diatoms, and planktonic and benthic foraminifers were examined in mudline and core catcher samples from Hole 1234A. Calcareous nannofossils and diatoms were also examined in additional samples from all sections of same hole. Drilling at Site 1234 revealed one major biostratigraphic unit of late Pleistocene age. The abundance of calcareous microfossils varies from rare to common, and a few samples are barren (Fig. F15). Preservation of the four groups (calcareous nannofossils, diatoms, and benthic and planktonic foraminifers) is generally moderate to good. Reworking of microfossils, mainly from Neogene sediments, is apparent to some extent in all the fossil groups examined. In particular, benthic diatoms are present in most of the samples, indicating relatively persistent redeposition from the upper continental margin. Changes in benthic foraminiferal assemblages likely reflect variations in the oxygenation of bottom water masses. Calcareous nannofossils suggest that the base of the cored sequence is younger than 0.26 Ma (Zone NN21).

F15. Calcareous nannofossils, planktonic and benthic foraminifers, and diatoms, p. 35.

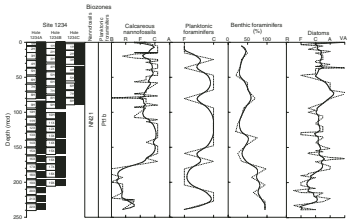

Calcareous Nannofossils

Calcareous nannofossils are common to abundant and well preserved in most of the samples examined, except for the core catcher samples from the lowermost six cores (Cores 202-1234A-17X through 22X [180.5–238.9 mcd]), where nannofossils are generally rare and poorly preserved. Reworking of nannofossils is minimal in the sequence, as only a few specimens of Neogene–Cretaceous nannofossil taxa were observed in a small proportion of the samples.

Calcareous nannofossil taxa commonly encountered at the site include various species of the genus *Gephyrocapsa, Emiliania huxleyi, Calcidiscus leptoporus, Coccolithus pelagicus,* and *Helicosphaera carteri* (Table T9). However, large fluctuations in the relative abundance of these taxa occur, presumably in response to changes in surface-water properties. The abundance of *E. huxleyi* also fluctuates significantly, which makes the placement for the base of the *E. huxleyi* acme zone (0.08 Ma) difficult at this site. The abundance of *E. huxleyi* first exceeds that of medium-sized gephyrocapsids (mainly *Gephyrocapsa muellerae*) at ~70 mcd. This abundance reversal generally occurs near the boundary between oxygen isotope Stages 4 and 5 in the Southern Ocean (Flores et al., 2000). More reliable and precise delineation of the *E. huxleyi* acme zone at this site awaits further detailed studies. *E. huxleyi* was found down to Sample 202-1234A-22X-5, 40 cm (237.1 mcd), in the last core, indicating an age younger than 0.26 Ma for the entire sedimentation sequence (Table T9). All of the sequence corresponds to Zone NN21 (Martini, 1971).

T9. Distribution of calcareous nannofossils, p. 54.

Planktonic Foraminifers

Planktonic foraminifers were examined in all core catcher samples from Hole 1234A. They are present in all samples, but abundance and preservation vary markedly (Table T10). At the base of Hole 1234A (Sections 202-1234A-17X through 22X; 180.9–238.9 mcd), the benthic to planktonic foraminiferal ratio is generally high and the abundance of planktonic foraminifers shows a marked decrease relative to the total foraminiferal abundance. The planktonic foraminiferal assemblage includes *Globorotalia truncatulinoides, Globorotalia inflata, Globorotalia scitula, Globorotalia ungulata, Globigerina bulloides, Globigerinita glutinata, Neogloboquadrina dutertrei, Neogloboquadrina pachyderma,* and *Orbulina universa*. This assemblage is present down to 238.9 mbsf, indicating the upper Pleistocene Subzone Pt1a of Berggren et al. (1995) (Fig. F12, p. 63, in the "Explanatory Notes" chapter). Changes in assemblage composition offer the potential to monitor variations in the intensity and position of the upwelling system with time.

T10. Distribution of foraminifers, p. 56.

Benthic Foraminifers

Benthic foraminifers were studied in all core catcher samples from Hole 1234A. They are generally frequent to common (representing between 20% and 98% of the total foraminiferal assemblage) and are moderately or well preserved, although a significant proportion of tests are pyritized at some levels. To assess assemblage composition and variability downhole, ~200 specimens from the >150-µm fraction were picked from each core catcher sample and mounted onto slides, prior to identification and counting. A total of 34 taxa were identified (Table T10). Common species are *Bolivina seminuda, Bolivina costata, Bulimina mexicana, Cassidulina teretis, Chilostomella ovoidea, Eubuliminella exilis, Globobulimina pyrula, Globobulimina affinis, Nonionella auris, Nonionella stella, Planulina wuellerstorfi, Praeglobobulimina spinescens, Rotaliatinopsis semiinvoluta, Rutherfordoides mexicanus,* and *Uvigerina peregrina*.

The assemblage is dominated by high carbon-flux indicators that are typical in assemblages from oxygen minimum zone (OMZ) environments. Oxygen often becomes the limiting factor in the central part of the modern OMZ, and the downslope succession of species reflects local variations in carbon flux and oxygen gradients. At Site 1234, marked

changes in assemblage composition are recorded downhole, particularly for *Bolivina* spp., *Globobulimina* spp., *Uvigerina* spp., and *Nonionella* spp. As these taxa have different tolerance of oxygen depletion, they can be used to detect shifts in bottom water oxygenation related to upwelling and circulation patterns. For instance, the distinct peak in the abundance of *Bolivina* spp. at ~175–215 mcd (>40% of total benthic foraminifers) points to an intense episode of seafloor dysoxia (Fig. F16) that may be linked to the intensification of nutrient-rich PCW and the decreased influence of AAIW.

F16. Variations in percent of benthic foraminifers, p. 36.

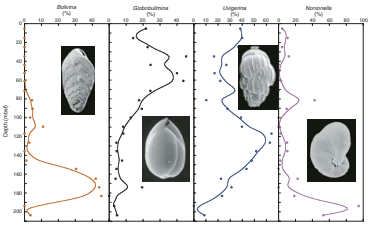

Diatoms

Diatoms are abundant and generally well preserved both in the core catcher and the split-core samples. Silicoflagellates, radiolarians, sponge spicules, and phytoliths are also observed in most samples.

This site is within the highly productive coastal upwelling area near Concepción, and diatom floras are dominated by the upwelling-related genus *Chaetoceros* spores, bristles, and vegetative cells (Schuette, 1980; Abrantes, 1988; Schrader and Sorknes, 1990; Abrantes and Moita, 1999). *Thalassiosira* sp., *Delphineis* sp., *Pseudonitzschia* sp., and *Thalassionema nitzschioides* appear as secondary components of the flora.

Despite the dominance of the coastal upwelling forms, the presence of more oceanic species gives indications of cold- and warm-water masses at various times. Warm water–related species such as *Azpeitia nodulifer, Fragilariopsis doliolus,* and *Nitzschia marina* are present in higher abundances (frequent/common) below ~68 mcd, from Samples 202-1234A-7H-CC through 8H-CC; 11H-CC through 12X-CC; 14X-3, 40 cm, to 18X-2, 40 cm; 18X-4, 40 cm, to 19X-3, 40 cm; and 21X-1, 40 cm, to 21X-3, 40 cm. Cold water–related forms, such as *Actinocyclus curvatulus* and the *Rhizosolenia hebetata* group, are found in higher abundances (frequent/common), mainly above ~78 mcd at the following levels: mudline to Samples 202-1234A-1H-CC; 4H-1, 40 cm, to 4H-5, 40 cm; 4H-CC to 5H-3, 40 cm; 6H-CC to 8H-3, 40 cm; and 13X-1, 40 cm, to 13X-5, 40 cm (Table T11).

T11. Distribution of diatoms, p. 58.

Floras are occasionally enriched in heavily silicified neritic forms, such as *Actinoptychus senarius* and *Stephanopyxis turris*. Freshwater diatoms are present (trace/rare) in the following intervals: mudline to Samples 202-1234A-1H-3, 42 cm; 2H-6, 40 cm, to 2H-CC; 5H-CC to 10H-4, 40 cm; and 16X-3, 40 cm, to 16X-4, 40 cm. Displaced shallow-water marine benthic diatoms are found throughout the core, with higher abundances between the mudline and Samples 202-1234A-2H-2, 40 cm, and from 14X-CC to 16X-4, 40 cm. Large diatom cells of the genus *Coscinodiscus* were found in the >63-µm fraction in Samples 202-1234A-2H-CC and 6H-CC. The presence of *F. doliolus* down to Sample 202-1234A-21X-CC places this sequence in the *F. doliolus* Zone; thus, the whole section cored at this site is of Quaternary age.

PALEOMAGNETISM

Natural Remanent Magnetization

The natural remanent magnetization (NRM) of the archive half of each core section was initially measured then remeasured after alternating-field (AF) demagnetization at selected levels. Sections obviously affected by drilling disturbance were not measured. Core 202-1234A-1H

was AF demagnetized at peak fields of 10, 15, and 20 mT. Cores 202-1234A-2H and 3H were AF demagnetized at 15 and 20 mT. Cores 202-1234A-4H through 22X were AF demagnetized at 20 and 25 mT. All other cores (202-1234B-1H through 19X and 202-1234C-1H through 8H) were measured after a single demagnetized step of 25 mT.

Initial NRM intensities were high, typically between 0.1 and 1 A/m except for a few discrete intervals discussed in more detail below (Fig. **F17**). The NRM intensities after demagnetization at 25 mT ranged from 1×10^{-3} to 8×10^{-2} A/m (Figs. **F17, F18**). The high NRM intensities prior to demagnetization are characterized by a steep positive inclination (averaging +76° in the upper 50 mcd of Hole 1234A) that is consistent with a drill string magnetic overprint. Though substantially reduced, this overprint was incompletely removed after AF demagnetization up to 25 mT. Within the upper 50 mcd, the inclinations after AF demagnetization at 20 or 25 mT were about –30° on average (Figs. **F17, F19**), much shallower than expected for the location of Site 1234 (expected inclination based on an axial geocentric dipole ≈ 56°). Before demagnetization, declinations tend to have values close to 0°/360°. This bias is likely the result of a drilling-induced magnetic overprint. Demagnetized (25 mT) declinations in the upper ~80 mcd deviate significantly from the 0°/360° values, and declination variability can be correlated between holes. Both of these are indicators that most of the overprint has been removed from the 25-mT declinations. Demagnetized (25 mT) inclinations have anomalously positive inclinations below 50 mcd and demagnetized (25 mT) declinations have a strong bias toward 0°/360° below 80 mcd, indicating the continued severe effect on the NRM of the drill string overprint below these depths (Fig. **F17**). The fact that the declination overprint is deeper than its inclination counterpart suggests that declination is more resistant to the drill string overprint. For more details on the overprint see **Lund et al.,** this volume.

Directional Variability

Biostratigraphic constraints (see **"Biostratigraphy,"** p. 8) based on calcareous nannofossils indicate that the base of the cored sequence is younger than 0.26 Ma (Zone NN21); therefore, these sediments should all have normal polarity (negative inclinations) associated with the Bruhnes Chron (0–0.78 Ma).

Within the uppermost 60 mcd, high positive inclinations associated with the drill string overprint are at least partially removed through AF demagnetization (Fig. **F19**). Inclinations are dominantly negative, as would be expected from sediment deposited during a normal polarity interval, and variations are consistent in all three holes (Fig. **F19**). The most significant of these variations is an interval of anomalous directions recorded between 21 and 23 mcd (Fig. **F19**). Steep positive inclinations and declinations ~180° opposed to the background declination values are observed (Fig. **F20B**). This interval, which is ~1 m thick in Core 202-1234-3H, is interpreted to be a magnetic field excursion and is remarkably similar in both inclination and declination to an excursion found at Site 1233 (Fig. **F20**). This interval may represent the Laschamp Excursion (~41 ka). The comparison of selected inclination and declination data with Site 1233 (Fig. **F20**) suggests that regionally correlative directional paleomagnetic secular variation can be observed at Site 1234. Clearly, caution must be used because this record suffers from magnetic overprints and distinct intervals appear to be affected by time-dependent magnetic dissolution.

F17. NRM inclination, declination, and intensity after demagnetization, p. 37.

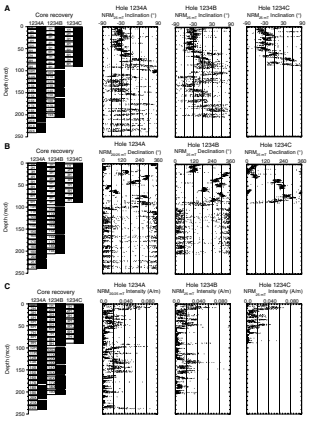

F18. NRM before and after AF demagnetization, p. 38.

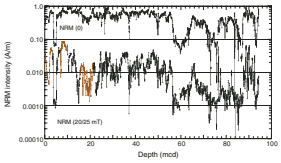

F19. NRM inclination after demagnetization, p. 39.

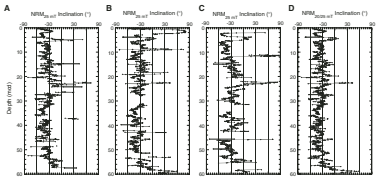

F20. Possible geomagnetic field excursion, p. 40.

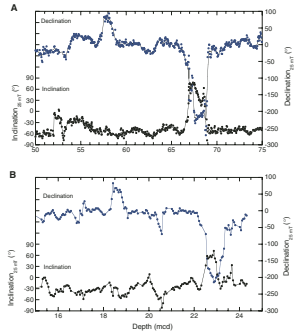

Several intervals below 60 mcd have NRM intensities that are more than one order of magnitude lower than background, from ~0.05 to 2 × 10^{-3} A/m (Fig. F18). These intervals may represent times when magnetic mineral dissolution associated with more significant early sediment diagenesis was occurring.

GEOCHEMISTRY

Sediment Gases

Concentrations of headspace and vacutainer gases were routinely monitored in Hole 1234A sediments according to shipboard safety and pollution prevention considerations. The high gas pressure in the cores required perforating the core liners to prevent excessive core expansion. Low methane concentrations were first detected in the shallowest headspace gas sample at 1.5 mcd (Fig. F21; Table T12). Methane (C_1) increased rapidly by 9.7 mcd, and vacutainer samples had high methane concentrations (>95 vol%) at all depths. Low ethane (C_2) concentrations were detected in the vacutainer samples. Ethane values gradually increase with depth, from 2.7 ppmv at 31.1 mcd to 81 ppmv at 221.3 mcd. No significant amounts of higher molecular weight hydrocarbons were observed.

High methane concentrations, low ethane concentrations, and the resulting high C_1/C_2 ratios (Fig. F21) indicate that the methane originates from in situ fermentation (methanogenesis) of sedimentary organic matter. A biogenic origin for methane is supported by the disappearance of dissolved sulfate by 9.7 mcd, where methane increased, because interstitial sulfate inhibits methanogenesis in marine sediments (Claypool and Kvenvolden, 1983).

Interstitial Water Geochemistry

We collected 22 interstitial water samples from Hole 1234A. Chemical gradients at this site (Table T13; Fig. F22) reflect the influence of organic matter diagenesis by microbially mediated oxidation reactions, a limited degree of biogenic opal dissolution, and the effects of authigenic mineralization reactions on fluid composition.

Chlorinity increases from 550 mM at 1.5 mcd to 572 mM at 51.8 mcd then decreases to values <565 mM by 87.9 mcd (Fig. F22). Salinity, measured refractively as total dissolved solids, increases from 35 to 37 from 29.7 to 51.8 mcd then decreases to values typically ≤33 by 111.5 mcd (Table T13). Sodium concentrations measured by inductively coupled plasma–atomic emission spectrophotometry averaged 3% lower than those estimated by charge balance reported here (Table T13). Sodium concentrations parallel salinity and chlorinity, with a total range from 470 mM at 1.5 mcd to a maximum of 504 mM at 51.8 mcd.

Organic matter diagenesis, driven by microbial oxidation reactions, dominates many of the interstitial water profiles. The relatively low organic carbon contents are apparently counterbalanced by high total sedimentation rates to result in pronounced depth variations in interstitial water chemistry, as typically observed in more organic carbon–rich, continental margin settings. Sulfate concentration at 1.5 mcd is 18.2 mM, already substantially lower than typical seawater values of 29 mM, and concentrations from 9.7 to 111.5 mcd are below the detection limit (~0.6 mM). Sulfate increases slightly with greater depth to values

F21. Headspace and vacutainer methane and C_1/C_2 vs. depth, p. 41.

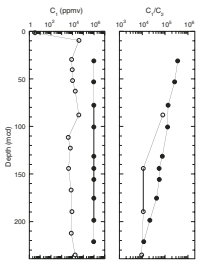

T12. Headspace and vacutainer gas concentrations and C_1/C_2 ratio, p. 60.

T13. Interstitial water geochemical data, p. 61.

F22. Interstitial water geochemical data, p. 42.

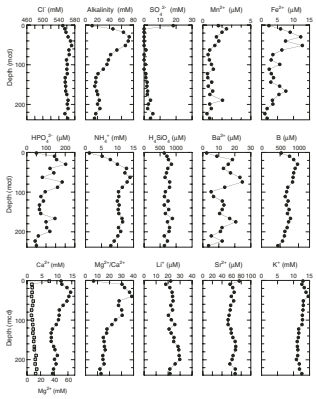

as high as 4 mM at 189.6 mcd and concentrations of 2–6 mM to the base of the drilled section. This minor sulfate maximum is coincident with a zone of locally elevated alkalinity, although it may reflect drilling fluid contamination.

Organic matter decomposition by sulfate reduction and methanogenesis drives large increases in alkalinity, which increases to peak values of >60 mM from 17.9 to 51.8 mcd then decreases to values <20 mM from 132.8 to 166.8 mcd. A secondary alkalinity maximum, with values >20 mM, occurs from 175.0 to 210.8 mcd. Lower alkalinity values correspond to the depth interval with a higher proportion of authigenic calcite (>120 mcd) (see **"Lithostratigraphy,"** p. 5), indicating that authigenic mineralization reactions of inorganic carbonates are an effective alkalinity sink in these sediments.

The profiles of the reduced forms of the secondary oxidants manganese and iron show variations with depth, although not simply related to that of sulfate. Dissolved manganese concentrations average 1 µM, with a small maximum at 9.7 mcd (2.5 µM) and an isolated peak value (2.1 µM) at 189.6 mcd. Dissolved iron concentrations have a broad maximum of >10 µM from 29.7 to 51.8 mcd, decrease to minimum values of <4 µM from 74.7 to 144.1 mcd, increase to 7.6 µM at 166.8 mcd, and then decrease with increasing depth.

Organic matter decomposition generates increases in phosphate and ammonium in interstitial water. Phosphate concentrations are >120 µM from 9.7 to 51.8 mcd and are <100 µM from 99.3 to 154.1 mcd, with a secondary maximum from 167.8 to 199.1 mcd approximately centered on the minor sulfate peak. Ammonium concentrations increase from 1.2 mM at 1.5 mcd to values >11 mM from 40.4 to 87.9 mcd and remain >8 mM throughout. Ammonium concentrations at Site 1234 are significantly higher throughout than even the peak values at Site 1233, indicating that the balance of ammonium generation by organic matter degradation and ammonium consumption differs for the two sites. The maximum in ammonium concentration is broader, deeper, and more smoothly defined than the phosphate maxima.

Dissolved silicate concentrations average ~720 µM with little depth variation (Fig. **F22**). Mean values are ~25% higher than those at Site 1233 but are undersaturated with respect to biogenic opal. Undersaturation may reflect the limited amount of biogenic opal available for dissolution or other controls on opal solubility, such as effects of opal composition, in these sediments. Barium concentrations are generally higher than those at Site 1233 but lack the sharp subsurface maximum seen there. Both sites experience complete depletion of seawater sulfate at shallow depths, which would drive barite dissolution and increase interstitial water barium concentrations. Barium concentrations are generally elevated in the zone of maximum alkalinity (e.g., 25 µM at 74.7 mcd) but decrease to minimum values from 99.3 to 111.5 mcd. Boron concentrations increase to values >840 µM from 17.9 to 62.9 mcd then generally decrease with increasing depth to 443 µM at 235.1 mcd. The resemblance of the boron and ammonium profiles indicates that adsorption/desorption reactions may influence the boron profile, although the maximum boron values are found shallower than maximum ammonium concentrations.

Calcium concentrations decrease sharply from 7.5 mM at 1.5 mcd to values generally <2 mM from 9.7 to 111.5 mcd then increase to >2.8 mM by 189.6 mcd. Magnesium concentrations increase to >58 mM from 17.9 to 51.8 mcd then generally decrease with increasing depth to 38 mM at 235.1 mcd. A broad minimum, with values <40 mM, occurs

from 122.8 to 166.9 mcd, starting in the zone of increased authigenic carbonate (see "Lithostratigraphy," p. 5). The very strong decrease in calcium by 9.7 mcd is consistent with authigenic mineralization reactions driven by the alkalinity increase. Increasing magnesium/calcium ratios with the calcium decrease indicate that calcite precipitation is the most likely reaction taking place in shallow sediments. Magnesium/calcium ratios are generally >30 from 9.7 to 87.9 mcd but decrease to ~12 in the deepest samples from 223.7 to 235.1 mcd.

Lithium concentrations first decrease sharply then generally increase with increasing depth before decreasing in the deepest samples. Strontium concentrations decrease with increasing depth to a broad minimum before increasing to 67 µM at 235.1 mcd, and potassium concentrations increase to >13 mM from 17.9 to 74.7 mcd, then decrease with increasing depth before increasing again in the deepest three samples (Fig. F22).

Sedimentary Inorganic Carbon and Organic Carbon, Nitrogen, and Sulfur Concentrations

Inorganic carbon (IC), TOC, total nitrogen (TN), and total sulfur (TS) concentrations were determined on sediment samples from Hole 1234A (Table T14). Organic matter carbon/nitrogen ratios and Rock-Eval pyrolysis were employed to characterize the organic matter.

Calcium carbonate concentrations range between 0.8 and 11.7 wt% (average = 3.5 wt%) (Fig. F23). In the uppermost 115.8 mcd, calcium carbonate concentrations vary around a mean of 3.0 wt%. A pronounced carbonate maximum up to 11.7 wt% is present between 118.6 and 123.6 mcd. At greater depths, the carbonate contents decrease gradually from ~6.0 to ~3.0 wt%. Calcium carbonate originates mainly from calcareous plankton, although diagenetically formed IC is visible in some intervals (see "Lithostratigraphy," p. 5). Low calcium carbonate concentrations in sediment from throughout the hole most likely reflect dilution by terrigenous sediment components. Changes in the carbonate contents may indicate changes in the fluvial supply of siliciclastics (see "Lithostratigraphy," p. 5), although fluctuations in carbonate flux may also be linked to changes in surface productivity triggered by the upwelling zone of Concepción (Chile). Fluctuations in carbonate dissolution may also have contributed to the variations in carbonate content because preservation of calcareous microfossils varied from poor to good (Tables T9, T10).

TOC concentrations range between 0.2 and 3.0 wt% (average = 1.1 wt%) (Fig. F23). The shallowest sample at 0.7 mcd has a high value of 2.0 wt%. TOC concentrations remain around a mean value of 1.0 wt% to a depth of 50 mcd, with small fluctuations. At greater depths, a more TOC-rich interval is observed between 54.5 and 90.2 mcd, with concentrations typically >1.5 wt% and up to 3.0 wt%. At greater depth, TOC concentrations are similar to the uppermost 50 mcd, but with larger fluctuations. Another maximum in TOC of 2.3 wt% is present at 223 mcd. The TN record contains very similar trends (Fig. F23). The good correlation between TOC concentrations and diatom abundance (see "Biostratigraphy," p. 8) suggests that the variations observed in both indicators should be linked primarily to productivity changes.

These upper Pleistocene sediments are poor in TOC compared to other coastal upwelling systems. For instance, in the Namibia and California margins, upper Pleistocene TOC concentrations are as high as 17 and 7 wt%, respectively (Lyle, Koizumi, Richter, et al., 1997; Berger et

T14. IC, $CaCO_3$, TC, TOC, TN, TOC/TN ratio, TS, and TOC/TS ratio, p. 62.

F23. Calcium carbonate, TOC, TN, and TS vs. depth, p. 43.

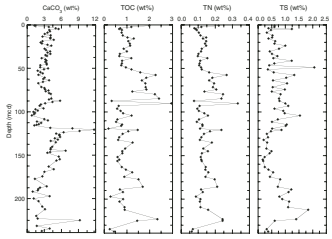

al., 1998). Lower TOC concentrations in the Chile margin sediments most likely result from greater dilution with siliciclastic material.

TS concentrations are high throughout the record, varying between 0.2 and 2.1 wt% (Table T14). In the uppermost 120 mcd, the TS profile presents large fluctuations (Fig. F23). TS concentrations gradually increase below 120 mcd to reach a maximum between 210 and 220 mcd then decrease. This TS maximum, which corresponds to the maximum in TOC and TN concentrations, could be attributed to the formation of pyrite during the microbial degradation of the organic matter by sulfate reduction.

TOC/TN ratios typically range between 5 and 10, which indicates a predominantly marine origin of the organic material (Fig. F24) (Bordovskiy, 1965; Emerson and Hedges, 1988; Meyers, 1997). Lower TOC/TN ratios are associated with lower TOC concentrations (Fig. F24), indicating that terrigenous organic matter supply and/or preservation effects during diagenesis control at least part of the organic matter variations.

Seven samples with different TOC concentrations and TOC/TN ratios were selected for Rock-Eval measurements. Low T_{max} values indicate that the organic matter is thermally immature (Table T15). The relationship between S_2 and TOC shows that the organic matter is dominantly Type II (Fig. F25) (i.e., marine algal organic matter) (Tissot and Welte, 1984; Langford and Blanc-Valleron, 1990), which is consistent with the TOC/TN ratios.

Fresh marine plankton has a relatively high lipid content, thus high H/C ratios. Therefore, well-preserved organic matter of marine algal origin yields high hydrogen index (HI) values when subjected to pyrolysis. The HIs measured in these samples range from 189 to 299 (Table T15), which indicates that the organic matter in sediments from the Chile margin is significantly degraded. Moreover, keeping in mind that TOC contents are low throughout the sedimentary record and that only a few samples have been measured with the Rock-Eval, the correspondence between decreases in both TOC concentrations and HI values (Fig. F25) could indicate that preservation of marine organic matter during diagenesis is important in controlling the organic carbon contents of sediments on the Chile margin.

AGE MODEL AND MASS ACCUMULATION RATES

A 239-mcd-thick (203.8 mbsf) late Quaternary hemipelagic sediment sequence was recovered at Site 1234, with a basal age <0.26 Ma (Zone NN21; see "Biostratigraphy," p. 8). The entire record is of normal polarity and within the Bruhnes Chron (1n; see "Paleomagnetism," p. 10). A conservative estimate of the average sedimentation rate is therefore ~788 m/m.y. A detailed age-depth model was not created shipboard, as datums are not abundant enough at this site of extremely high sedimentation rates.

F24. TN vs. TOC and TOC/TN vs. TOC, p. 44.

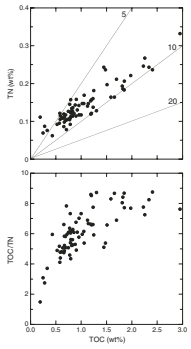

T15. Results of Rock-Eval pyrolysis, p. 64

F25. S_2 vs. TOC and HI vs. TOC, p. 45.

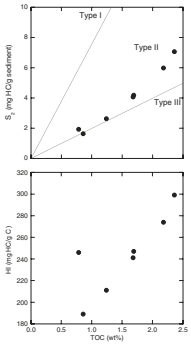

REFERENCES

Abrantes, F., 1988. Diatom assemblages as upwelling indicators in surface sediments off Portugal. *Mar. Geol.,* 85:15–39.

Abrantes, F., and Moita, T., 1999. Water column and recent sediment data on diatoms and coccolithophorids, off Portugal, confirm sediment record as a memory of upwelling events. *Oceanol. Acta,* 22:319–336.

Berger, W.H., Wefer G., Richter, C., Lange, C.B., Giraudeau, J., Hermelin, O., and Shipboard Scientific Party, 1998. The Angola-Benguela upwelling system: paleoceanographic synthesis of shipboard results from Leg 175. *In* Wefer, G., Berger, W.H., and Richter, C., et al., *Proc. ODP, Init. Repts.,* 175: College Station, TX (Ocean Drilling Program), 505–531.

Berggren, W.A., Kent, D.V., Swisher, C.C., III, and Aubry, M.-P., 1995. A revised Cenozoic geochronology and chronostratigraphy. *In* Berggren, W.A., Kent, D.V., Aubry, M.-P., and Hardenbol, J. (Eds.), *Geochronology, Time Scales and Global Stratigraphic Correlation*. Spec. Publ.—SEPM, 54:129–212.

Bordovskiy, O.K., 1965. Accumulation and transformation of organic substances in marine sediments, 2. Sources of organic matter in marine basins. *Mar. Geol.,* 3:5–31.

Brandhorst, W., 1971. Condiciones oceanográficas extivales frente a la costa de Chile. *Revista Biologica Marina* (Valparaiso), 14:45–84.

Claypool, G.E., and Kvenvolden, K., 1983. Methane and other hydrocarbons gases in marine sediment. *Ann. Rev. Earth Planet. Sci.,* 11:299–327.

Dettinger, M.D., Battisti, D.S., Garreaud, R.D., McCabe, G.J., Jr., and Blitz, C.M., 2001. Interhemispheric effects of interannual and decadal ENSO-like climate variations on the Americas. *In* Markgraf, V. (Ed.), *Interhemispheric Climate Linkages:* San Diego (Academic Press), 1–16.

Emerson, S., and Hedges, J.I., 1988. Processes controlling the organic carbon content of open ocean sediments. *Paleoceanography,* 3:621–634.

Flores, J.A., Gersonde, R., Sierro, F.J., and Niebler, H.S., 2000. Southern Ocean Pleistocene calcareous nannofossil events: calibration with isotope and geomagnetic stratigraphies. *Mar. Micropaleontol.,* 40:377–402.

Fonseca, T.R., 1989. An overview of the poleward undercurrent and upwelling along the Chilean coast. *In* Neshyba, S.J., Mooers, C.N.K., Smith, R.L., and Barber, R.T. (Eds.), *Poleward Flows along Eastern Ocean Boundaries:* New York (Springer), 203–228.

Hebbeln, D., Marchant, M., and Wefer, G., 2000. Seasonal variations of the particle flux in the Peru Chile Current at 30°S under "normal" and El Niño conditions. *Deep-Sea Res. II,* 47:2101–2128.

Lamy, F., Rühlemann, C., Hebbeln, D., and Wefer, G., 2002. High and low latitude control on the position of the southern Peru-Chile current during the Holocene. *Paleoceanography,* 17:10.1029/2001PA000727.

Langford, F.F., and Blanc-Valleron, M.M., 1990. Interpreting Rock-Eval pyrolysis data using graphs of pyrolizable hydrocarbons vs. total organic carbon. *AAPG Bull.,* 74:799–804.

Lyle, M., Koizumi, I., Richter, C., et al., 1997. *Proc. ODP, Init. Repts.,* 167: College Station, TX (Ocean Drilling Program).

Martini, E., 1971. Standard Tertiary and Quaternary calcareous nannoplankton zonation. *In* Farinacci, A. (Ed.), *Proc. 2nd Int. Conf. Planktonic Microfossils Roma:* Rome (Ed. Tecnosci.), 2:739–785.

Meyers, P.A., 1997. Organic geochemical proxies of paleoceanographic, paleolimnologic, and paleoclimatic proxies. *Org. Geochem.,* 27:213–250.

Mix, A.C., Pisias, N.G., Bloomer, S.F., and Mayer, LA., 1998. *Southeast Pacific Paleoceanographic Transects, Site Survey Data Package 3: 3.5 kHz Data, Genesis Leg III, R/V* Roger Revelle, *Feb.–Apr. 1997:* Corvallis (Oregon State Univ.).

Ocean Climate Laboratory, 1999. *World Ocean Atlas 1998 (WOA98)* [CD-ROM]. Available from: National Climatic Data Center, Asheville NC 28801-5001, USA.

Schrader, H., and Sorknes, R., 1990. Spatial and temporal variation of Peruvian coastal upwelling during the latest Quaternary. *In* Suess, E., von Huene, R., et al., *Proc. ODP, Sci. Results,* 112: College Station, TX (Ocean Drilling Program), 391–406.

Schuette, G., 1980. Recent marine diatom taphocoenoses off Peru and off southwest Africa: reflection of coastal upwelling [Ph.D. dissert.]. Oregon State Univ., Corvallis.

Strub, P.T., Mesias, J.M., Montecino, V., Rutllant, J., and Salinas, S., 1998. Coastal ocean circulation off western South America. *In* Robinson, A.R., and Brink, K.H. (Eds.), *The Sea* (Vol. 11): Coastal Oceans: New York (Wiley), 273–313.

Thornburg, T.M., and Kulm, L.D., 1987. Sedimentation in the Chile Trench: depositional morphologies, lithofacies, and stratigraphy. *Geol. Soc. Am. Bull.,* 98:33–52.

Tissot, B.P., and Welte, D.H., 1984. *Petroleum Formation and Occurrence* (2nd ed.): Heidelberg (Springer-Verlag).

Wiedecke-Hombach, M., and Shipboard Party, 2002. Cruise Report *Sonne,* SO 161/5, SPOC (Subduction Processes of Chile)-Geology-Geochemistry-Heatflow. Archive Number 11241/02, March 2002: Hannover (BGR).

Figure F1. Three-dimensional bathymetry image of the upper continental margin and locations of Sites 1234 and 1235, based on Parasound data (SO161-5, *Sonne,* Wiedecke-Hombach et al., 2002).

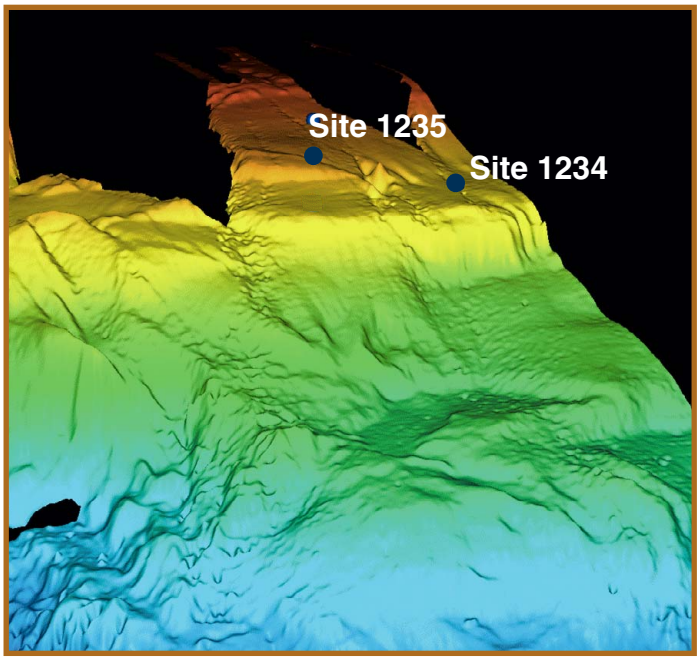

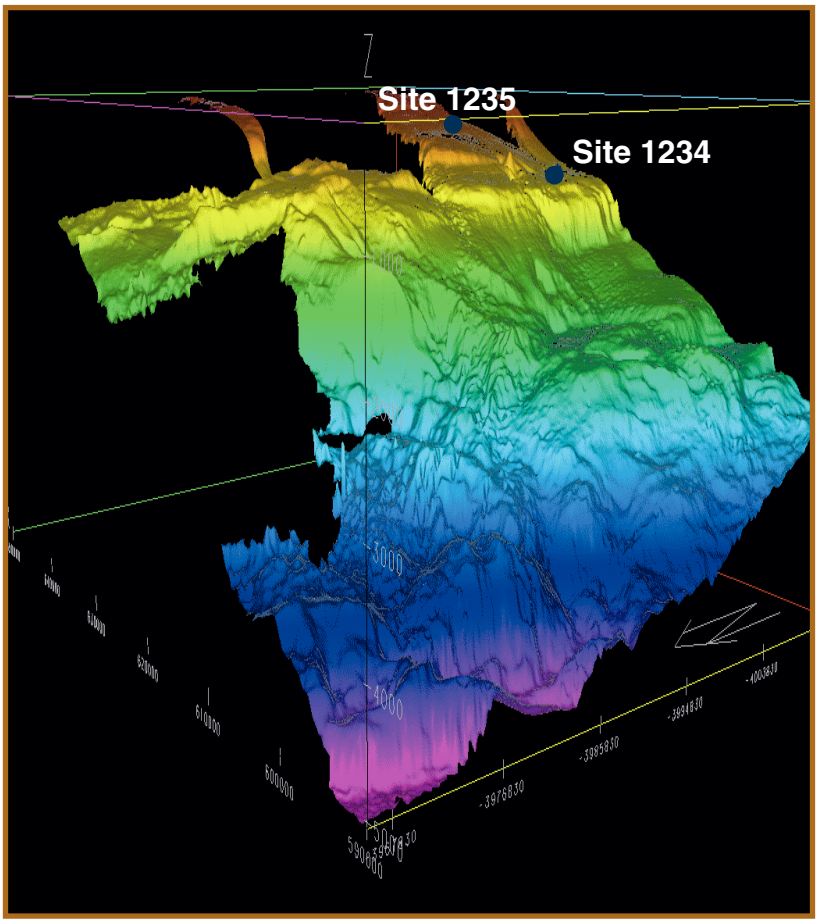

Figure F2. Seismic profile at Site 1234 (line 970308, *Revelle,* 80-in³ water gun at 30–400 Hz).

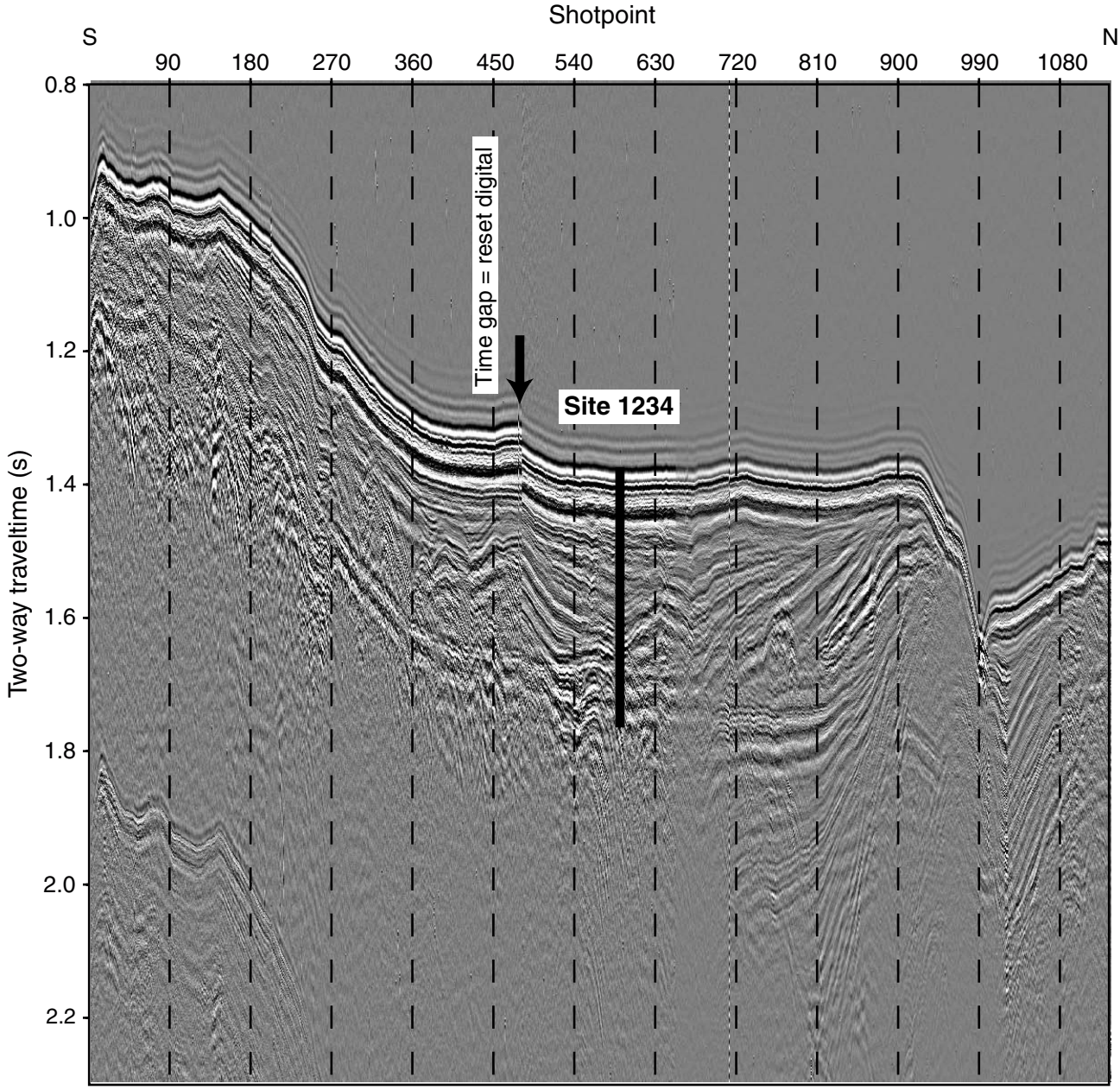

Figure F3. Locations of Sites 1232–1235 and oceanographic features off southern and central Chile (ACC = Antarctic Circumpolar Current, PCC = Peru-Chile Current, PCCC = Peru-Chile Countercurrent, CC = Chile Coastal Current, CFW = Chilean Fjord Water) after Strub et al. (1998) and Lamy et al. (2002). **A.** Modern mean annual sea-surface temperatures (SSTs) (contours are in degrees Celsius, after Ocean Climate Laboratory, 1999; dashed isotherms are extrapolated). **B.** Modern sea-surface salinities (SSSs) measured during the *Marchile* cruise in February to March 1960 (Brandhorst, 1971).

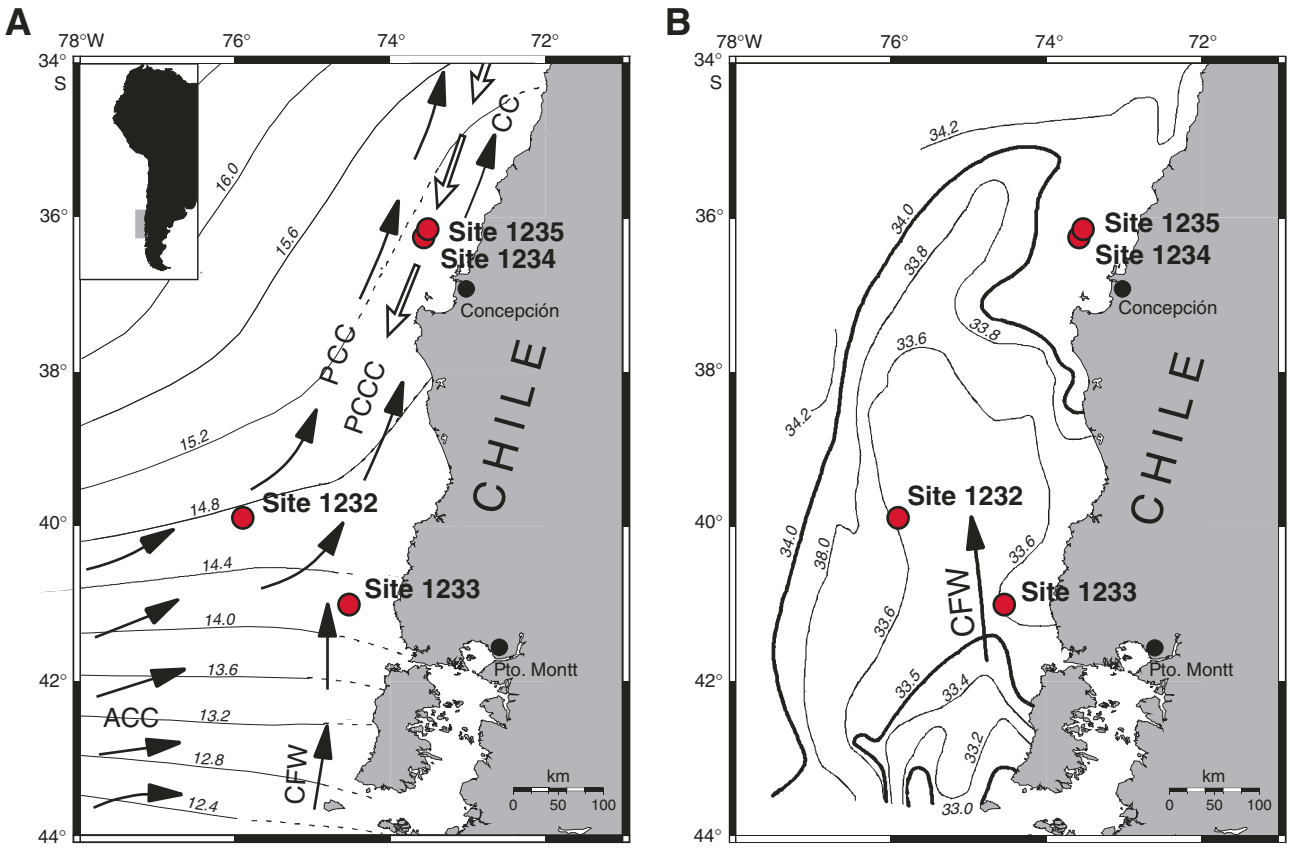

Figure F4. North-south cross section of water masses, characterized by dissolved oxygen concentrations in the southeast Pacific (Ocean Climate Laboratory, 1999). Southward-spreading mid-depth waters (PCW = Pacific Central Water) are characterized by relatively low oxygen and salinity and high nutrients. Northward-spreading Antarctic Intermediate Water (AAIW), above 1 km depth, is high in oxygen but is low in both salinity and nutrients. The Gunther Undercurrent (GUC) flows southward between 100 and 400 m water depth and is characterized by relatively low oxygen, high nutrients, and high salinity. Vertical bars indicate the water depth range of Sites 1233, 1234, and 1235 relative to the last glacial sea level lowering of ~130 m.

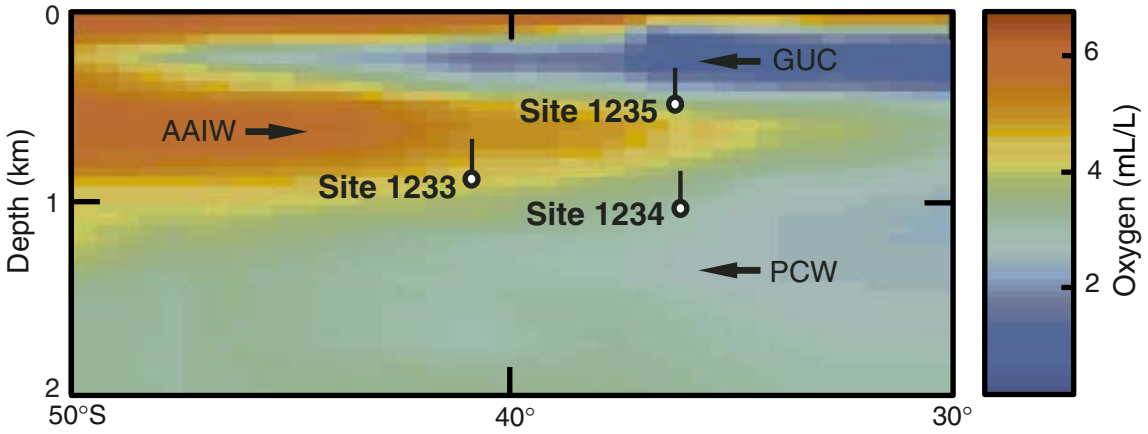

Figure F5. OSU Fast Track magnetic susceptibility data (OSUS-MS) vs. mcd for the spliced record and Holes 1234A though 1234C. Gray boxes indicate the portions of cores that are in the splice. **A.** 0–40 mcd. **B.** 30–70 mcd. (Continued on next three pages.)

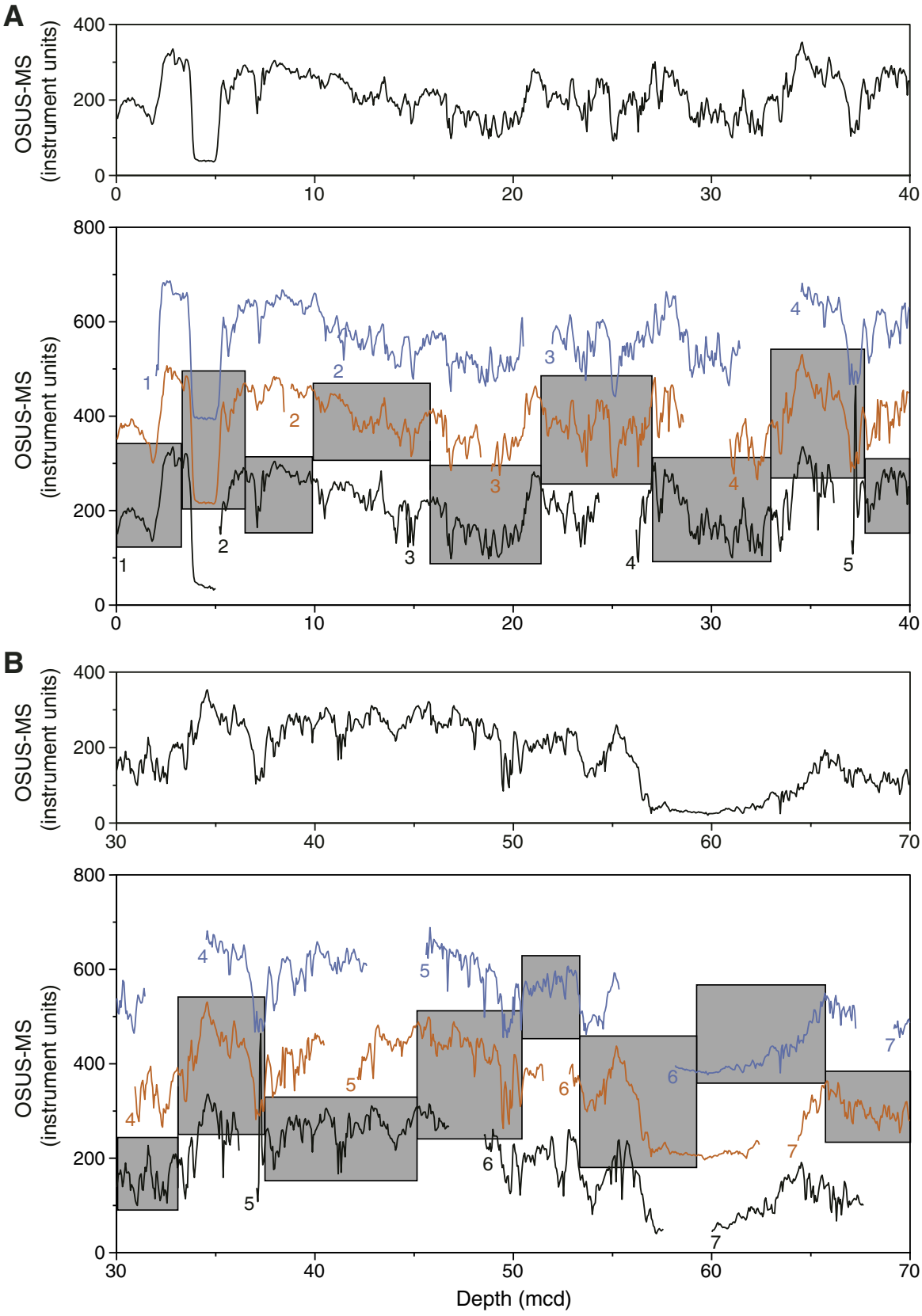

Figure F5 (continued). C. 60–100 mcd. D. 90–130 mcd.

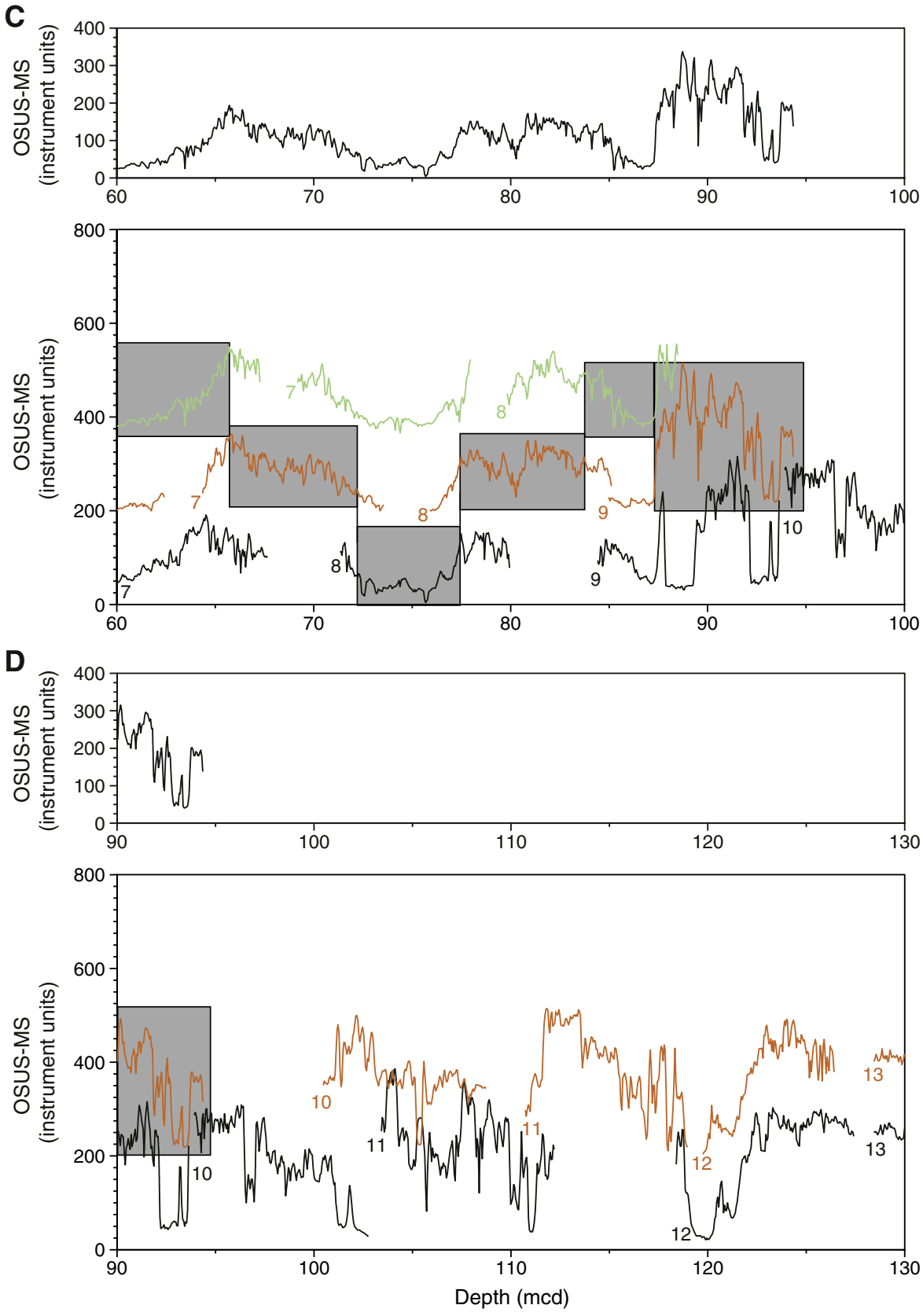

Figure F5 (continued). E. 120–160 mcd. F. 150–190 mcd.

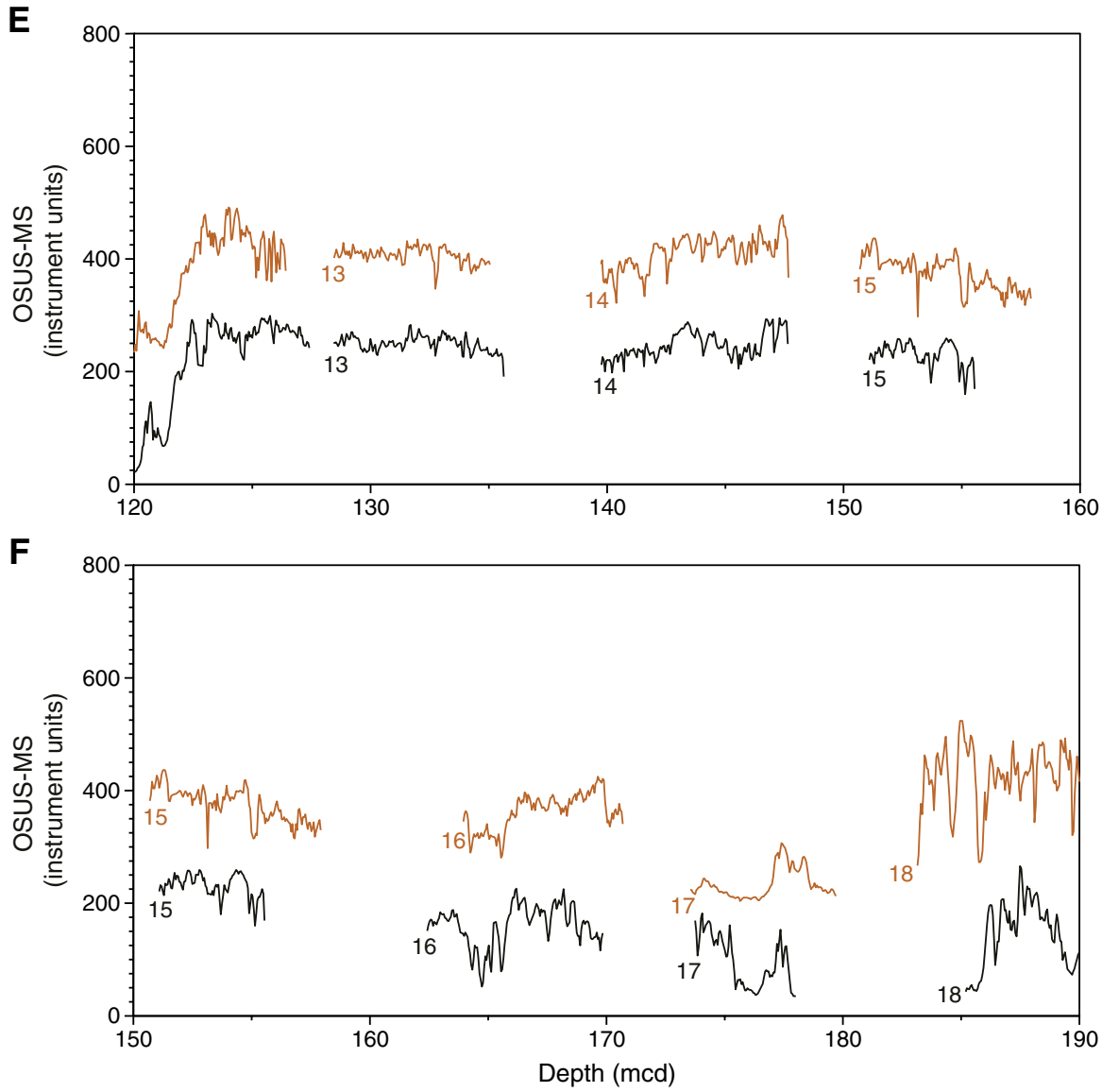

Figure F5 (continued). **G.** 180–220 mcd. **H.** 210–250 mcd.

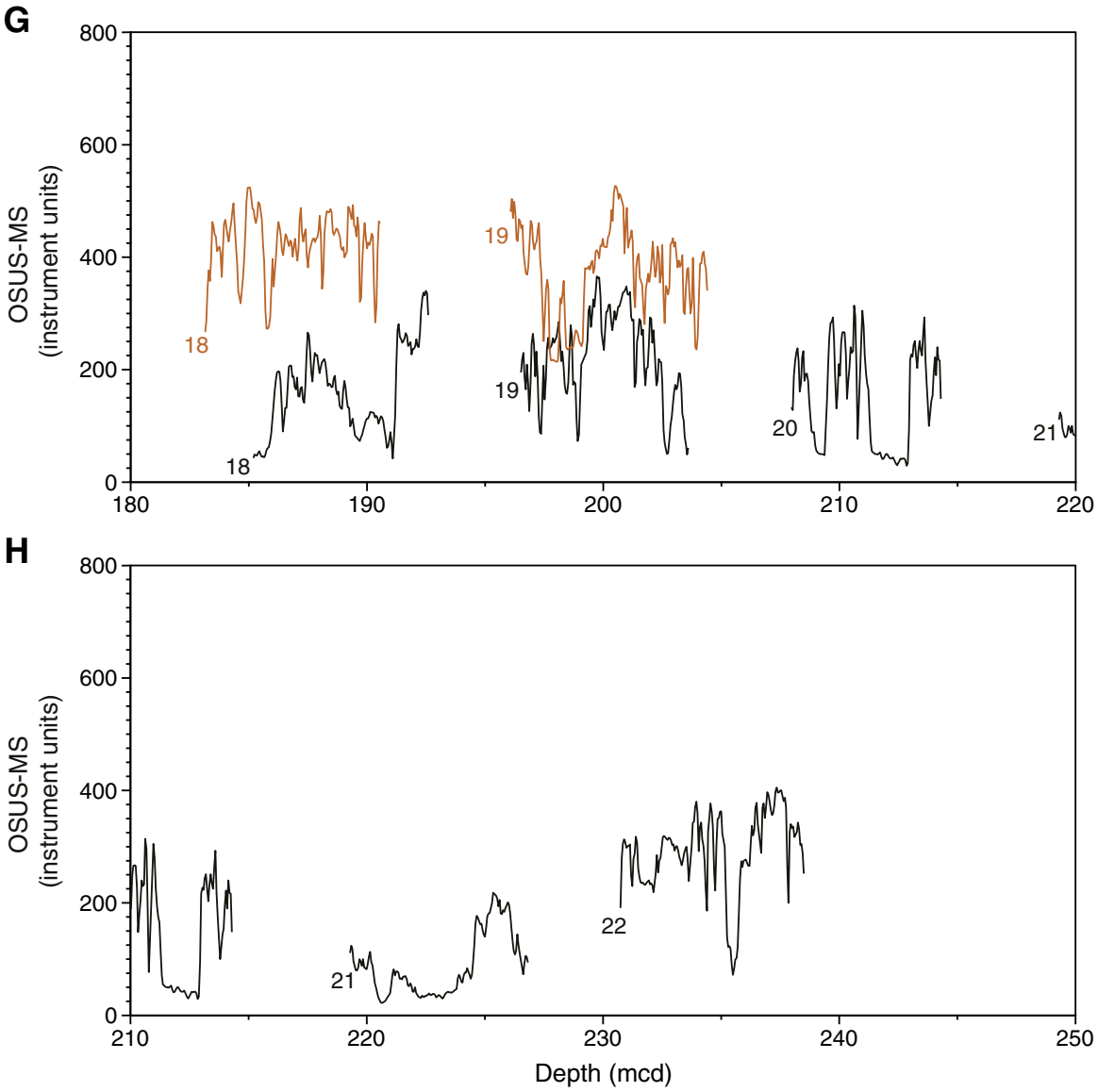

Figure F6. Spliced records of reflectance (L*), natural gamma radiation (NGR), gamma ray attenuation (GRA) bulk density, and multisensor track magnetic susceptibility (MST-MS) data from Site 1234.

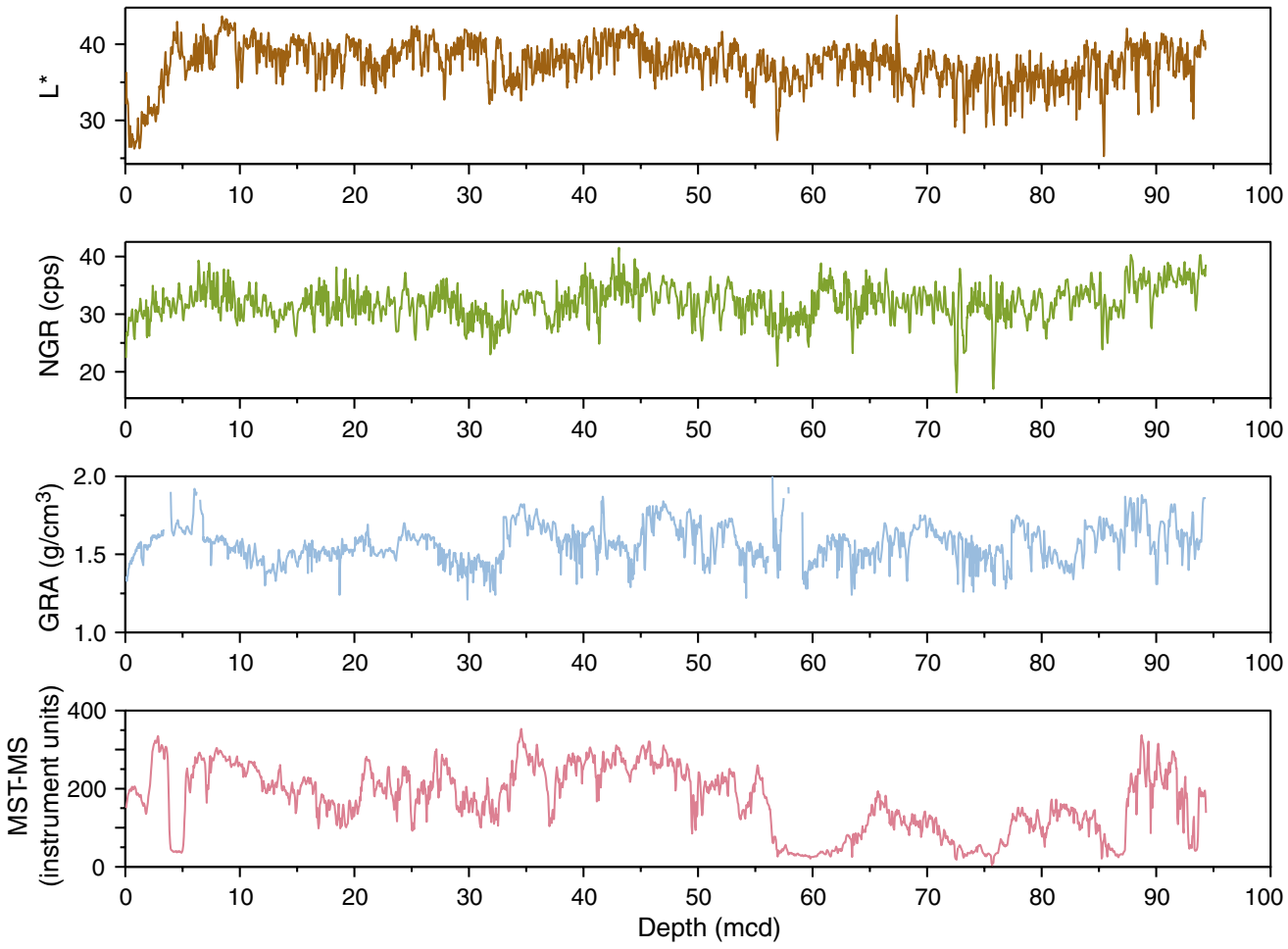

Figure F7. A comparison of the drillers depth (mbsf) and meters composite depth (mcd) scales in Holes 1234A through 1234C. The purple box shows the extent of the spliced record. On average, mcd is 18% greater than mbsf. The 1:1 (mbsf:mcd) line is also shown for comparison. GF = growth factor.

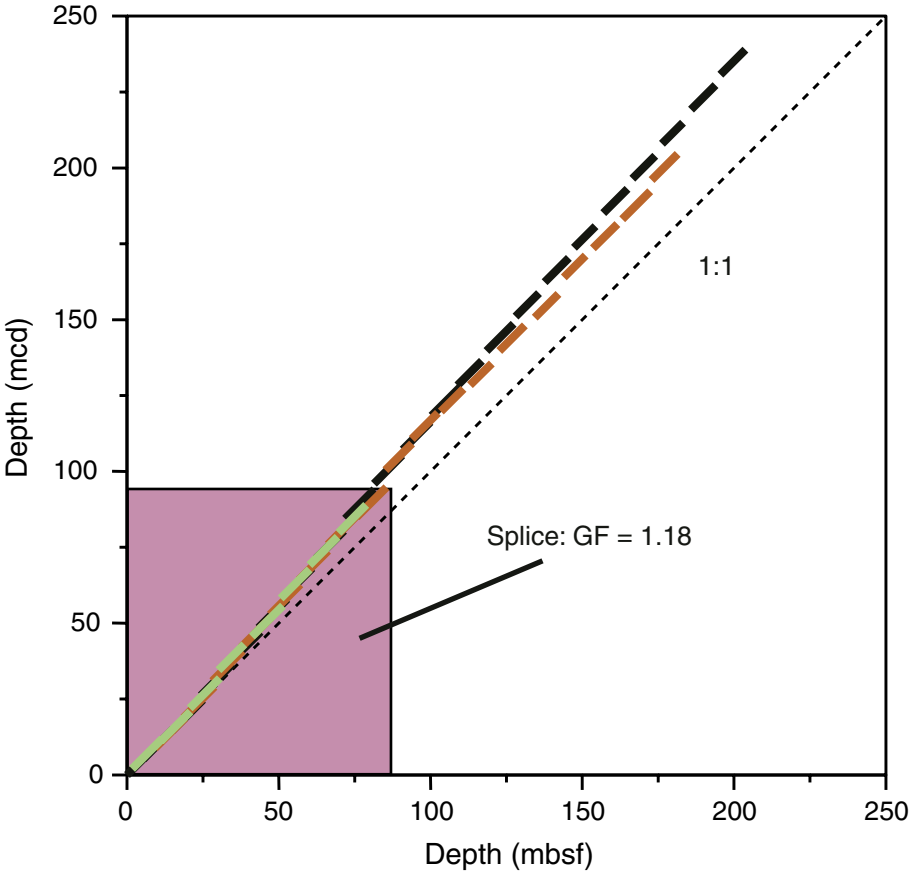

Figure F8. Core recovery, lithostratigraphy, age, color reflectance, gamma ray attenuation (GRA) and moisture and density (MAD) bulk density, magnetic susceptibility, and natural gamma radiation of recovered sediments from Site 1234. The gray lines show the original data, and the dark lines are 50-point smoothing averages of the original data.

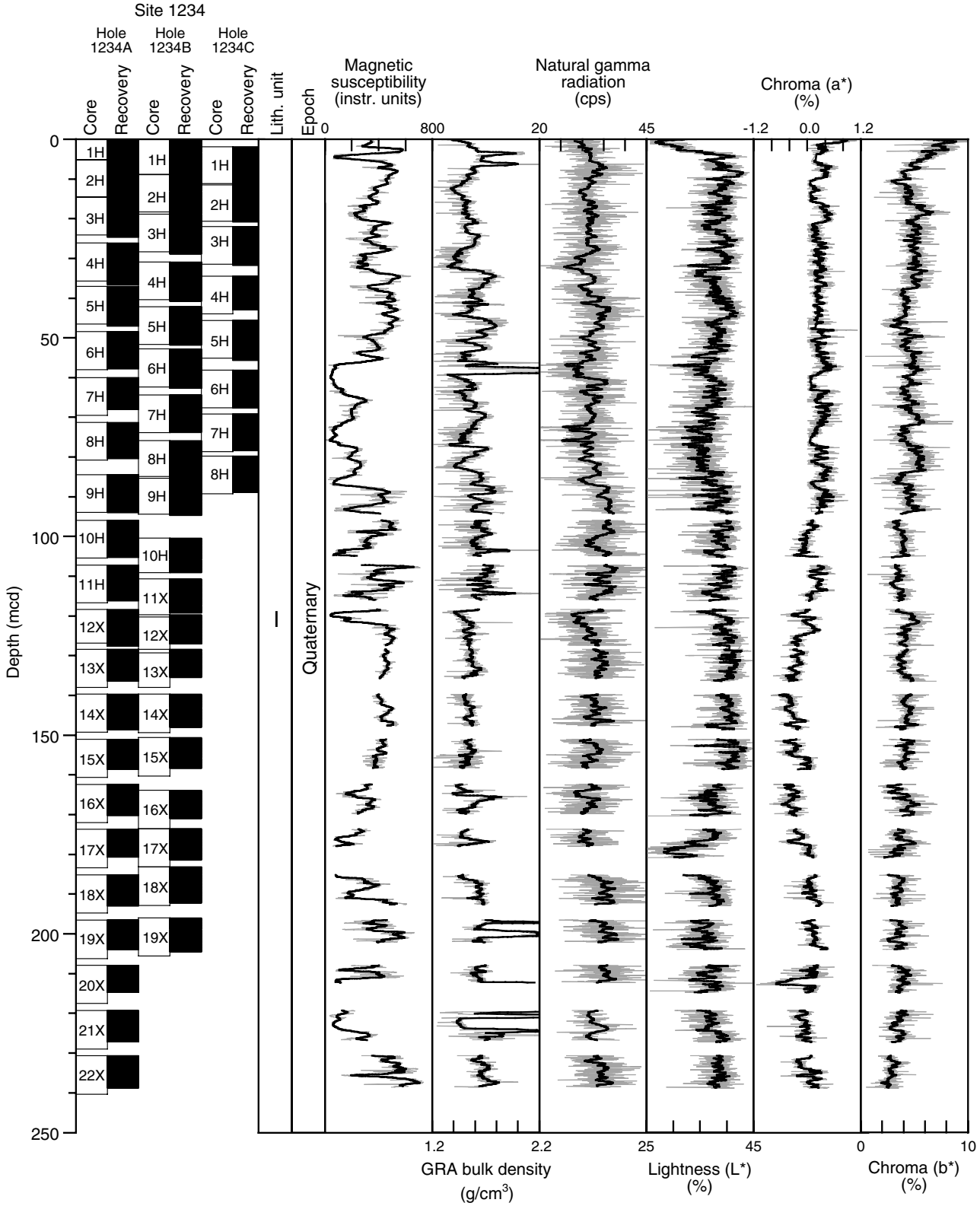

Figure F9. Major siliciclastic, biogenic, and authigenic components observed from smear slide analyses and compared to magnetic susceptibility (MS) data from Hole 1234A.

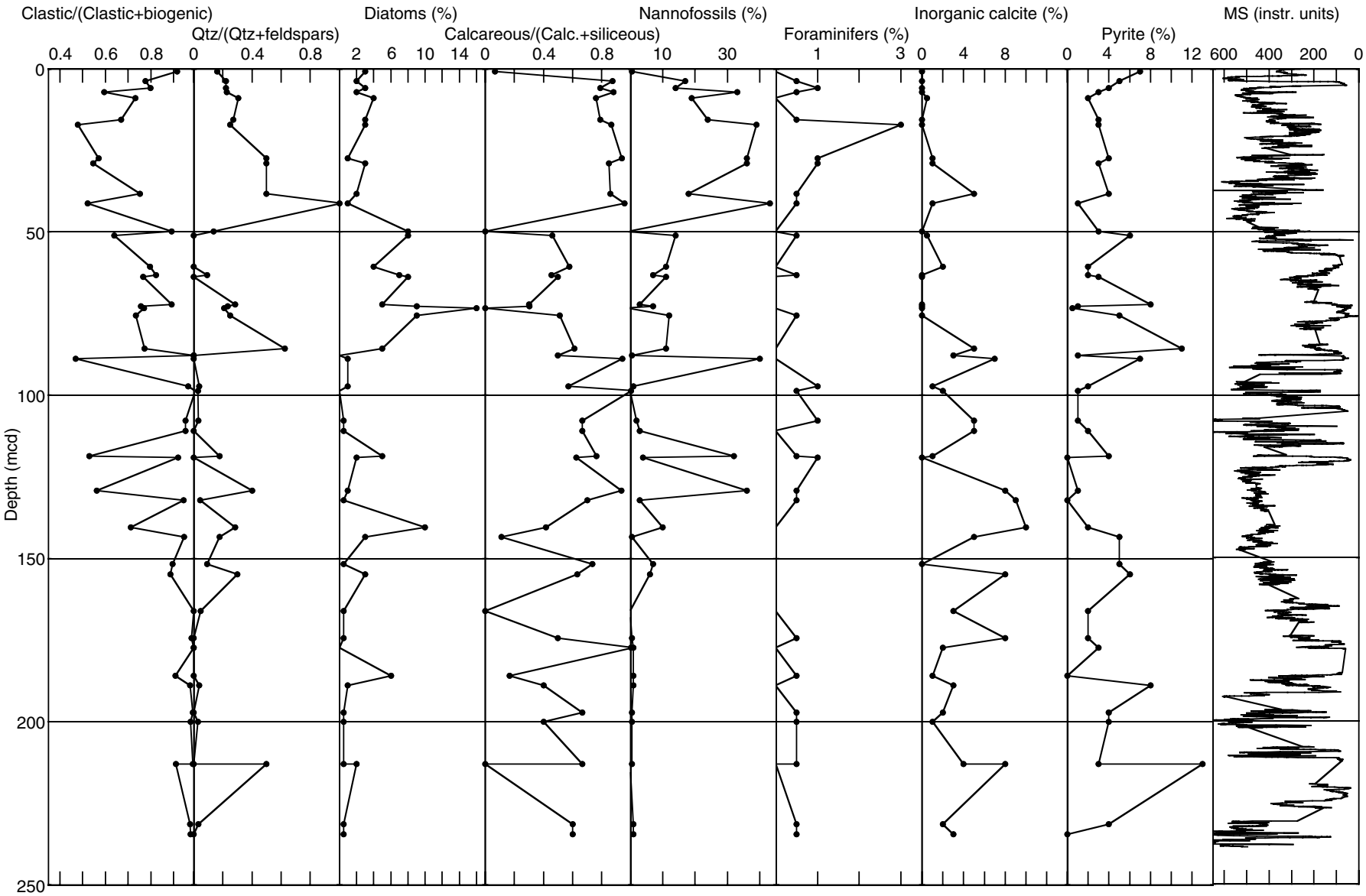

Figure F10. Close-up photograph of dark green layer interbedded in Site 1234 sediments (interval 202-1234A-12X-4, 10–35 cm).

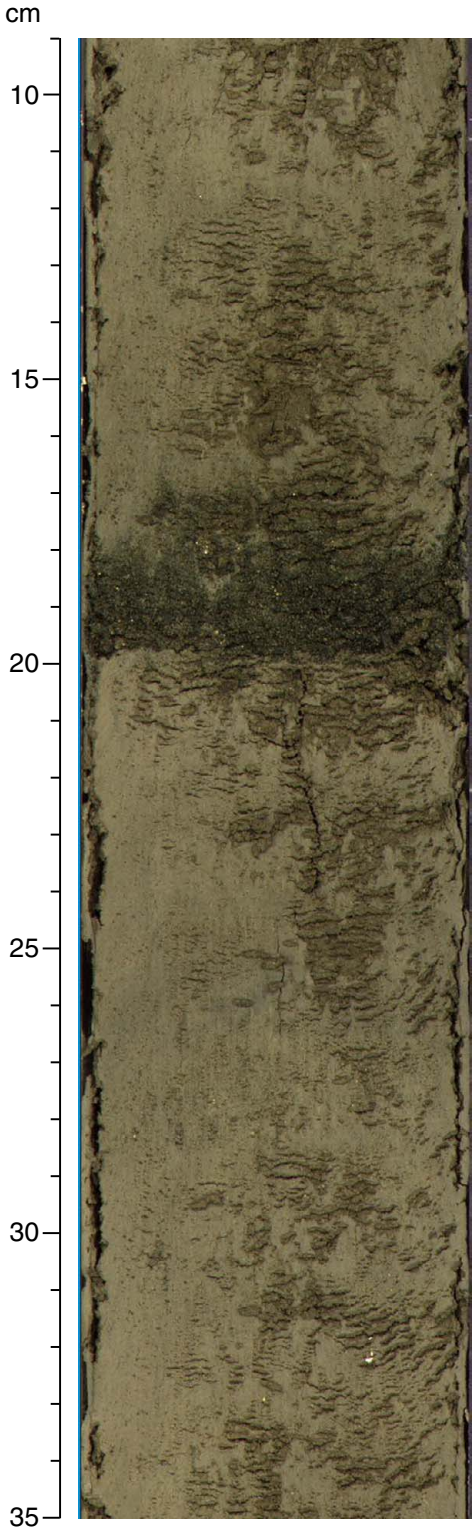

Figure F11. Close-up photograph of brownish white ash layer interbedded in Site 1234 sediments (interval 202-1234A-3H-3, 40–60 cm).

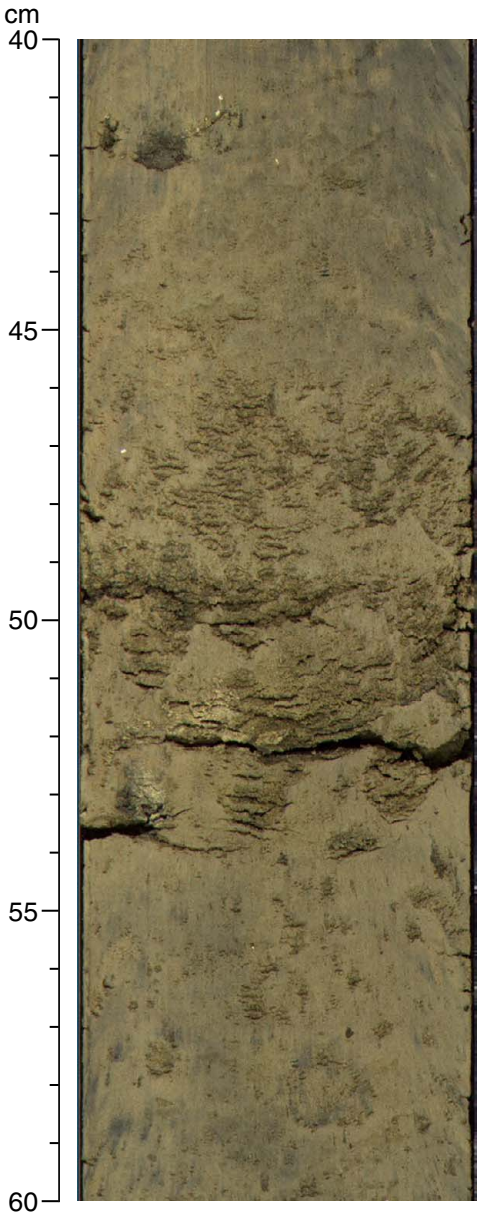

Figure F12. A. Moisture and density (MAD) (blue circles) and gamma ray attenuation (GRA) (gray line) bulk densities. **B.** Linear regression of MAD and GRA bulk densities at MAD measurement locations.

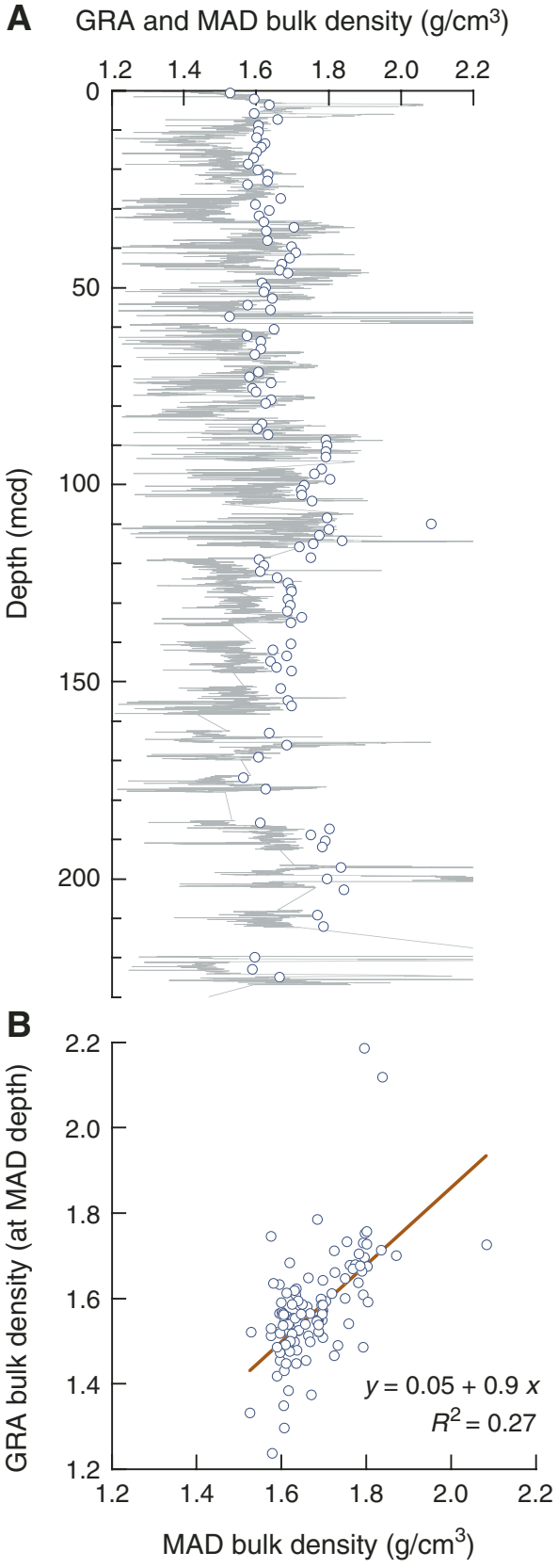

Figure F13. Core recovery and bulk density, grain density, porosity, and water content of sediments from Site 1234. Diagenetically controlled, increase in lithification probably occurs in highlighted intervals leading to increased bulk density and reduced porosity and water content.

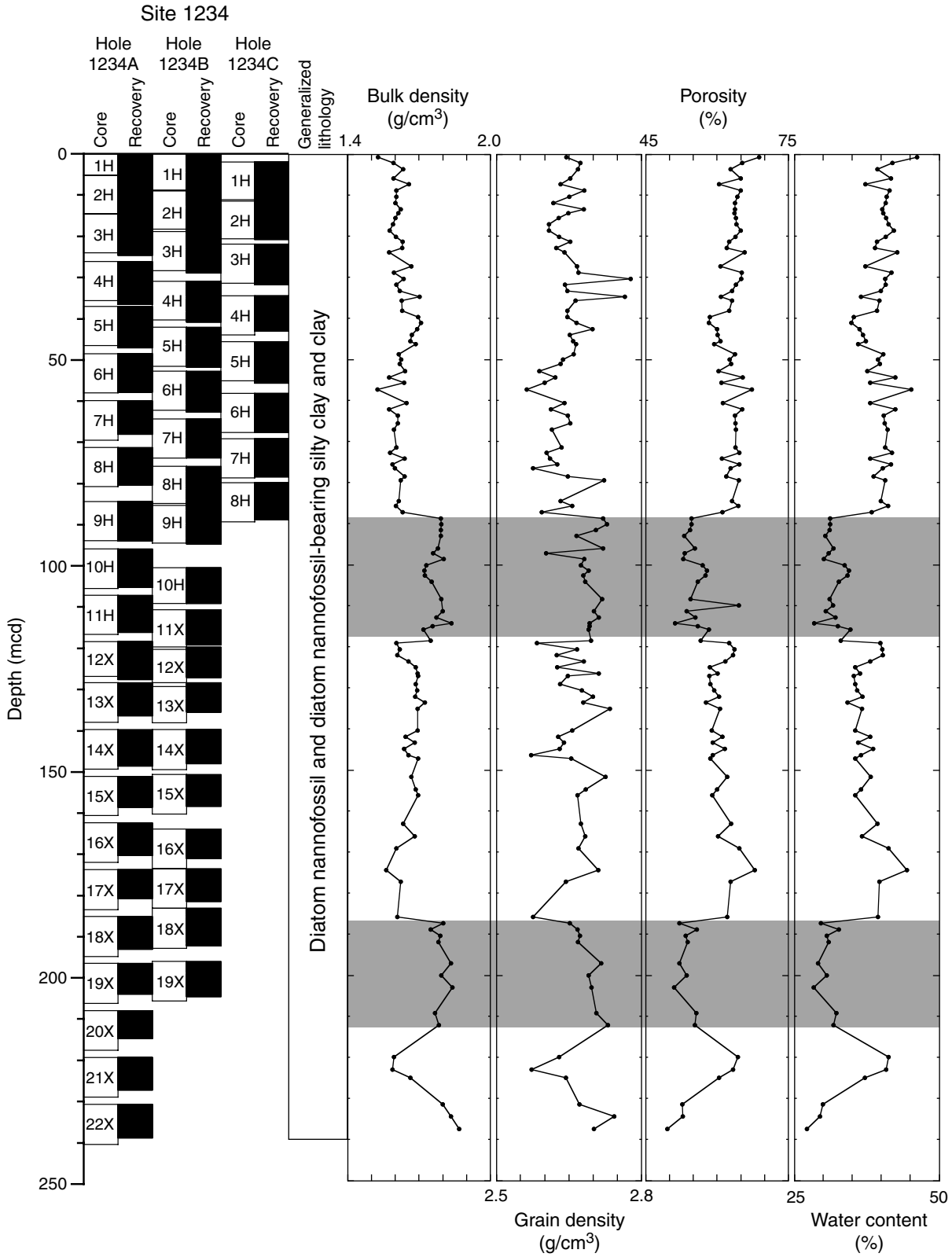

Figure F14. Color measurements plotted in the a*-b* color plane. Note the weak bimodal distribution with one trend characteristic of brownish sediments (a* > 0) and the other typical for more greenish sediments (a* < 0).

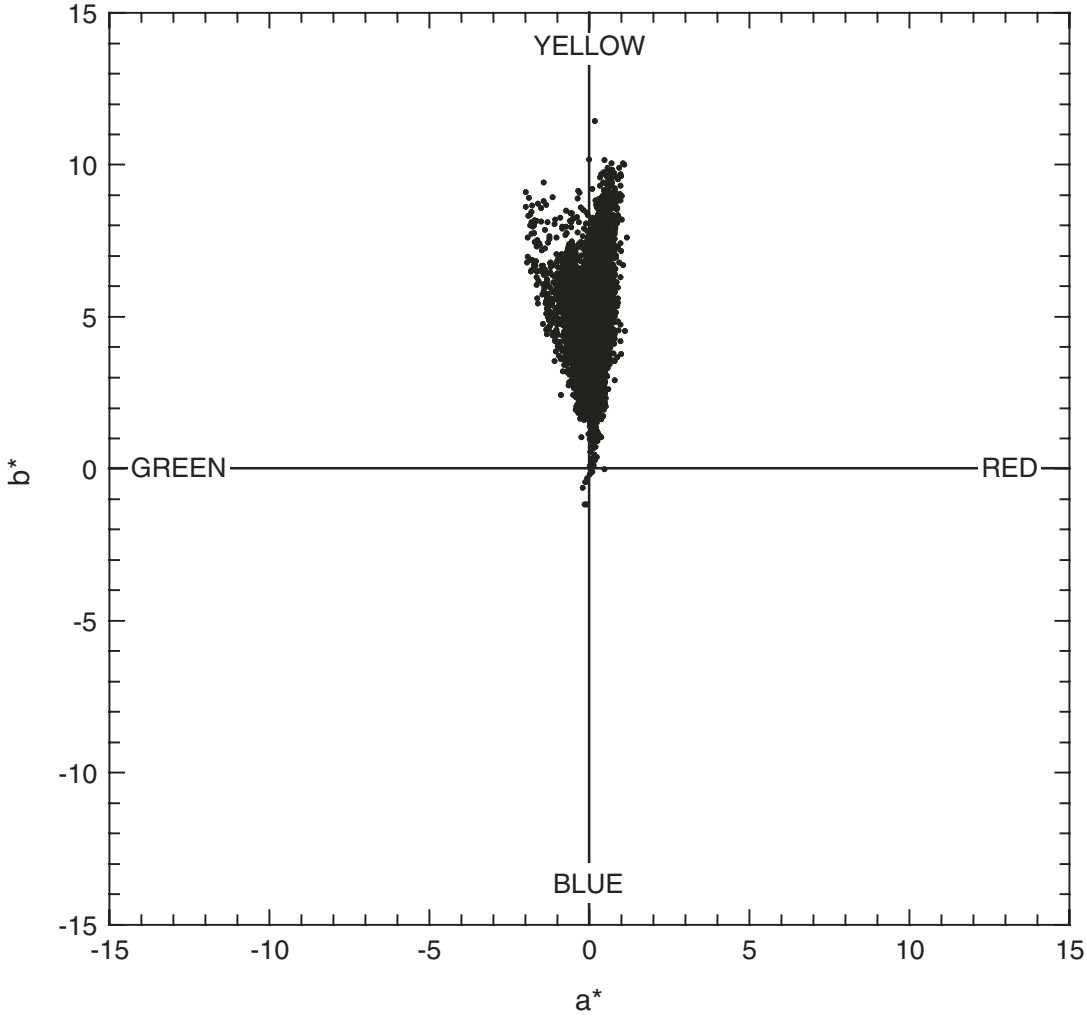

Figure F15. Core recovery, calcareous nannofossil and planktonic foraminifer abundance, benthic foraminifer percentage of total foraminifers, and diatom abundance at Hole 1234A (smoothed lines). B = barren, R = rare, F = few, C = common, A = abundant, VA = very abundant.

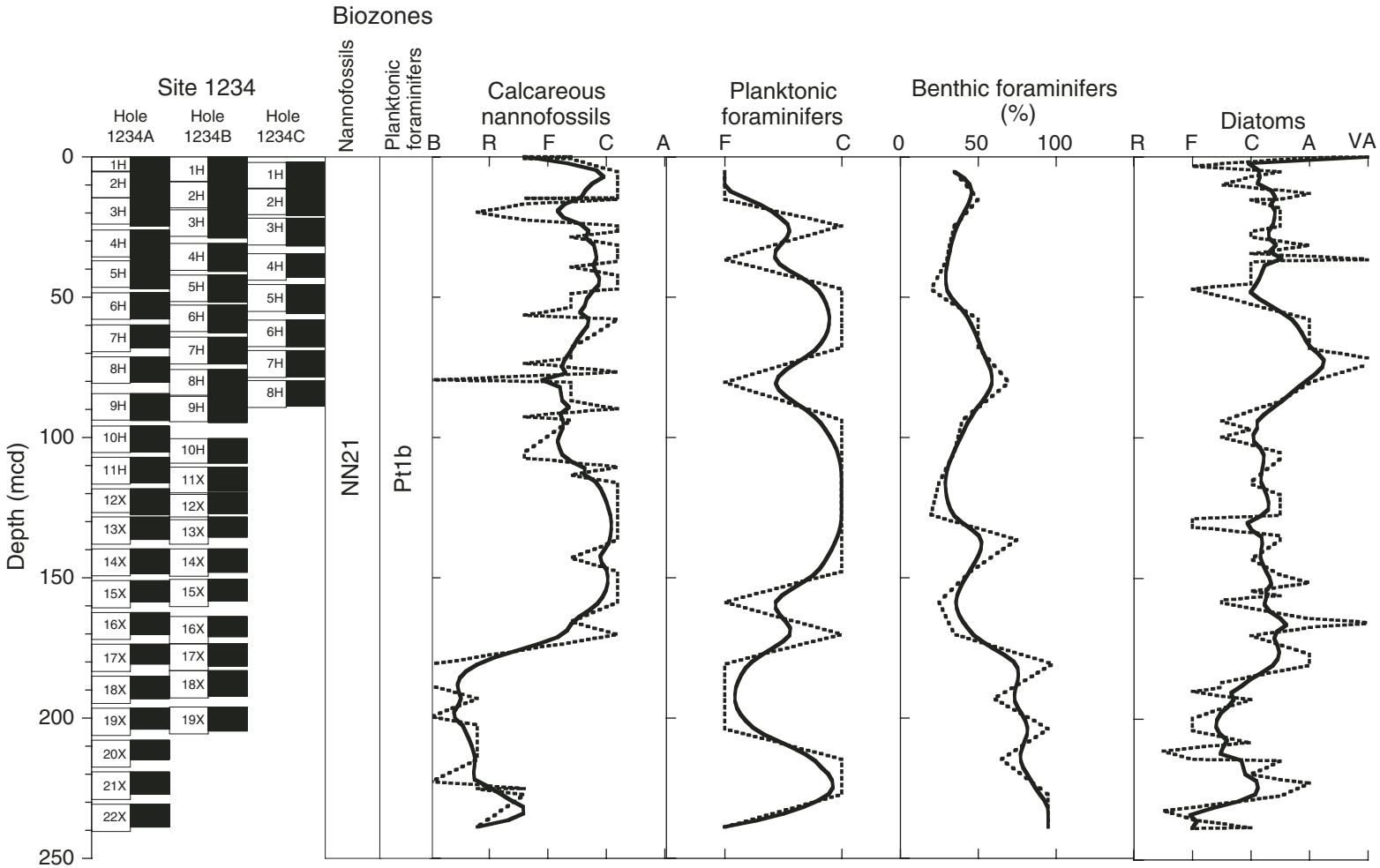

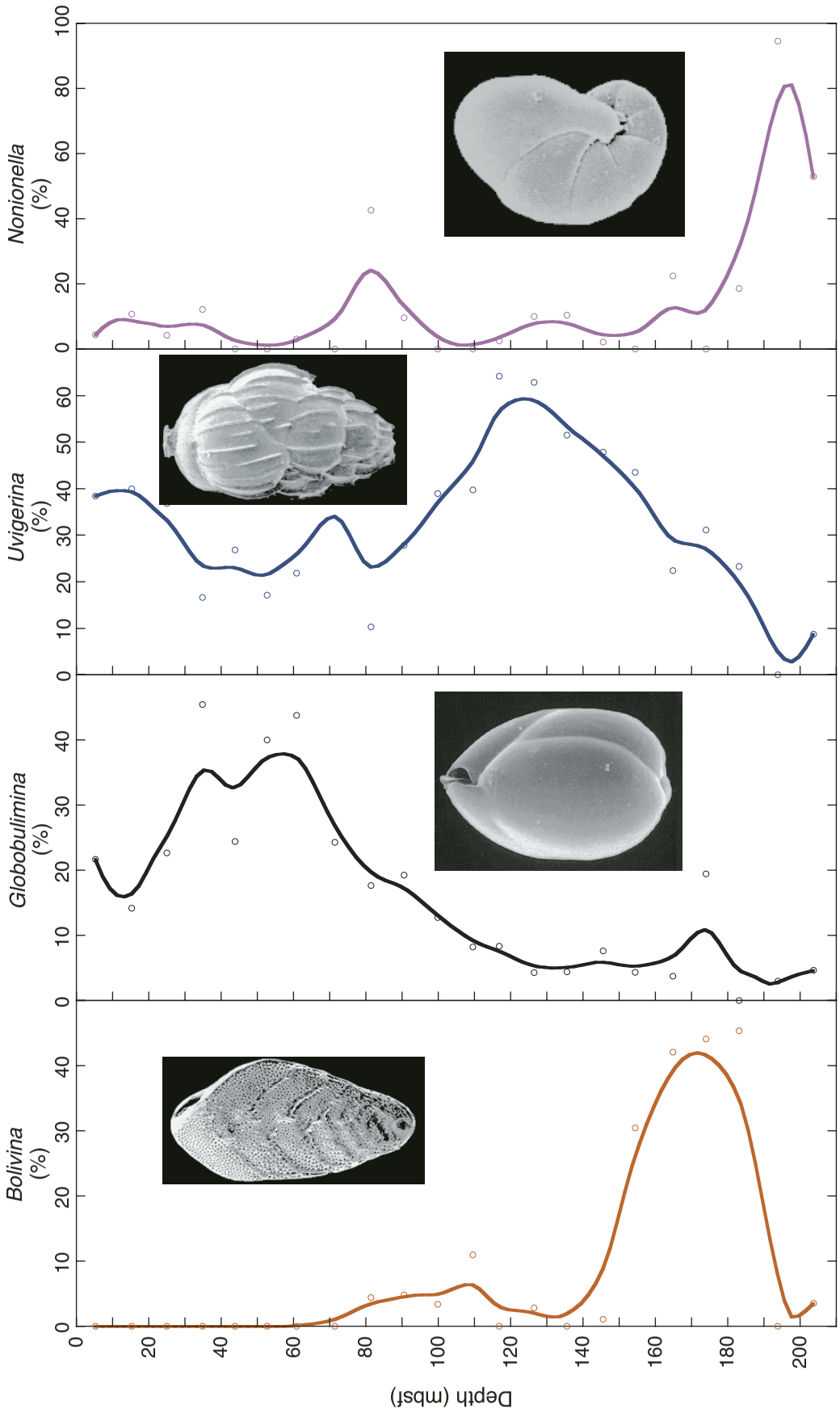

Figure F16. Variations in percent of dysoxic indicators (*Bolivina, Globobulimina, Uvigerina,* and *Nonionella*) in Hole 1234A (smoothed lines).

Figure F17. (**A**) Natural remanent magnetization (NRM) inclination, (**B**) declination, and (**C**) intensity after demagnetization at 20 or 25 mT vs. depth for Holes 1234A, 1234B, and 1234C. Core recovery is plotted for reference.

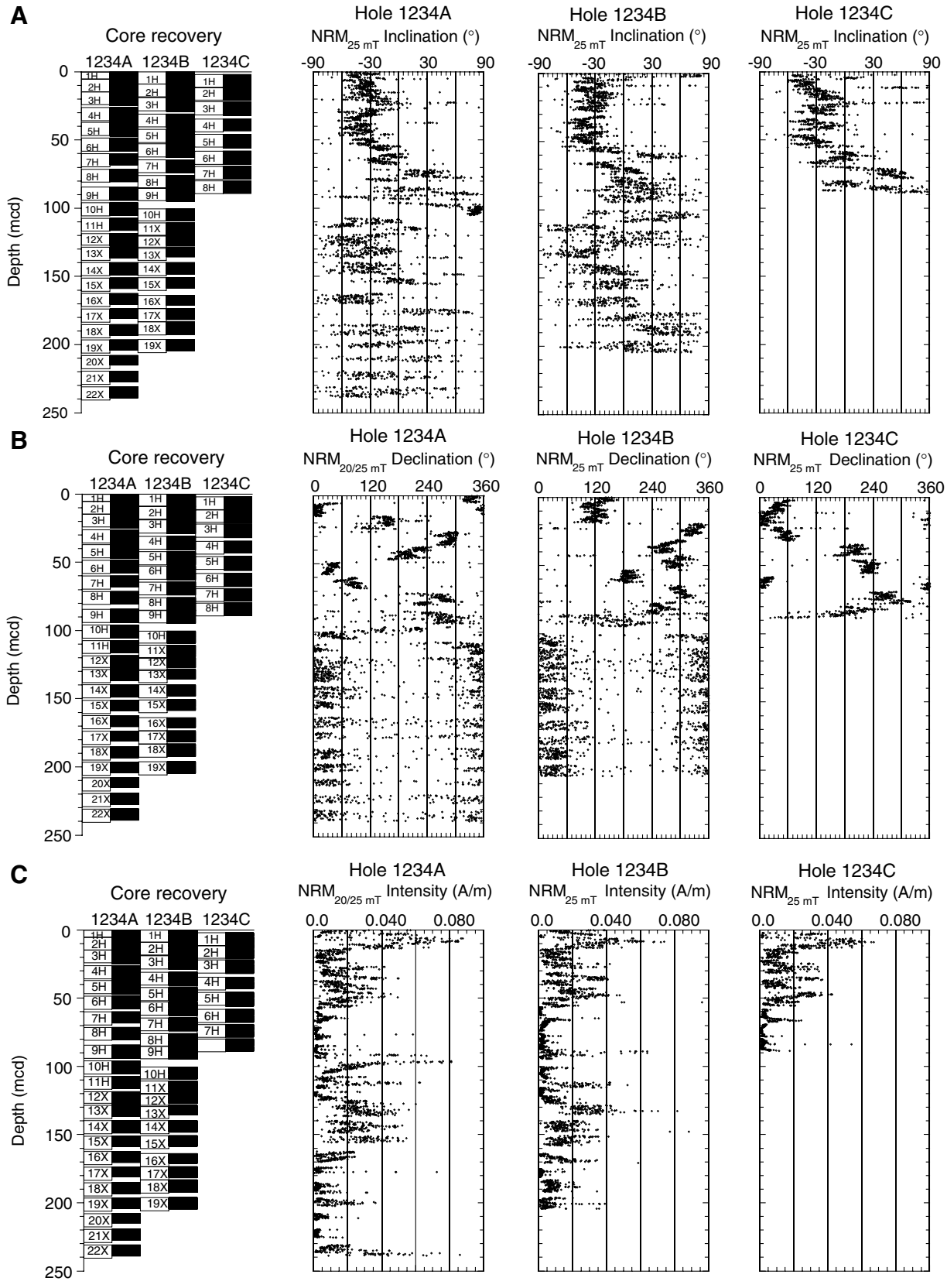

Figure F18. The natural remanent magnetization (NRM) intensity before and after AF demagnetization at peak field of either 20 or 25 mT for the Site 1234 splice.

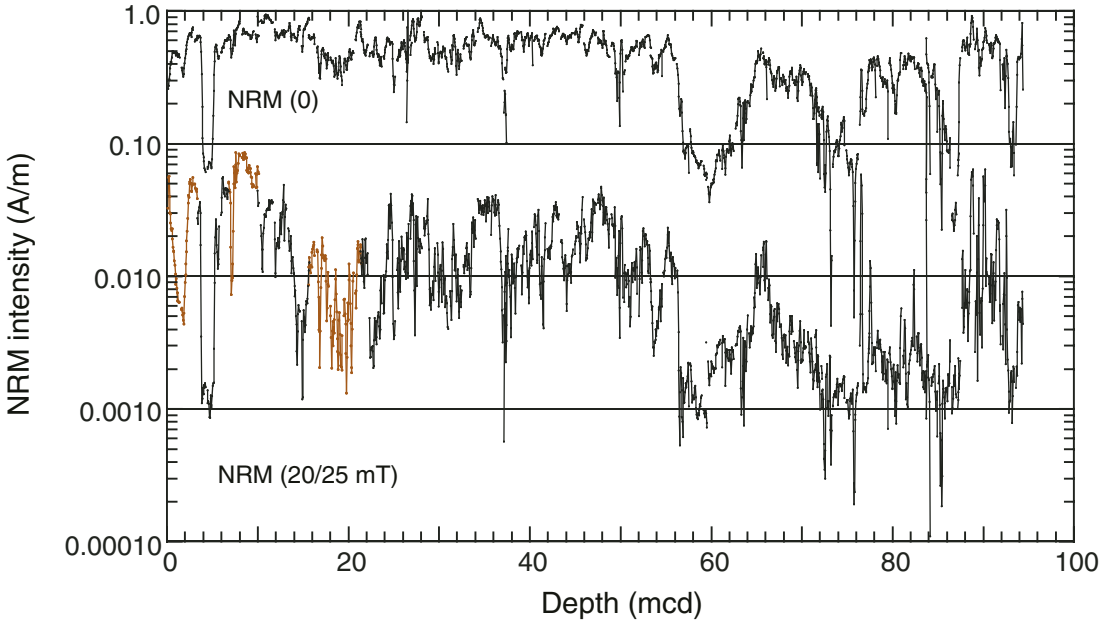

Figure F19. Natural remanent magnetization (NRM) inclination after demagnetization at 20 or 25 mT for the upper 60 mcd for the (**A**) Hole 1234A, (**B**) Hole 1234B, (**C**) Hole 1234C, and (**D**) Site 1234 splice.

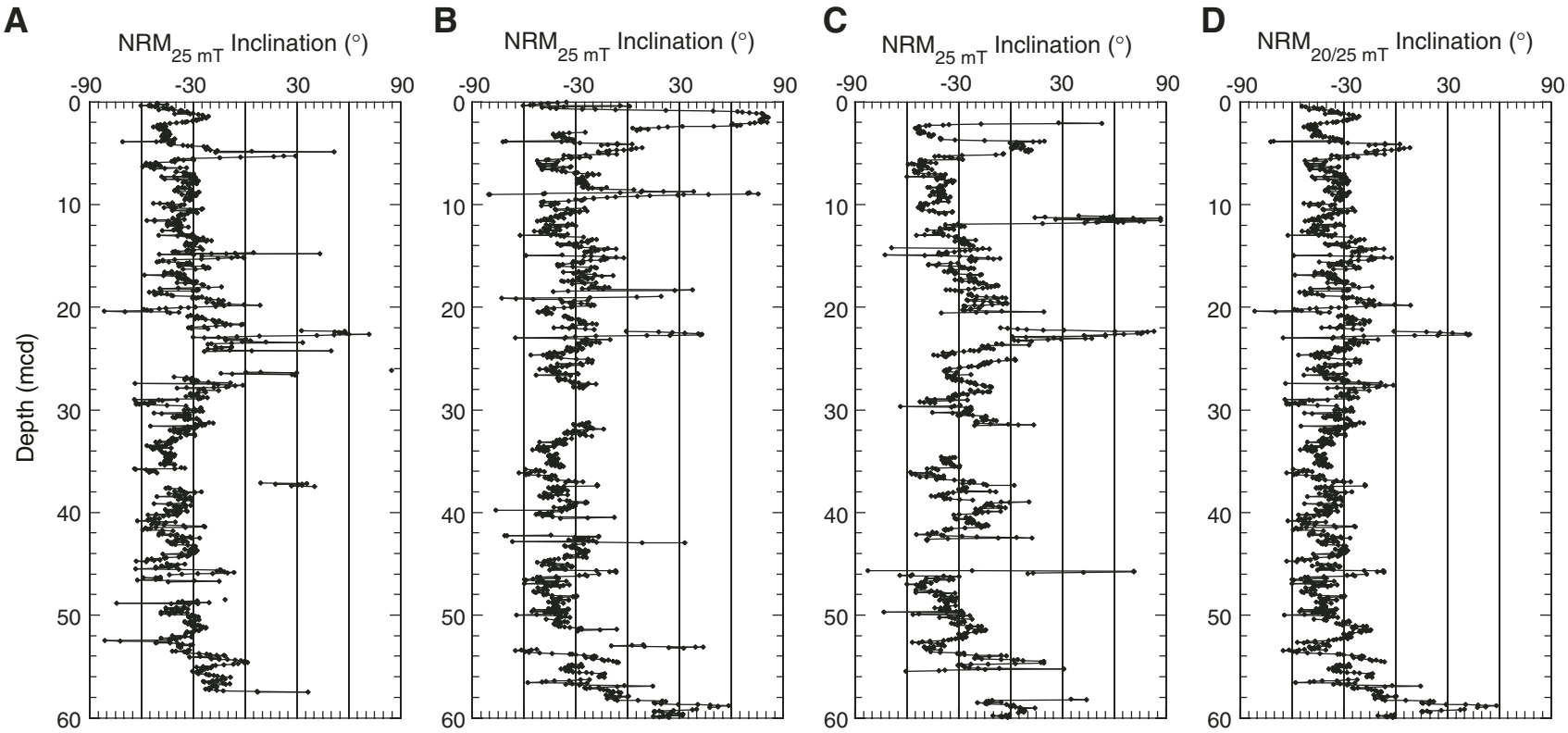

Figure F20. Possible geomagnetic field excursion (Laschamp Event?) recorded at Site 1234 compared with a similar record from Site 1233. Inclination and declination data after 25-mT AF demagnetization from (**A**) the Site 1233 splice and (**B**) Core 202-1234A-3H.

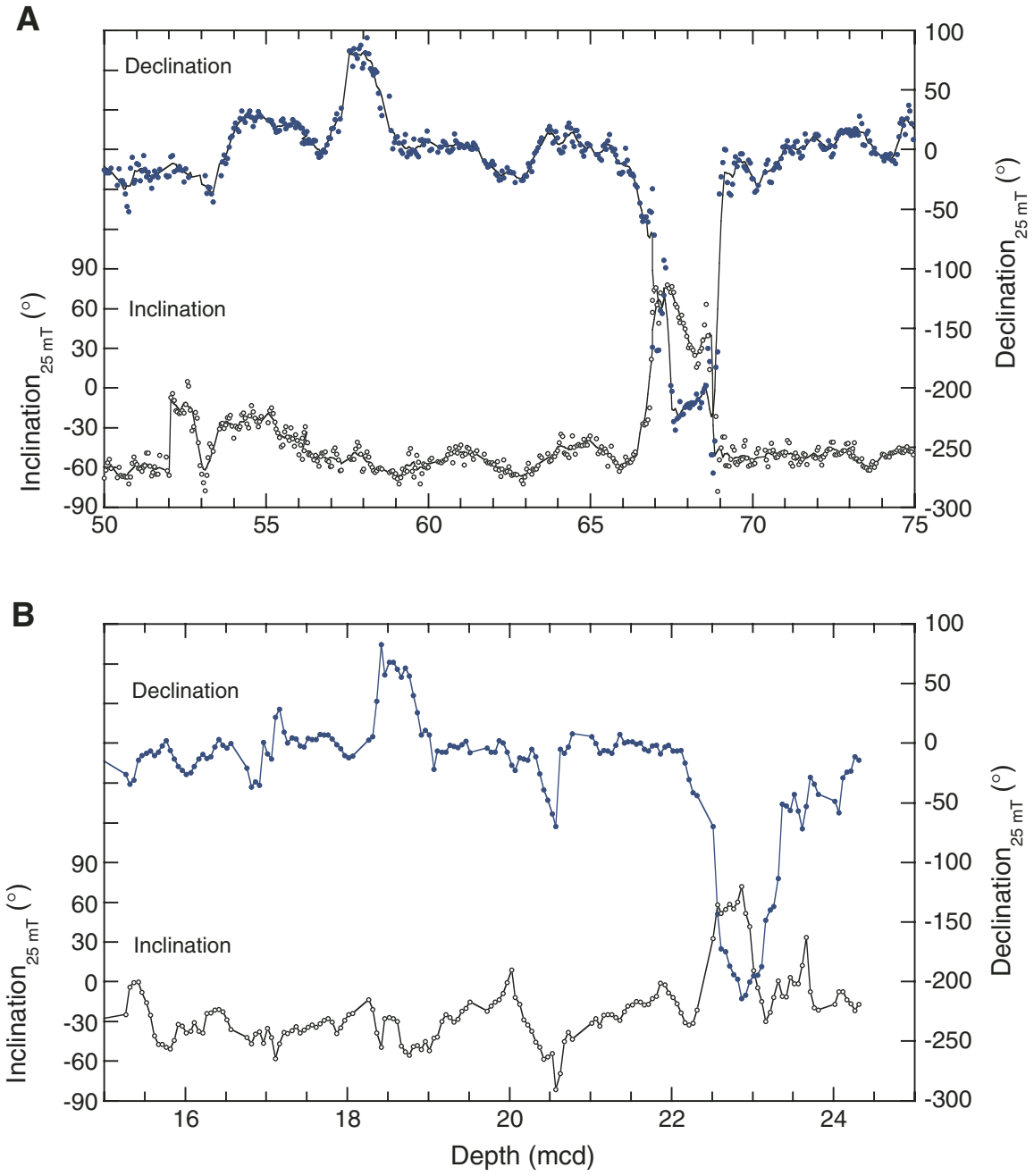

Figure F21. Headspace and vacutainer methane (C_1) concentrations and C_1/C_2 ratio in sediments from Hole 1234A vs. depth. Open circles = headspace, solid circles = vacutainer. Because of the direct sampling method, vacutainer gas concentrations are higher than headspace gas concentrations.

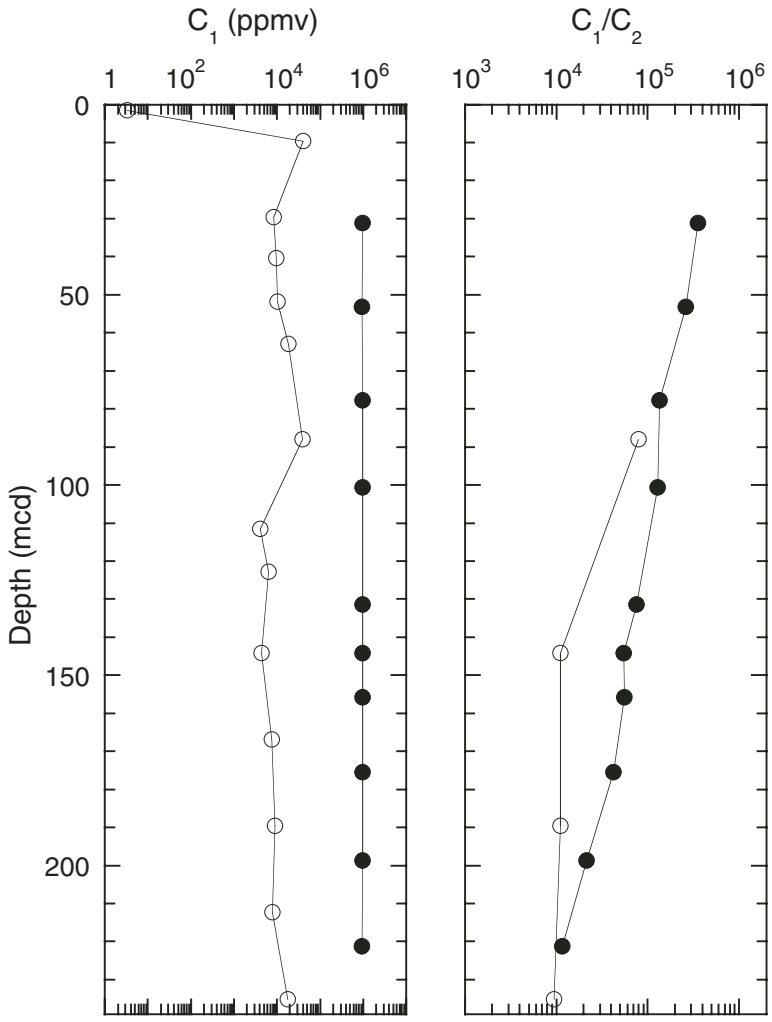

Figure F22. Interstitial water geochemical data, Site 1234. Sulfate values below the detection limit (~0.6 mM) are plotted at zero. Open squares = calcium concentrations.

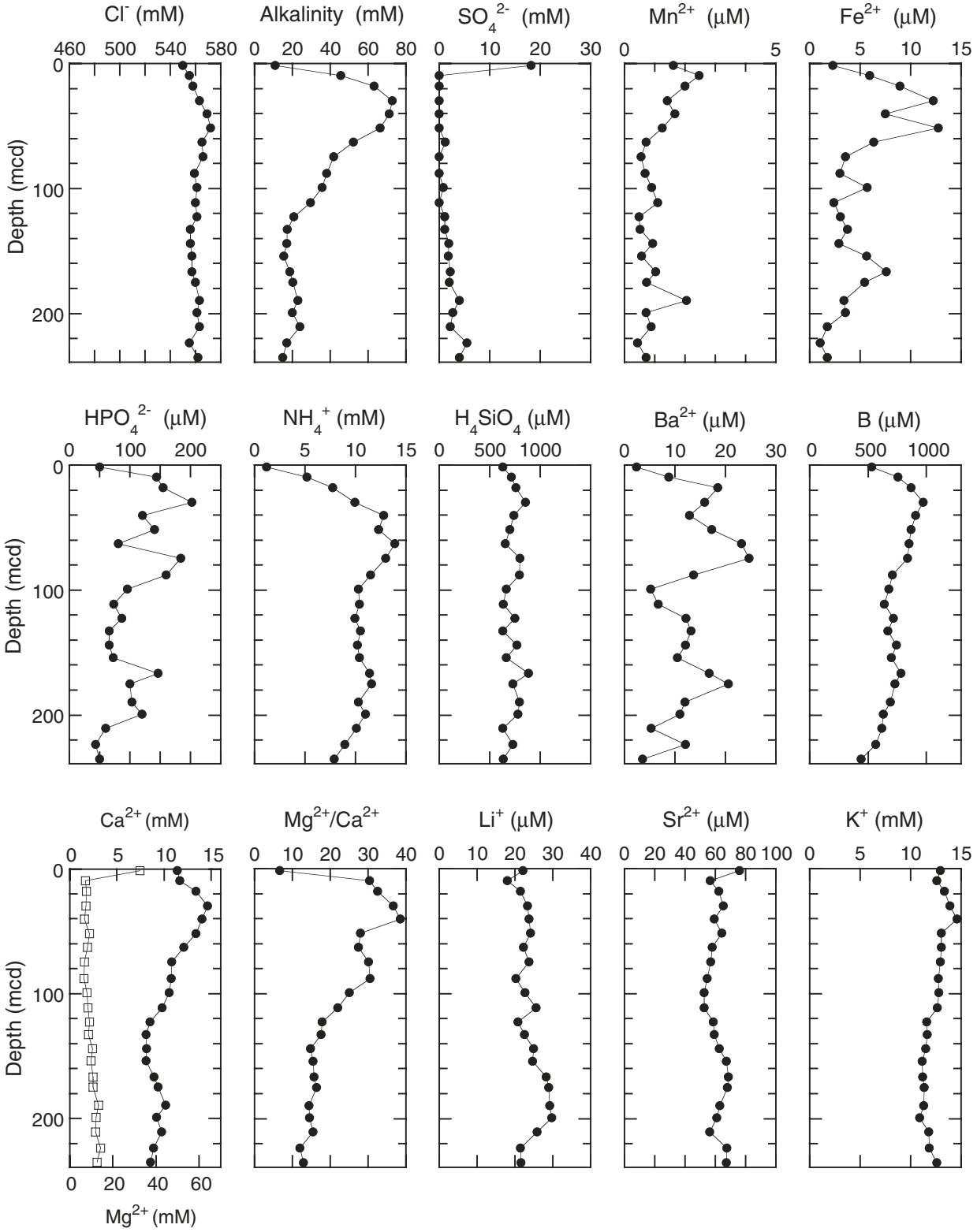

Figure F23. Calcium carbonate ($CaCO_3$), total organic carbon (TOC), total nitrogen (TN), and total sulfur (TS) concentrations vs. depth in sediments of Site 1234.

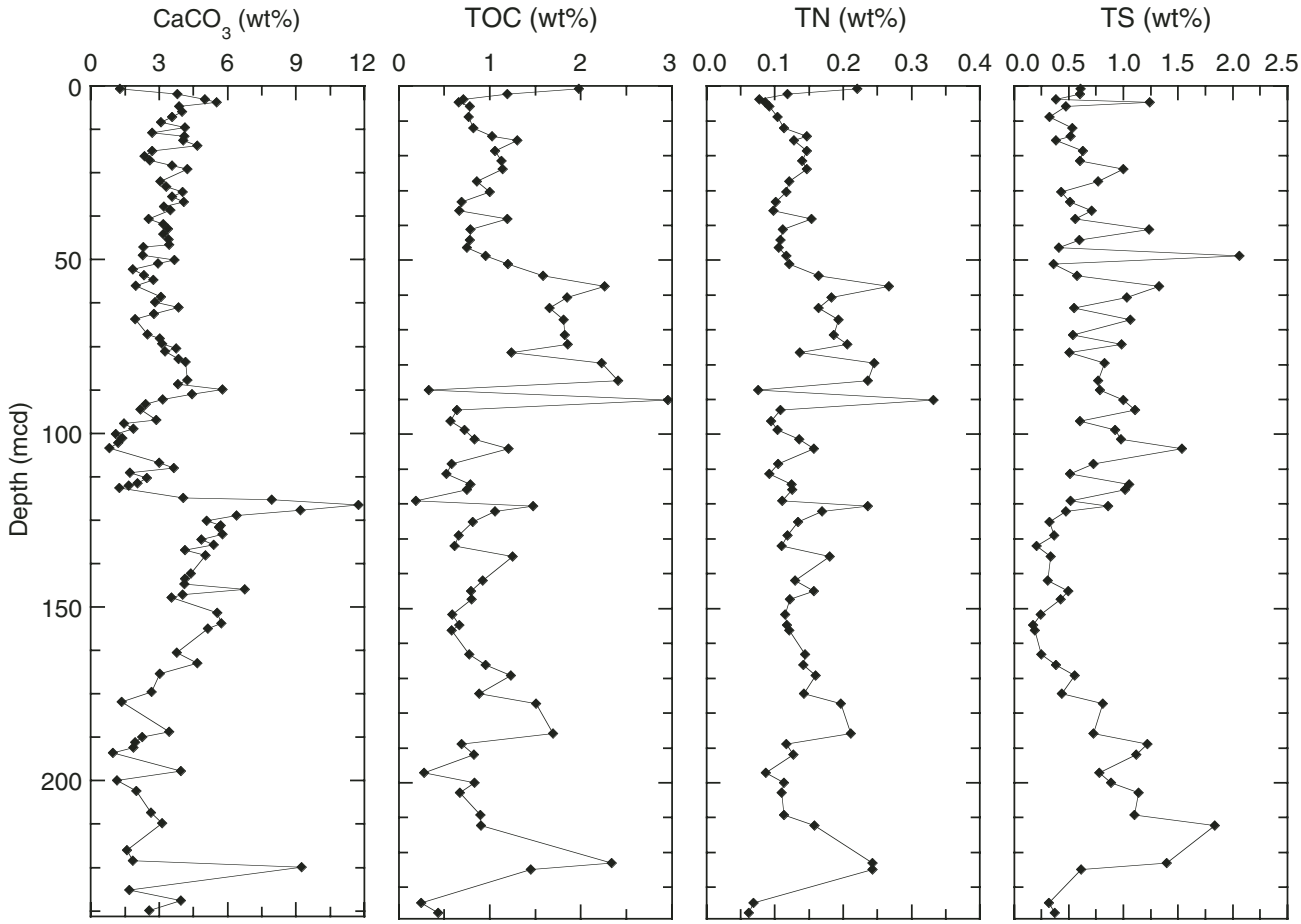

Figure F24. Total nitrogen (TN) vs. total organic carbon (TOC) and TOC/TN vs. TOC in sediments at Site 1234.

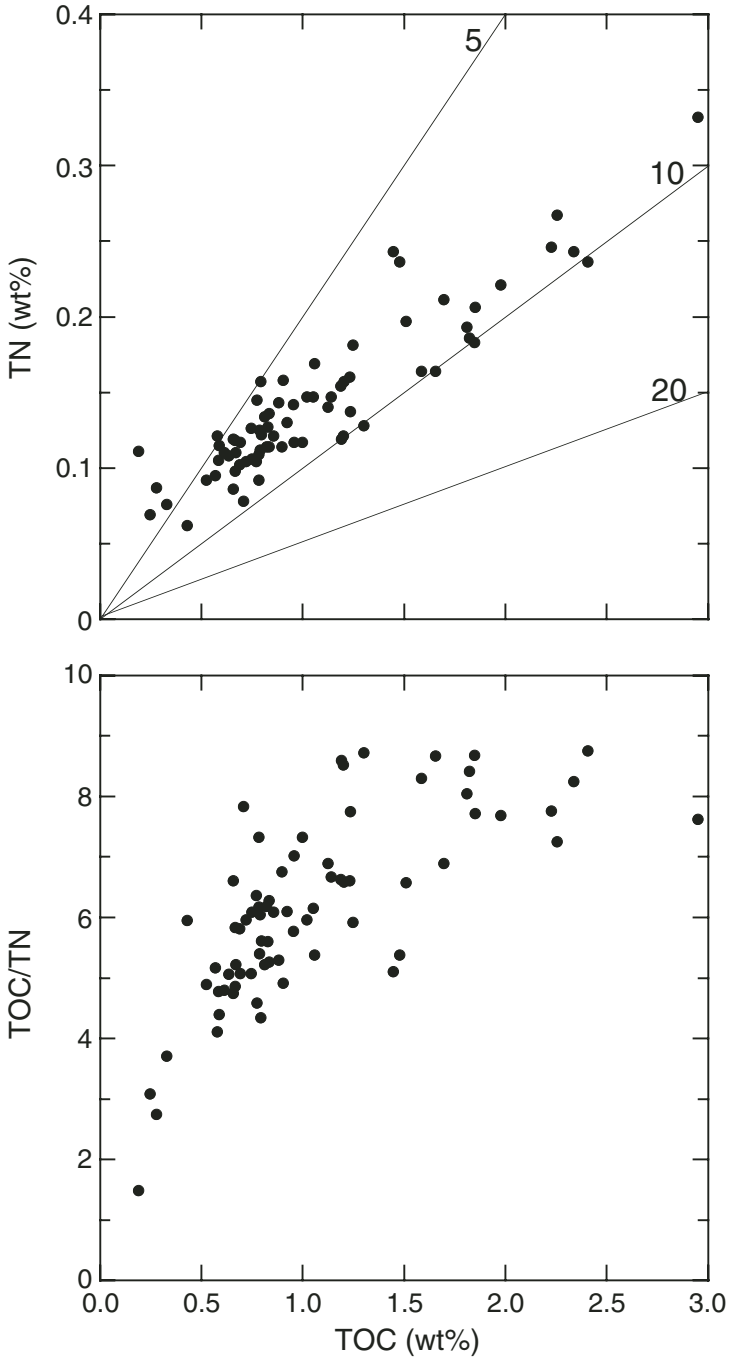

Figure F25. S_2 vs. total organic carbon (TOC) and hydrogen index (HI) vs. TOC in selected samples from Site 1234. Boundaries for Types I, II, and III kerogen fields are taken from Langford and Blanc-Valleron (1990).

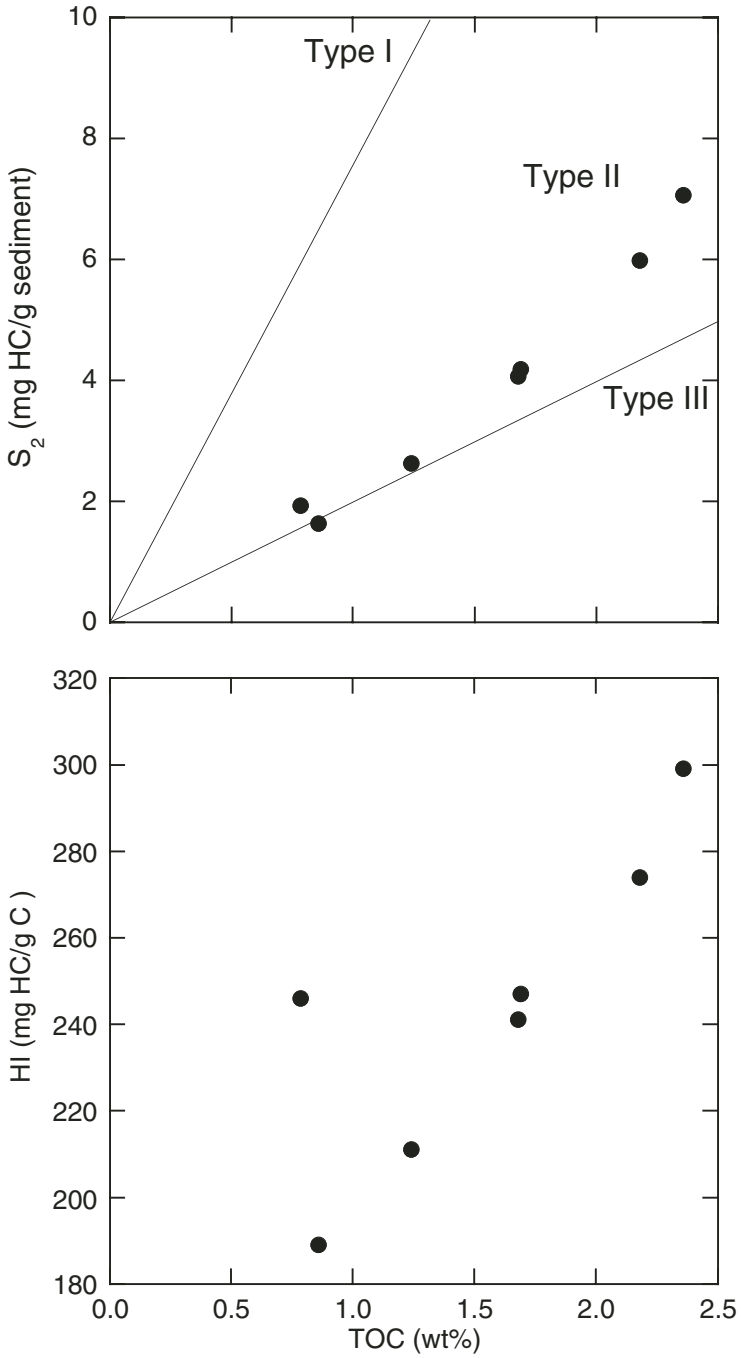

Table T1. Operations summary, Site 1234.

Core	Date (Apr 2002)	Local time (hr)	Depth (mbsf) Top	Depth (mbsf) Bottom	Length (m) Cored	Length (m) Recovered	Recovery (%)	APCT	Orientation
202-1234A-									
1H	15	1015	0.0	5.3	5.3	5.30	100.0		
2H	15	1100	5.3	14.8	9.5	9.97	105.0		
3H	15	1135	14.8	24.3	9.5	10.20	107.4		
4H	15	1230	24.3	33.8	9.5	10.48	110.3	X	Tensor
5H	15	1255	33.8	43.3	9.5	10.15	106.8		Tensor
6H	15	1325	43.3	52.8	9.5	9.44	99.4		Tensor
7H	15	1415	52.8	62.3	9.5	8.20	86.3	X	Tensor
8H	15	1445	62.3	71.8	9.5	9.17	96.5		Tensor
9H	15	1525	71.8	81.3	9.5	9.66	101.7		Tensor
10H	15	1610	81.3	90.8	9.5	9.36	98.5	X	Tensor
11H	15	1645	90.8	100.3	9.5	9.15	96.3		Tensor
12X	15	1759	100.3	108.8	8.5	9.33	109.8		
13X	15	1830	108.8	118.4	9.6	8.08	84.2		
14X	15	1910	118.4	128.0	9.6	8.97	93.4		
15X	15	1955	128.0	137.6	9.6	7.68	80.0		
16X	15	2025	137.6	147.2	9.6	7.98	83.1		
17X	15	2110	147.2	156.9	9.7	7.11	73.3		
18X	15	2145	156.9	166.5	9.6	7.96	82.9		
19X	15	2225	166.5	176.2	9.7	7.56	77.9		
20X	15	2305	176.2	185.8	9.6	6.95	72.4		
21X	15	2335	185.8	195.5	9.7	8.08	83.3		
22X	16	0035	195.5	205.2	9.7	8.24	85.0		
			Cored totals:		205.2	189.02	92.1		
202-1234B-									
1H	16	0325	0.0	9.1	9.1	9.17	100.8	X	
2H	16	0400	9.1	18.6	9.5	10.05	105.8		
3H	16	0435	18.6	28.1	9.5	10.15	106.8		Tensor
4H	16	0510	28.1	37.6	9.5	10.00	105.3		Tensor
5H	16	0545	37.6	47.1	9.5	9.78	103.0		Tensor
6H	16	0620	47.1	56.6	9.5	10.01	105.4		Tensor
7H	16	0645	56.6	66.1	9.5	9.59	101.0		Tensor
8H	16	0715	66.1	75.6	9.5	9.70	102.1		Tensor
9H	16	0750	75.6	85.1	9.5	9.88	104.0		Tensor
10H	16	0830	85.1	93.8	8.7	8.75	100.6		Tensor
11X	16	0925	93.8	103.4	9.6	8.65	90.1		
12X	16	0955	103.4	113.0	9.6	7.49	78.0		
13X	16	1025	113.0	122.6	9.6	7.15	74.5		
14X	16	1100	122.6	132.3	9.7	8.45	87.1		
15X	16	1125	134.3	143.9	9.6	7.80	81.3		
16X	16	1159	143.9	153.5	9.6	7.21	75.1		
17X	16	1235	153.5	163.1	9.6	8.02	83.5		
18X	16	1305	163.1	172.8	9.7	9.24	95.3		
19X	16	1355	172.8	182.4	9.6	8.62	89.8		
			Cored totals:		180.4	169.71	94.1		
202-1234C-									
1H	16	1600	1.6	11.1	9.5	9.93	104.5		
2H	16	1630	11.1	20.6	9.5	9.76	102.7		
3H	16	1710	20.6	30.1	9.5	9.93	104.5		Tensor*
4H	16	1735	30.1	39.6	9.5	8.55	90.0		Tensor*
5H	16	1840	41.1	50.6	9.5	10.23	107.7		Tensor
6H	16	1915	50.6	60.1	9.5	9.56	100.6		Tensor
7H	16	1950	60.1	69.6	9.5	9.30	97.9		Tensor
8H	16	2100	69.6	79.1	9.5	9.16	96.4		Tensor
			Cored totals:		76.0	76.42	100.6		
			Site totals:		461.6	435.15	94.3		

Notes: APCT = advanced piston corer temperature tool (stainless-steel housing is cutting shoe). X = APCT was used. Tensor = brand name for core-barrel orientation tool. * = tensor measurement was attempted but a problem occurred, resulting in bad or no data.

Table T2. Composite depth scale, Site 1234.

Core	Depth of core top		Depth offset		Translation to cmcd	
	Drillers (mbsf)	Composite (mcd)	Cumulative (m)	Differential (m)	Growth factor*	Depth (cmcd)†
202-1234A-						
1H	0.0	0.00	0.00		1.18†	0.00
2H	5.3	5.15	–0.15	–0.15	1.18†	4.36
3H	14.8	14.55	–0.25	–0.10	1.18†	12.33
4H	24.3	26.16	1.86	2.11	1.18†	22.17
5H	33.8	37.02	3.22	1.36	1.18†	31.37
6H	43.3	48.47	5.17	1.95	1.18†	41.08
7H	52.8	59.96	7.16	1.99	1.18†	50.81
8H	62.3	71.28	8.98	1.82	1.18†	60.41
9H	71.8	84.37	12.57	3.59	1.18†	71.50
10H	81.3	95.93	14.63	2.06	1.18‡	81.30
11H	90.8	107.14	16.34	1.71	1.18‡	90.80
12X	100.3	118.35	18.05	1.71	1.18‡	100.30
13X	108.8	128.38	19.58	1.53	1.18‡	108.80
14X	118.4	139.71	21.31	1.73	1.18‡	118.40
15X	128.0	151.04	23.04	1.73	1.18‡	128.00
16X	137.6	162.37	24.77	1.73	1.18‡	137.60
17X	147.2	173.70	26.50	1.73	1.18‡	147.20
18X	156.9	185.14	28.24	1.74	1.18‡	156.90
19X	166.5	196.47	29.97	1.73	1.18‡	166.50
20X	176.2	207.92	31.72	1.75	1.18‡	176.20
21X	185.8	219.24	33.44	1.72	1.18‡	185.80
22X	195.5	230.69	35.19	1.75	1.18‡	195.50
202-1234B-						
1H	0.0	–0.16	–0.16		1.18†	–0.14
2H	9.1	8.75	–0.35	–0.19	1.18†	7.42
3H	18.6	18.86	0.26	0.61	1.18†	15.98
4H	28.1	30.88	2.78	2.52	1.18†	26.17
5H	37.6	42.09	4.49	1.71	1.18†	35.67
6H	47.1	52.78	5.68	1.19	1.18†	44.73
7H	56.6	64.30	7.70	2.02	1.18†	54.49
8H	66.1	75.85	9.75	2.05	1.18†	64.28
9H	75.6	84.90	9.30	–0.45	1.18†	71.95
10H	85.1	100.42	15.32	6.02	1.18‡	85.10
11X	93.8	110.68	16.88	1.56	1.18‡	93.80
12X	103.4	119.70	16.30	–0.58	1.18‡	101.44
13X	113.0	128.40	15.40	–0.90	1.18‡	108.81
14X	122.6	139.69	17.09	1.69	1.18‡	118.38
15X	134.3	150.64	16.34	–0.75	1.18‡	127.66
16X	143.9	163.90	20.00	3.66	1.18‡	138.90
17X	153.5	173.50	20.00	0.00	1.18‡	147.03
18X	163.1	183.10	20.00	0.00	1.18‡	155.17
19X	172.8	196.03	23.23	3.23	1.18‡	166.13
202-1234C-						
1H	1.6	1.95	0.35		1.18†	1.65
2H	11.1	11.11	0.01	–0.34	1.18†	9.42
3H	20.6	21.92	1.32	1.31	1.18†	18.58
4H	30.1	34.47	4.37	3.05	1.18†	29.21
5H	41.1	45.55	4.45	0.08	1.18†	38.60
6H	50.6	58.11	7.51	3.06	1.18†	49.25
7H	60.1	69.13	9.03	1.52	1.18†	58.58
8H	69.6	79.77	10.17	1.14	1.18†	67.60

Notes: * = calculated based on mbsf-mcd relationship for splice shown in Figure F7, p. 27. † = within the splice, the following equations apply: cmcd = mcd/growth factor, mcd = mbsf + cumulative depth offset, mcd = cmcd × growth factor, mbsf = cmcd × growth factor – cumulative offset. ‡ = assumed growth factor for interval below the splice. This table is also available in ASCII.

Table T3. Splice tie points, Site 1234.

Hole, core, section, interval (cm)	Depth (mbsf)	Depth (mcd)	Depth (cmcd)		Hole, core, section, interval (cm)	Depth (mbsf)	Depth (mcd)	Depth (cmcd)
202-					202-			
1234A-1H-3, 0	0.00	0.00	0.00					
1234A-1H-3, 35	3.35	3.35	2.84	Tie to	1234B-1H-3, 50	3.51	3.35	2.84
1234B-1H-5, 95	6.96	6.80	5.76	Tie to	1234A-2H-2, 15	6.95	6.80	5.76
1234A-2H-4, 40	10.20	10.05	8.52	Tie to	1234B-2H-1, 130	10.40	10.05	8.52
1234B-2H-5,90	16.01	15.66	13.27	Tie to	1234A-3H-2, 73.5	15.91	15.66	13.27
1234A-3H-6, 75	21.65	21.40	18.14	Tie to	1234B-3H-3, 62	21.14	21.40	18.14
1234B-3H-7, 20	26.69	26.95	22.84	Tie to	1234A-4H-2, 25	25.09	26.95	22.84
1234A-4H-6, 45	31.16	33.02	27.98	Tie to	1234B-4H-3, 35	30.24	33.02	27.98
1234B-4H-6, 45	34.84	37.62	31.88	Tie to	1234A-5H-2, 15	34.40	37.62	31.88
1234A-5H-7, 30	41.94	45.16	38.27	Tie to	1234B-5H-3, 75	40.67	45.16	38.27
1234B-5H-7, 20	45.96	50.45	42.75	Tie to	1234C-5H-5, 2	46.00	50.45	42.75
1234C-5H-6, 140	48.87	53.32	45.19	Tie to	1234B-6H-2, 10	47.64	53.32	45.19
1234B-6H-6, 47.5	53.86	59.54	50.46	Tie to	1234C-6H-1, 142.5	52.03	59.54	50.46
1234C-6H-6, 15	58.25	65.76	55.73	Tie to	1234B-7H-2, 95	58.06	65.76	55.73
1234B-7H-7, 20	64.53	72.23	61.21	Tie to	1234A-8H-2, 20	63.25	72.23	61.21
1234A-8H-5, 115	68.40	77.38	65.58	Tie to	1234B-8H-2, 60	67.63	77.38	65.58
1234B-8H-6, 125	73.97	83.72	70.95	Tie to	1234C-8H-3, 95	73.55	83.72	70.95
1234C-8H-7, 25	77.11	87.28	73.97	Tie to	1234B-9H-2, 120	77.98	87.28	73.97
1234B-9H-7, 85	85.05	94.35	79.96					

Note: This table is also available in **ASCII.**

Table T4. OSUS-MS measurements, Hole 1234A.

Core, section, interval (cm)	Depth (mbsf)	Depth (mcd)	Magnetic susceptibility (instrument units)	Run number	Depth from top of core (cm)
202-1234A-					
1H-1, 5	0.05	0.05	150	271	5
1H-1, 10	0.10	0.10	161	271	10
1H-1, 15	0.15	0.15	169	271	15
1H-1, 20	0.20	0.20	180	271	20
1H-1, 25	0.25	0.25	187	271	25
1H-1, 30	0.30	0.30	189	271	30
1H-1, 35	0.35	0.35	196	271	35
1H-1, 40	0.40	0.40	198	271	40
1H-1, 45	0.45	0.45	199	271	45
1H-1, 50	0.50	0.50	194	271	50
1H-1, 55	0.55	0.55	203	271	55
1H-1, 60	0.60	0.60	205	271	60
1H-1, 65	0.65	0.65	198	271	65
1H-1, 70	0.70	0.70	198	271	70
1H-1, 75	0.75	0.75	201	271	75
1H-1, 80	0.80	0.80	206	271	80
1H-1, 85	0.85	0.85	202	271	85
1H-1, 90	0.90	0.90	200	271	90
1H-1, 95	0.95	0.95	189	271	95
1H-1, 100	1.00	1.00	184	271	100
1H-1, 105	1.05	1.05	187	271	105
1H-1, 110	1.10	1.10	188	271	110
1H-1, 115	1.15	1.15	185	271	115
1H-1, 120	1.20	1.20	181	271	120
1H-1, 125	1.25	1.25	179	271	125
1H-1, 130	1.30	1.30	184	271	130
1H-1, 135	1.35	1.35	184	271	135
1H-1, 140	1.40	1.40	171	271	140
1H-2, 5	1.56	1.56	156	272	155
1H-2, 10	1.61	1.61	163	272	160
1H-2, 15	1.66	1.66	160	272	165
1H-2, 20	1.71	1.71	154	272	170
1H-2, 25	1.76	1.76	142	272	175
1H-2, 30	1.81	1.81	135	272	180
1H-2, 35	1.86	1.86	139	272	185
1H-2, 40	1.91	1.91	151	272	190
1H-2, 45	1.96	1.96	164	272	195
1H-2, 50	2.01	2.01	180	272	200
1H-2, 55	2.06	2.06	189	272	205
1H-2, 60	2.11	2.11	199	272	210
1H-2, 65	2.16	2.16	209	272	215
1H-2, 70	2.21	2.21	228	272	220
1H-2, 75	2.26	2.26	248	272	225
1H-2, 80	2.31	2.31	266	272	230
1H-2, 85	2.36	2.36	295	272	235
1H-2, 90	2.41	2.41	301	272	240
1H-2, 95	2.46	2.46	309	272	245
1H-2, 100	2.51	2.51	315	272	250
1H-2, 105	2.56	2.56	317	272	255
1H-2, 110	2.61	2.61	323	272	260
1H-2, 115	2.66	2.66	321	272	265
1H-2, 120	2.71	2.71	317	272	270
1H-2, 125	2.76	2.76	322	272	275
1H-2, 130	2.81	2.81	331	272	280
1H-2, 135	2.86	2.86	335	272	285
1H-2, 140	2.91	2.91	324	272	290
1H-2, 145	2.96	2.96	294	272	295
1H-3, 5	3.07	3.07	296	273	305
1H-3, 10	3.12	3.12	306	273	310
1H-3, 15	3.17	3.17	312	273	315
1H-3, 20	3.22	3.22	311	273	320
1H-3, 25	3.27	3.27	305	273	325
1H-3, 30	3.32	3.32	300	273	330

Note: Only a portion of this table appears here. The complete table is available in **ASCII**.

Table T5. OSUS-MS measurements, Hole 1234B.

Core, section Interval (cm)	Depth (mbsf)	Depth (mcd)	Magnetic susceptibility (instrument units)	Run number	Depth from top of core (cm)
202-1234B-					
1H-1, 5	0.05	-0.11	132	328	5
1H-1, 10	0.10	-0.06	148	328	10
1H-1, 15	0.15	-0.01	123	328	15
1H-1, 20	0.20	0.04	173	328	20
1H-1, 25	0.25	0.09	182	328	25
1H-1, 30	0.30	0.14	193	328	30
1H-1, 35	0.35	0.19	200	328	35
1H-1, 40	0.40	0.24	207	328	40
1H-1, 45	0.45	0.29	197	328	45
1H-1, 50	0.50	0.34	202	328	50
1H-1, 55	0.55	0.39	199	328	55
1H-1, 60	0.60	0.44	206	328	60
1H-1, 65	0.65	0.49	203	328	65
1H-1, 70	0.70	0.54	201	328	70
1H-1, 75	0.75	0.59	202	328	75
1H-1, 80	0.80	0.64	202	328	80
1H-1, 85	0.85	0.69	207	328	85
1H-1, 90	0.90	0.74	216	328	90
1H-1, 95	0.95	0.79	216	328	95
1H-1, 100	1.00	0.84	213	328	100
1H-1, 105	1.05	0.89	205	328	105
1H-1, 110	1.10	0.94	200	328	110
1H-1, 115	1.15	0.99	201	328	115
1H-1, 120	1.20	1.04	198	328	120
1H-1, 125	1.25	1.09	198	328	125
1H-1, 130	1.30	1.14	190	328	130
1H-1, 135	1.35	1.19	183	328	135
1H-1, 140	1.40	1.24	186	328	140
1H-1, 145	1.45	1.29	192	328	145
1H-2, 5	1.57	1.41	174	329	156
1H-2, 10	1.62	1.46	173	329	161
1H-2, 15	1.67	1.51	168	329	166
1H-2, 20	1.72	1.56	164	329	171
1H-2, 25	1.77	1.61	166	329	176
1H-2, 30	1.82	1.66	166	329	181
1H-2, 35	1.87	1.71	157	329	186
1H-2, 40	1.92	1.76	141	329	191
1H-2, 45	1.97	1.81	127	329	196
1H-2, 50	2.02	1.86	123	329	201
1H-2, 55	2.07	1.91	129	329	206
1H-2, 60	2.12	1.96	136	329	211
1H-2, 65	2.17	2.01	146	329	216
1H-2, 70	2.22	2.06	168	329	221
1H-2, 75	2.27	2.11	189	329	226
1H-2, 80	2.32	2.16	207	329	231
1H-2, 85	2.37	2.21	219	329	236
1H-2, 90	2.42	2.26	235	329	241
1H-2, 95	2.47	2.31	262	329	246
1H-2, 100	2.52	2.36	268	329	251
1H-2, 105	2.57	2.41	296	329	256
1H-2, 110	2.62	2.46	315	329	261
1H-2, 115	2.67	2.51	319	329	266
1H-2, 120	2.72	2.56	329	329	271
1H-2, 125	2.77	2.61	315	329	276
1H-2, 130	2.82	2.66	323	329	281
1H-2, 135	2.87	2.71	325	329	286
1H-2, 140	2.92	2.76	324	329	291
1H-2, 145	2.97	2.81	300	329	296
1H-3, 5	3.07	2.91	317	330	306
1H-3, 10	3.12	2.96	317	330	311
1H-3, 15	3.17	3.01	308	330	316
1H-3, 20	3.22	3.06	307	330	321
1H-3, 25	3.27	3.11	302	330	326

Note: Only a portion of this table appears here. The complete table is available in **ASCII**.

Table T6. OSUS-MS measurements, Hole 1234C.

Core, section, interval (cm)	Depth (mbsf)	Depth (mcd)	Magnetic susceptibility (instrument units)	Run number	Depth from top of core (cm)
202-1234C-					
1H-1, 5	1.65	2.00	129	454	5
1H-1, 10	1.70	2.05	153	454	10
1H-1, 15	1.75	2.10	143	454	15
1H-1, 20	1.80	2.15	223	454	20
1H-1, 25	1.85	2.20	267	454	25
1H-1, 30	1.90	2.25	283	454	30
1H-1, 35	1.95	2.30	318	454	35
1H-1, 40	2.00	2.35	327	454	40
1H-1, 45	2.05	2.40	327	454	45
1H-1, 50	2.10	2.45	321	454	50
1H-1, 55	2.15	2.50	325	454	55
1H-1, 60	2.20	2.55	331	454	60
1H-1, 65	2.25	2.60	328	454	65
1H-1, 70	2.30	2.65	328	454	70
1H-1, 75	2.35	2.70	331	454	75
1H-1, 80	2.40	2.75	324	454	80
1H-1, 85	2.45	2.80	311	454	85
1H-1, 90	2.50	2.85	302	454	90
1H-1, 95	2.55	2.90	302	454	95
1H-1, 100	2.60	2.95	304	454	100
1H-1, 105	2.65	3.00	305	454	105
1H-1, 110	2.70	3.05	303	454	110
1H-1, 115	2.75	3.10	304	454	115
1H-1, 120	2.80	3.15	302	454	120
1H-1, 125	2.85	3.20	302	454	125
1H-1, 130	2.90	3.25	290	454	130
1H-1, 135	2.95	3.30	293	454	135
1H-1, 140	3.00	3.35	305	454	140
1H-1, 145	3.05	3.40	294	454	145
1H-2, 5	3.16	3.51	299	455	155
1H-2, 10	3.21	3.56	306	455	160
1H-2, 15	3.26	3.61	297	455	165
1H-2, 20	3.31	3.66	255	455	170
1H-2, 25	3.36	3.71	225	455	175
1H-2, 30	3.41	3.76	157	455	180
1H-2, 35	3.46	3.81	96	455	185
1H-2, 40	3.51	3.86	62	455	190
1H-2, 45	3.56	3.91	45	455	195
1H-2, 50	3.61	3.96	41	455	200
1H-2, 55	3.66	4.01	41	455	205
1H-2, 60	3.71	4.06	43	455	210
1H-2, 65	3.76	4.11	40	455	215
1H-2, 70	3.81	4.16	39	455	220
1H-2, 75	3.86	4.21	40	455	225
1H-2, 80	3.91	4.26	41	455	230
1H-2, 85	3.96	4.31	42	455	235
1H-2, 90	4.01	4.36	40	455	240
1H-2, 95	4.06	4.41	38	455	245
1H-2, 100	4.11	4.46	41	455	250
1H-2, 105	4.16	4.51	38	455	255
1H-2, 110	4.21	4.56	37	455	260
1H-2, 115	4.26	4.61	40	455	265
1H-2, 120	4.31	4.66	41	455	270
1H-2, 125	4.36	4.71	41	455	275
1H-2, 130	4.41	4.76	39	455	280
1H-2, 135	4.46	4.81	40	455	285
1H-2, 140	4.51	4.86	40	455	290
1H-2, 145	4.56	4.91	37	455	295
1H-3, 5	4.66	5.01	38	456	305
1H-3, 10	4.71	5.06	49	456	310
1H-3, 15	4.76	5.11	60	456	315
1H-3, 20	4.81	5.16	67	456	320
1H-3, 25	4.86	5.21	97	456	325

Note: Only a portion of this table appears here. The complete table is available in **ASCII**.

Table T7. Lithologic Unit I, Site 1234.

Unit	Top Hole, core	Top Depth (mbsf)	Top Depth (mcd)	Base Hole, core	Base Depth (mbsf)	Base Depth (mcd)	Description	Interpretation
I	202-			202-				
	1234A-1H	0.0	0.0	1234A-22X	203.8	239.0	Dark olive gray to dark gray diatom nannofossil and diatom- or nannofossil-bearing silty clay and clay	Hemipelagic sequences
	1234B-1H	0.0	0.0	1234B-19X	181.4	204.7		
	1234C-1H	1.6	2.0	1234C-8H	78.8	88.9		

Table T8. Ash layers, Site 1234.

Core, section, interval (cm)	Depth (mcd)		Thickness (cm)	Associate minerals					Plagioclase composition
	Top	Bottom		Quartz	Mica	Amphiboles	Ortho-pyroxene	Clino-pyroxene	
202-1234A-									
3H-3, 47–54	16.91	23.91	7	P	P		P	P	Andesine
3H-5, 115–122	20.57	27.57	7	P	P	P	P	P	Andesine
6H-4, 80–86	52.68	58.68	6	P	P	P	P	P	Andesine
10H-2, 83–91	97.35	105.35	8	P		P	P		Labradorite
202-1234B-									
6H-7, 64–72	61.23	69.23	8	P	P	P	P	P	NM
6H-7, 119–126	61.78	68.78	7	P	P	P	P	P	Andesine
202-1234C-									
5H-3, 30–38	47.77	55.77	8	P	P	P	P	P	Labradorite
6H-3, 47–53	61.60	67.60	6	P	P	P	P	P	NM

Notes: P = present. NM = not measured.

Table T9. Distribution of calcareous nannofossils, Hole 1234A. (**See table notes.** Continued on next page.)

Core, section, interval (cm)	Depth (mbsf)	Depth (mcd)	Preservation	Abundance	*Braarudosphaera bigelowii*	*Calcidiscus leptoporus*	*Coccolithus pelagicus*	*Emiliania huxleyi*	*Gephyrocapsa oceanica* (large)	*Gephyrocapsa* spp. (*G. caribbeanica*) (medium)	*Gephyrocapsa* spp. (*G. muellerae*) (medium)	*Gephyrocapsa* spp. (small)	*Helicosphaera carteri*
202-1234A-													
1H-1, 0	0.00	0.00	G	F		R		F			R	F	R
1H-1, 1	0.01	0.01	M	G		R		R	C		R	C	
1H-1, 76	0.76	0.76	M	F	R	R		R	F		F	F	
1H-1, 76	0.76	0.76	M	C		C		C	F		C	A	R
1H-CC, 22	5.29	5.29	G	A		F	R	C			F	C	C
2H-1, 40	5.70	5.55	G	A	R	C	F	C			C	A	C
2H-3, 40	8.75	8.60	M	A		R	F	A			C	A	F
2H-5, 40	11.79	11.64	G	A		F	F	A			C	A	C
2H-7, 40	14.82	14.67	M	A		F	F	C			C	A	F
3H-1, 20	15.00	14.75	G	F		R	R	F			F	F	R
2H-CC, 24	15.35	15.20	G	A		C	F	C			A	C	F
3H-3, 40	17.09	16.84	M	F		F	R	R			F	F	R
3H-5, 40	20.07	19.82	M	R		R	R	R			R	R	R
3H-7, 40	22.86	22.61	M	F		F	R	R			F	F	
4H-1, 40	24.70	26.56	G	A		R	F	F			A	C	R
3H-CC, 27	24.99	24.74	G	A		F	R	A			F	C	R
4H-3, 40	26.76	28.62	M	C		F	R	F			C	F	R
4H-5, 40	29.66	31.52	M	A		F	C	F			A	C	F
4H-7, 40	32.55	34.41	M	A		F	R	F		R	A	C	R
5H-1, 40	34.20	37.42	G	A			C	F			A	C	
4H-CC, 38	34.78	36.64	G	A		F	F	F			A	F	
5H-3, 40	36.15	39.37	M	C		R	R	C	R		C	C	
5H-5, 40	39.05	42.27	M	A		R	F	F	R		F	F	F
5H-7, 40	42.06	45.28	M	A		R	R	F			A	C	F
6H-1, 40	43.70	48.87	M	A		R	F	F	R		A	A	R
5H-CC, 30	43.92	47.14	G	C		R	R	R			C	F	R
6H-3, 40	45.60	50.77	M	C		R	R	F			F	A	
6H-5, 40	48.52	53.69	M	C		R	R	R		R	F	C	
6H-7, 40	51.36	56.53	M	F				R			F	F	
6H-CC, 25	52.71	57.88	G	A		F	R	R			F	F	
7H-CC, 34	60.97	68.13	G	C		R	R	F			R	F	
8H-1, 40	62.70	71.68	M	C		R	R	R			C	C	R
8H-3, 40	64.76	73.74	M	F		R	R	R			R	F	
8H-5, 40	67.73	76.71	M	A		C	R	F			F	A	
8H-7, 40	70.71	79.69		B									
8H-CC, 35	71.44	80.42	G	C		R	R	R			F	F	
9H-1, 40	72.20	84.77	M	C		R	R	F			R	A	
9H-3, 40	74.38	86.95	M	C		R	R	R	C		F	F	R
9H-5, 40	77.28	89.85	M	A		R	R	R		R	A	A	R
9H-7, 40	80.16	92.73	M	F		R	R	R			F	F	R
9H-CC, 24	81.44	94.01	G	C			R	R			F	F	R
10H-CC, 33	90.69	105.32	P	F		R	F					F	
11H-1, 40	91.20	107.54	G	F		R		R			F	F	R
11H-3, 40	94.18	110.52	G	A		F	R	F			A	A	R
11H-5, 40	97.07	113.41	M	C		R		R			C	F	
11H-CC, 23	99.95	116.29	G	A		F	F	R			C	C	
12X-3, 40	103.70	121.75	G	A		F	R	R	C		A	A	F
12X-5, 40	106.71	124.76	G	A	F	F	R	R			A	A	R
12X-CC, 17	109.62	127.67	G	A		R	R	R			C	C	F
13X-3, 40	112.22	131.80	M	A		F	F	F	F		A	A	F
13X-CC, 69	116.89	136.47	G	A		F	R	R			C	C	F

Table T9 (continued).

Core, section, interval (cm)	Depth (mbsf)	Depth (mcd)	Preservation	Abundance	*Braarudosphaera bigelowii*	*Calcidiscus leptoporus*	*Coccolithus pelagicus*	*Emiliania huxleyi*	*Gephyrocapsa oceanica* (large)	*Gephyrocapsa* spp. (*G. caribbeanica*) (medium)	*Gephyrocapsa* spp. (*G. muellerae*) (medium)	*Gephyrocapsa* spp. (small)	*Helicosphaera carteri*
14X-3, 40	121.80	143.11	G	C		R	R	R			C	A	R
14X-CC, 15	126.54	147.85	G	A		F	R	R			A	C	
15X-3, 40	131.42	154.46	G	A		R	R	R			A	A	R
15X-CC, 34	135.68	158.72	G	A		R		R			A	C	
16X-3, 40	141.02	165.79	M	C		F	R	R			C	C	R
16X-CC, 43	145.57	170.34	G	A		F					A	C	R
17X-CC, 38	154.40	180.90		B									
18X-3, 40	160.32	188.56		B									
18X-CC, 41	164.87	193.11	P	R		C	R	R			R		R
19X-3, 40	169.67	199.64		B									
19X-5, 40	172.66	202.63	M	R				R	R		R	R	
19X-CC, 33	174.05	204.02	P	R		R	R				R		
20X-3, 40	179.61	211.33	M	R			R		R	R			
20X-CC, 47	183.10	214.82	P	R		R				R	R		R
21X-3, 40	189.22	222.66		B									
21X-5, 40	191.74	225.18	M	F		F	R		F	R	F	F	
21X-5, 40	191.74	225.18	M	R				R	R		R	R	
21X-CC, 39	193.88	227.32	M	F			R	R		F	R	R	
22X-CC, 28	203.74	238.93	P	R			R	R	R	F			R

Notes: Preservation: G = good, M = moderate, P = poor. Abundance: A = abundant, C = common, F = few, R = rare, B = barren.

Table T10. Distribution of foraminifers, Hole 1234A. (See table notes. Continued on next page.)

Core, section	Depth (mbsf)	Depth (mcd)	Preparation	Preservation	Abundance	Benthic/planktonic foraminifers (%)	Remarks	*Globigerina bulloides*	*Globigerinita glutinata*	*Globorotalia inflata*	*Globorotalia scitula*	*Globorotalia truncatulinoides*	*Globorotalia ungulata*	*Neogloboquadrina dutertrei*	*Neogloboquadrina pachyderma* (d)	*Orbulina universa*	*Sphaeroidinella* sp.	*Bolivina costata*	*Bolivina seminuda*	*Bulimina mexicana*	*Cassidulina teretis*	*Cibicidoides* spp.	*Cyclammina* sp. 1	*Ehrenbergina serrata*	*Eubuliminella exilis*	*Globigerinella*	*Globobulimina affinis*	*Globobulimina pyrula*	*Globulina prisca*	*Gyroidinoides orbicularis*	*Hoeglundina elegans*	*Laevidentalina* sp.	*Marginulina obesa*	*Martinotiella communis*	*Melonis affinis*	*Neogloboquadrina pachyderma* (s)	*Nonionella auris*
202-1234A-																																					
1H-CC	5.29	5.29	S	M	F	35/65		C	F	C		F		F	F	F				18	3	8					60	4	6		2		4	8	1	R	14
2H-CC	15.35	15.20	S	G	F	50/50	Radiolarians: C; Diatoms: R	C	F	F		F	F	F	F					38	1				2		17	4			1	1			9		25
3H-CC	24.99	24.74	S	G	C	35/65		C	F	F	R	F	C	F	F					17							24	6							1		7
4H-CC	34.78	36.64	S	M	F	30/70	Radiolarians: F	C	F	C	F	C		F	R					5							14	3	1						1		8
5H-CC	43.92	47.14	S	M	C	20/80	Radiolarians: F; pyritized tests	F	F			F	C			R											9	1		2							
6H-CC	52.71	57.88	S	M	C	50/50	Diatoms: F, Radiolarians: R	F	F	F			F												4		11		2								
7H-CC	60.97	68.13	S	M	C	50/50	Radiolarians: F	R	F				F	R	R					4							8	2									1
8H-CC	71.44	80.42	S	M	F	70/30	Radiolarians: F	F	F	F			F	F		R				4					6		14										
9H-CC	81.44	94.01	S	P	C	40/60	Radiolarians: R; large agglutinated tests reproduced?	F	F	C			R	F					3				6		4		10								1		29
10H-CC	90.69	105.32	S	M	C	35/65	Radiolarians: R; pyritized burrow	F	F	C		F	R	F				3	2	8				1	18		9								1		10
11H-CC	99.95	116.29	S	M	C	25/75	Radiolarians: R; pyritized burrow	C	F	C		F	F	R	F		R	2	2	32					5	R	7						1		1		
12X-CC	109.62	127.67	S	G	C	20/80		F	F	C		F	F	F	R			7	1	12	1				4		1					1					
13X-CC	116.89	136.47	S	M	C	75/25	Radiolarians: R	F	F	F			F	F	R					4	1				1		6										3
14X-CC	126.54	147.85	S	M	C	45/55	Radiolarians: R	F	F					F				2		2					5		2								1		7
15X-CC	135.68	158.72	S	M	F	25/75	Radiolarians: R	R	R	F	R		C	R						11					4		1								2		7
16X-CC	145.57	170.34	S	M	C	35/65	Radiolarians: F	F	F	F	F	R		R	R			1		15					2		6			2							2
17X-CC	154.4	180.90	S	P	F	98/2	Glauconite: A; Radiolarians: R; teeth	R	F	F		R		F		R		12	2						4									2		
18X-CC	164.87	193.11	S	M	F	60/40	Glauconite: R	R	F	F		R	F	R				17	28			1			1												24
19X-CC	174.05	204.02	S	M	F	95/5		R	F	F		C		R		R		17	17								15										
20X-CC	183.1	214.82	S	M	C	65/35	Bivalve fragments, Radiolarians: R	F	F		R	F		F				23	16						8												16
21X-CC	193.88	227.32	S	G	C	95/5	Radiolarians: R	F	F	F				R											1												159
22X-CC	203.74	238.93	S	M	F	95/5	Bivalve fragments, Radiolarians: R	F		C									6		1				2										1		91

Table T10 (continued).

Core, section, interval (cm)	Depth (mbsf)	Depth (mcd)	Preparation	Preservation	Abundance	*Nuttalides umbonifera*	*Oolina* spp.	*Oolina sulcata*	*Peneroplis* sp.	*Planulina wuellerstorfi*	*Praeglobobulimina spinescens*	*Protoglobobulimina pupoides*	*Pullenia bulloides*	*Pullenia quinqueloba*	*Pyrgo serrata*	*Pyrgo* spp.	*Quinqueloculina* spp.	*Rotaliatinopsis semiinvoluta*	*Rutherfordoides mexicanus*	*Saracenaria* sp.	*Uvigerina peregrina*
202-1234A-																					
1H-CC	5.29	5.29	S	M	F	4				34	6				10	12	5				124
2H-CC	15.35	15.20	S	G	F	6				19	11						5		1		93
3H-CC	24.99	24.74	S	G	C	1	4	3		23	7					1	9				60
4H-CC	34.78	36.64	S	M	F	2	2	1		4	10				1				3		11
5H-CC	43.92	47.14	S	M	C	3	1			12					1	1					11
6H-CC	52.71	57.88	S	M	C		1			4	2	1	2			1	1				6
7H-CC	60.97	68.13	S	M	C	1				2		1		1			1	1	3		7
8H-CC	71.44	80.42	S	M	F	2				5		3		1	1						34
9H-CC	81.44	94.01	S	P	C	1			3		2					1				1	7
10H-CC	90.69	105.32	S	M	C			1		4		3			1	2	1	3	8		29
11H-CC	99.95	116.29	S	M	C					7		7					2	5	1		46
12X-CC	109.62	127.67	S	G	C					7	5			1	3	1					29
13X-CC	116.89	136.47	S	M	C	4					1							20	3		77
14X-CC	126.54	147.85	S	M	C	2				2		1				1	1				44
15X-CC	135.68	158.72	S	M	F					4		1		1				1	1		35
16X-CC	145.57	170.34	S	M	C	4				14				1					1		44
17X-CC	154.4	180.90	S	P	F		1			3	2										20
18X-CC	164.87	193.11	S	M	F					3							2	3	4		24
19X-CC	174.05	204.02	S	M	F					2							1	1			24
20X-CC	183.1	214.82	S	M	C												2	1			20
21X-CC	193.88	227.32	S	G	C												3		5		0
22X-CC	203.74	238.93	S	M	F												12	36	8		15

Notes: Preparation: S = sieve. Preservation: G = good, M = moderate, P = poor. Abundance: C = common, F = few, R = rare.

Table T11. Distribution of diatoms, Hole 1234A. (See table notes. Continued on next page.)

Core, section, interval (cm)	Depth (mbsf)	Depth (mcd)	Identification	Method	Abundance	Preservation	*Actinocyclus curvatulus*	*Actinoptychus senarius*	*Aulacoseira glanulata*	*Azpeitia nodulifer*	*Chaetoceros* spp. (resting spores)	*Delphineis* spp.	*Fragilariopsis doliolus*	*Hemidiscus cuneiformis*	*Paralia sulcata*	*Pseudonitzschia*	*Roperia tesselata*	*Thalassionema nitzschioides*	*Thalassiosira* spp.	Freshwater benthic	Freshwater species (planktonic)	Marine benthic species	Marine neritic species (other)	Marine pelagic species (other) COSM	Marine pelagic species (other) WW	Marine pelagic species (other) CW	Remarks
202-1234A-																											
Mudline	0.00	0.00	PAL	S	VA	VG	F	F	T		A							F	C		T		C	T		T	
1H-1, 40	0.40	0.40	Toothpick	S	A	G					A				R			C	R–F	T	T		C	F			
1H-3, 42	3.42	3.42	Toothpick	S	F	M					F	F				R		R	F	T	T	R	F	T		T	
1H-CC, 22–27	5.25	5.29	PAL	S	C–A	G–M	R	T			A							R	F			R					
2H-2, 40	7.20	7.05	Toothpick	S	C	M					C								F			F					
2H-4, 40	10.20	10.05	Toothpick	S	F–C	M					F					T			R–F				T				
2H-6, 40	13.20	13.05	Toothpick	S	A	G					A	T								T	T						
2H-CC, 24–29	15.22	15.20	PAL	S	C–A	G–M	T				A					T		F	F	T	T	T	T				>63-µm cells of *Coscinodiscus*
3H-2, 40	15.57	15.32	Toothpick	S	C	M					C								F								
3H-4, 40	18.57	18.32	Toothpick	S	C–A	M				R	A								F				T				
3H-6, 40	21.32	21.07	Toothpick	S	C–A	M					A								F								
4H-1, 40	24.70	26.56	Toothpick	S	C	M	F				C					T		F	F			T	F	R		R	
3H-CC, 27–32	24.91	24.74	PAL	S	C–A	G–M	T				A		T						F			T					
4H-3, 40	26.74	28.60	Toothpick	S	C	M–G	F				C	T				T			F				R				
4H-5, 40	29.63	31.49	Toothpick	S	A	G	F				A								C				F				
4H-7, 40	32.51	34.37	Toothpick	S	C	M					C								F			T			T		
5H-1, 40	34.20	37.42	Toothpick	S	C	M–G					C	F										T	C	R	R		
4H-CC, 38–43	34.73	36.64	PAL	S	D	G	F			T	D	R				T			F			T	F	T		R	
5H-3, 40	36.15	39.37	Toothpick	S	C	M–G	R				C	F			T	T		F	F			T	C	T–R			
5H-7, 40	42.06	45.28	Toothpick	S	C	M				R	C					T		R	F			R	F				
5H-CC, 30–35	43.90	47.14	PAL	S	F	M		T			F								F	T	T	T					
6H-CC, 25–30	52.69	57.88	PAL	S	A	G–M					A	T							R				R			R–F	>63-µm cells of *Coscinodiscus*
7H-CC, 34–39	60.95	68.13	PAL	S	A	M					A	F–C	T					R	F			R	F				
8H-1, 40	62.70	71.68	Toothpick	S	VA	G	R		T	T	VA		R			T		F	R		T					T	
8H-3, 40	64.76	73.74	Toothpick	S	VA	G		F		F	VA					R			R			T	F			R	
8H-CC, 35–40	71.42	80.42	PAL	S	A	G			T	R	A	T				R			F	T	R		C				
9H-3, 40	74.37	86.94	Toothpick	S	C–A	P–M		F			C	R						F	F				C–A	R			Important change in assemblage–*Cyclotella*
9H-CC, 24–29	81.41	94.01	PAL	S	F–C	M–P			T		F	F						R–F	R		T	T	R				
10H-2, 40	82.28	96.91	Toothpick	S	C	M				R	C	R				T			T	F			R					
10H-4, 40	85.17	99.80	Toothpick	S	F–C	G–M				T	CA								R	F	T	T	T					
10H-CC, 33–38	90.61	105.32	PAL	S	C–A	G–M					A	F							R	F			T					
11H-1, 40	91.20	107.54	Toothpick	S	C–A	M		F			C	F							F	C			R					
11H-7, 40	99.33	115.67	Toothpick	S	C	M					C									F				F				
11H-CC, 23–28	99.90	116.29	PAL	S	C	M				T	C	T							F	F			T	F				
12X-2, 40	102.20	120.25	Toothpick	S	C–A	G–M	T	R–F			A		R	T					F	F			T			T		
13X-1, 40	109.20	128.78	Toothpick	S	F	M					F	F				T	T		F				R	R	T	R–F	T	
12X-CC, 17–22	109.58	127.67	PAL	S	C–A	M–P	R			R	C	F				T			F	F			T	R		T		

Table T11 (continued).

Core, section, interval (cm)	Depth (mbsf)	Depth (mcd)	Identification	Method	Abundance	Preservation	*Actinocyclus curvatulus*	*Actinoptychus senarius*	*Aulacoseira glanulata*	*Azpeitia nodulifer*	*Chaetoceros* spp. (resting spores)	*Delphineis* spp.	*Fragilariopsis doliolus*	*Hemidiscus cuneiformis*	*Paralia sulcata*	*Pseudonitzschia*	*Roperia tesselata*	*Thalassionema nitzschioides*	*Thalassiosira* spp.	Freshwater benthic	Freshwater species (planktonic)	Marine benthic species	Marine neritic species (other)	Marine pelagic species (other) COSM	Marine pelagic species (other) WW	Marine pelagic species (other) CW	Remarks
13X-3, 40	112.20	131.78	Toothpick	S	F	P–M	F				F	R							F			R	R				
13X-5, 40	115.20	134.78	Toothpick	S	C–A	M	F		T	F	C	F				T			F		T		T				
13X-CC, 69–74	116.87	136.47	PAL	S	C–A	M	T				C	F–C						R	T				F	T			
14X-3, 40	121.80	143.11	Toothpick	S	C	M		T		F	C	R						R	F				F–C				
14X-CC, 95–100	127.32	148.65	PAL	S	C–A	M					A	F							F			R	T		T		
15X-1, 40	128.40	151.44	Toothpick	S	A	M					A	F	F					R	F				F				
15X-3, 40	131.40	154.44	Toothpick	S	C	P–M			T		C	R				T		R	F–C		T	F–C	F–C		T		Frequent *Cocconeis*
15X-5, 40	133.04	156.08	Toothpick	S	C–A	M	R	R		R	C					R		R	F			F	F				Frequent *Cocconeis*
15X-6, 40	134.54	157.58	Toothpick	S	F–C	M				T	C					R		R	F–C			T	R				
15X-CC, 34–39	135.63	158.72	PAL	S	F–C	M–P					F	R						T	F–C			R	F		T		
16X-2, 40	139.50	164.27	Toothpick	S	A	G		T		T	A								C–A			F	A				
16X-3, 40	141.00	165.77	Toothpick	S	VA	G			T	F–C	VA	F	R					C	C		T	T	R		T		
16X-4, 40	142.50	167.27	Toothpick	S	A	G–M			T		A								F–C		T	T					
16X-CC, 43–48	145.53	170.34	PAL	S	C	M–P		T		R	F–C	R–F						T	R				F				
17X-3, 40	150.45	176.95	Toothpick	S	A	G		R–F			A							C	C			R	T	T	T		
17X-CC, 38–43	154.26	180.90	PAL	S	A	G–M		T			A	F						F	R				T		T	T	
18X-2, 40	158.80	187.04	Toothpick	S	F–C	M–P		T			F–C	T	T					T			R	T					
18X-3, 40	160.30	188.54	Toothpick	S	F–C	M–P					F–C								F								
18X-4, 40	161.80	190.04	Toothpick	S	F	P					F							T	R–F			R		T	T		
18X-CC, 41–46	164.81	193.11	PAL	S	C	M		T		T	C	T						T	T			T	T	T			
19X-3, 40	169.65	199.62	Toothpick	S	F	P		R		F	F–C	R						T	F					T			
19X-CC, 33–38	174.01	204.02	PAL	S	F	M					F	F						F	F	T	T	R–F					
20X-1, 40	176.60	208.32	Toothpick	S	C	P–M					C							R	F				F				
20X-3, 40	179.60	211.32	Toothpick	S	R–F	P					F							T				T	R				
20X-5, 40	182.53	214.25	Toothpick	S	F	P			R–F		F								R								
20X-CC, 47–52	183.10	214.82	PAL	S	C–A	M		R			A	F						F–C	R				F				
21X-1, 40	186.20	219.64	Toothpick	S	C	M		F		F	C	R	R									R	F				
21X-3, 40	189.20	222.64	Toothpick	S	A	G		F–C		F–C	A		R					F	C			T	F		R		
21X-CC, 39–44	193.83	227.32	PAL	S	C–A	M					A	F						F	F				R	R		R	
22X-2, 40	197.40	232.59	Toothpick	S	R–F	P				T	F								R–F			T	R				
22X-4, 40	200.40	235.59	Toothpick	S	F	M					F	T						T	F				R				
22X-6, 30	203.30	238.49	Toothpick	S	C	M					C	T						T									
22X-CC, 28–33	203.69	238.93	PAL	S	F	M–P			R		F				T			F	F		R	T	F				

Notes: PAL = paleontology sample. S = smear slide. Abundance: VA = very abundant, A = abundant, C = common, F = few, R = rare. Preservation: VG = very good, G = good, M = moderate, P = poor. COSM = cosmopolitan forms, WW = warm-water forms, CW = cold-water forms.

Table T12. Headspace and vacutainer gas concentrations and C_1/C_2 ratio in sediments, Hole 1234A.

Core, section, interval (cm)	Depth (mbsf)	Depth (mcd)	Sample method	C_1 (ppmv)	C_2 (ppmv)	C_1/C_2	C_2= (ppmv)	C_3 (ppmv)
202-1234A-								
1H-2, 0–5	1.51	1.51	HS	3	0		0.0	0.0
2H-4, 0–5	9.87	9.72	HS	39,980	0		0.0	0.0
4H-4, 0–5	27.86	29.72	HS	8,385	0		0.0	0.0
4H-5, 0–5	29.26	31.12	VAC	957,128	3	354,492	0.0	0.0
5H-4, 0–5	37.21	40.43	HS	9,629	0		0.0	0.0
6H-4, 0–5	46.71	51.88	HS	10,104	0		0.0	0.0
6H-5, 0–5	48.12	53.29	VAC	951,542	4	264,317	0.0	0.0
7H-3, 0–5	55.82	62.98	HS	18,037	0		0.0	0.0
8H-6, 0–5	68.83	77.81	VAC	971,476	7	134,927	0.0	0.3
9H-4, 0–5	75.47	88.04	HS	39,571	1	79,143	0.4	0.0
10H-5, 0–5	86.11	100.74	VAC	970,587	8	129,412	0.0	0.0
11H-4, 0–5	95.25	111.59	HS	4,052	0		0.0	0.0
12X-4, 0–5	104.80	122.85	HS	6,266	0		0.0	0.0
13X-3, 0–5	111.82	131.40	VAC	959,946	13	7,6186	0.0	0.0
14X-4, 0–5	122.91	144.22	HS	4,365	0		0.0	0.0
14X-4, 0–5	122.91	144.22	VAC	965,586	18	54,863	0.0	0.0
15X-5, 5–6	132.73	155.77	VAC	964,921	17	55,776	0.0	0.8
16X-4, 0–5	142.13	166.90	HS	7,578	0		0.0	0.0
17X-2, 52–53	149.09	175.59	VAC	961,528	23	42,546	0.0	0.0
18X-4, 0–5	161.44	189.68	HS	8,943	1	11,179	0.0	0.0
19X-2, 82–83	168.83	198.80	VAC	958,937	45	21,453	0.0	0.0
20X-4, 0–5	180.64	212.36	HS	7,672	0		0.0	0.0
21X-2, 54–55	187.85	221.29	VAC	948,034	81	11,704	0.0	6.9
22X-4, 0–5	200.03	235.22	HS	17,953	2	9,449	0.0	0.0

Note: HS = headspace, VAC = vacutainer.

Table T13. Interstitial water geochemical data, Hole 1234A.

Core, section, interval (cm)	Depth (mbsf)	Depth (mcd)	pH	Alkalinity (mM)	Salinity	Cl^- (mM)	Na^+ (mM)	SO_4^{2-} (mM)	HPO_4^{2-} (μM)	NH_4^+ (mM)	H_4SiO_4 (μM)	Mn^{2+} (μM)	Fe^{2+} (μM)	Ca^{2+} (mM)	Mg^{2+} (mM)	B (μM)	Sr^{2+} (μM)	Ba^{2+} (μM)	Li^+ (μM)	K^+ (mM)
202-1234A-																				
1H-1, 145–150	1.45	1.45	7.83	11.0	35.0	550	470	18.2	50	1.2	627	1.6	2.3	7.5	49.8	532	76	2.4	22	13.0
2H-3, 145–150	9.80	9.65	7.93	45.4	35.0	555	482	BDL	144	5.2	716	2.5	6.0	1.7	51.0	759	57	8.8	18	12.6
3H-3, 145–150	18.14	17.89	7.94	63.1	36.0	558	487	BDL	155	7.7	761	2.0	9.0	1.8	58.4	870	62	18.4	21	13.3
4H-3, 145–150	27.81	29.67	7.82	72.8	37.0	563	491	BDL	202	9.9	856	1.4	12.3	1.8	63.9	974	65	15.9	23	13.9
5H-3, 140–145	37.15	40.37	8.08	71.1	37.0	569	499	BDL	121	12.8	737	1.7	7.5	1.6	61.4	909	60	12.9	24	14.6
6H-3, 140–150	46.60	51.77	7.88	66.5	37.0	572	504	BDL	141	12.3	697	1.3	12.8	2.1	58.6	869	64	17.3	24	13.0
7H-2, 140–150	55.71	62.87	7.97	52.2	35.0	565	497	1.2	81	13.9	654	0.7	6.4	1.9	52.9	855	58	23.2	22	13.0
8H-3, 140–150	65.76	74.74	7.88	41.8	35.0	566	497	BDL	184	13.0	799	0.6	3.6	1.6	47.3	839	57	24.7	24	13.0
9H-3, 138–148	75.36	87.93	7.95	38.0	35.0	559	487	BDL	160	11.5	792	0.7	3.0	1.6	47.1	709	55	13.7	20	12.7
10H-3, 133–143	84.69	99.32	8.06	35.8	34.0	561	489	0.8	96	10.3	662	0.9	5.7	1.9	46.2	681	53	5.2	23	12.8
11H-3, 136–146	95.14	111.48	8.13	29.6	32.0	560	487	BDL	73	10.4	636	1.1	2.4	2.0	43.0	642	53	6.7	26	12.7
12X-3, 140–150	104.70	122.75	8.07	20.8	33.0	561	493	1.1	87	9.9	747	0.5	3.1	2.1	37.3	718	59	12.1	21	11.6
13X-3, 140–150	113.22	132.80	8.04	17.2	33.0	556	489	1.1	66	10.5	627	0.5	3.7	2.0	35.3	672	59	13.2	23	11.6
14X-3, 140–150	122.80	144.11	7.90	16.9	35.0	556	489	1.9	66	10.2	770	0.9	2.9	2.4	35.6	746	63	12.1	25	11.5
15X-2, 140–150	130.91	153.95	7.93	15.4	33.0	557	490	1.8	72	10.4	662	0.6	5.6	2.3	35.4	699	67	10.5	25	11.2
16X-3, 140–150	142.02	166.79	7.81	18.5	33.0	557	485	2.2	147	11.4	883	1.0	7.6	2.5	39.2	783	69	16.8	28	11.2
17X-1, 125–135	148.45	174.95	7.81	20.2	33.0	560	486	2.0	100	11.6	730	0.7	5.4	2.5	41.0	731	68	20.6	29	11.4
18X-3, 140–150	161.32	189.56	7.64	22.8	34.0	563	487	4.0	103	10.3	792	2.1	3.4	3.1	44.5	694	63	12.0	29	11.3
19X-2, 115–125	169.16	199.13	7.63	20.0	33.0	561	489	2.7	120	11.0	780	0.7	3.6	2.8	40.4	633	61	11.0	30	10.9
20X-2, 140–150	179.10	210.82	7.99	24.1	33.0	563	489	2.2	60	10.1	629	0.9	1.7	2.8	42.5	618	56	5.3	26	11.8
21X-3, 140–150	190.22	223.66	7.86	17.2	33.0	555	487	5.5	43	9.0	730	0.4	1.0	3.3	39.0	568	68	12.1	22	11.8
22X-3, 140–150	199.93	235.12	8.04	15.0	33.0	562	491	4.0	50	7.9	632	0.7	1.8	2.9	37.5	443	67	3.5	22	12.6

Note: BDL = below detection limit (SO_4^{2-} = ~0.6 mM).

Table T14. Inorganic carbon, calcium carbonate, total carbon, total organic carbon, and total nitrogen concentrations, TOC/TN ratios, total sulfur concentrations, and TOC/TS ratios in sediments, Hole 1234A. (See table note. Continued on next page.)

Core, section, interval (cm)	Depth (mbsf)	Depth (mcd)	IC (wt%)	$CaCO_3$ (wt%)	TC (wt%)	TOC (wt%)	TN (wt%)	TOC/TN (atomic)	TS (wt%)	TOC/TS (atomic)
202-1234A-										
1H-1, 74–75	0.74	0.74	0.15	1.3	2.13	1.98	0.22	7.68	0.61	3.26
1H-2, 74–75	2.25	2.25	0.46	3.8	1.65	1.19	0.12	8.59	0.60	1.97
1H-3, 74–75	3.76	3.76	0.60	5.0	1.31	0.71	0.08	7.83	0.39	1.84
1H-4, 20–21	4.73	4.73	0.66	5.5	1.32	0.66	0.09	6.60	1.24	0.53
2H-1, 74–75	6.04	5.89	0.47	3.9	1.26	0.79	0.09	7.32	0.47	1.66
2H-2, 74–75	7.56	7.41	0.48	4.0						
2H-3, 74–75	9.09	8.94	0.43	3.6	1.20	0.77	0.10	6.36	0.32	2.38
2H-4, 74–75	10.61	10.46	0.37	3.1						
2H-5, 74–75	12.13	11.98	0.50	4.1	1.32	0.82	0.11	6.18	0.53	1.55
2H-6, 74–75	13.64	13.49	0.32	2.7						
2H-7, 20–21	14.62	14.47	0.49	4.1	1.51	1.02	0.15	5.96	0.52	1.97
3H-2, 74–75	15.92	15.67	0.49	4.1	1.79	1.30	0.13	8.72	0.38	3.41
3H-3, 74–75	17.43	17.18	0.56	4.7						
3H-4, 74–75	18.94	18.69	0.32	2.7	1.38	1.06	0.15	6.15	0.63	1.68
3H-5, 74–75	20.41	20.16	0.28	2.4						
3H-6, 74–75	21.69	21.44	0.31	2.6	1.44	1.13	0.14	6.89	0.60	1.87
3H-7, 74–75	23.20	22.95	0.43	3.6						
3H-8, 20–21	24.18	23.93	0.51	4.2	1.65	1.14	0.15	6.67	1.00	1.14
4H-2, 74–75	25.59	27.45	0.37	3.1	1.23	0.86	0.12	6.09	0.77	1.11
4H-3, 74–75	27.10	28.96	0.40	3.3						
4H-4, 74–75	28.60	30.46	0.48	4.0	1.48	1.00	0.12	7.33	0.43	2.33
4H-5, 74–75	30.00	31.86	0.43	3.6						
4H-6, 74–75	31.49	33.35	0.49	4.1	1.18	0.69	0.10	5.81	0.51	1.35
4H-7, 74–76	32.89	34.75	0.39	3.2						
4H-8, 20–21	33.86	35.72	0.42	3.5	1.09	0.67	0.10	5.83	0.71	0.94
5H-2, 74–75	34.99	38.21	0.30	2.5	1.49	1.19	0.15	6.62	0.56	2.12
5H-3, 74–75	36.49	39.71	0.38	3.2						
5H-4, 74–75	37.95	41.17	0.41	3.4	1.20	0.79	0.11	6.05	1.24	0.64
5H-5, 74–75	39.39	42.61	0.38	3.2						
5H-6, 74–75	40.89	44.11	0.41	3.4	1.20	0.79	0.11	6.17	0.60	1.31
5H-7, 74–75	42.40	45.62	0.41	3.4						
5H-8, 20–21	43.17	46.39	0.28	2.3	1.03	0.75	0.11	6.08	0.41	1.82
6H-1, 30–31	43.60	48.77	0.27	2.3	1.23	0.96	0.12	7.02	2.06	0.47
6H-2, 100–101	44.92	50.09	0.44	3.7						
6H-3, 74–75	45.94	51.11	0.35	3.0	1.55	1.20	0.12	8.52	0.36	3.34
6H-4, 100–101	47.71	52.88	0.22	1.8						
6H-5, 120–121	49.32	54.49	0.28	2.3	1.87	1.59	0.16	8.30	0.58	2.75
6H-6, 110–111	50.58	55.75	0.33	2.8						
6H-7, 130–131	52.26	57.43	0.24	2.0	2.50	2.26	0.27	7.25	1.33	1.70
7H-1, 74–75	53.54	60.70	0.37	3.1	2.22	1.85	0.18	8.67	1.03	1.80
7H-2, 74–75	55.05	62.21	0.34	2.8						
7H-3, 74–75	56.56	63.72	0.46	3.9	2.12	1.66	0.16	8.66	0.55	3.02
7H-4, 130–131	58.48	65.64	0.33	2.8						
7H-5, 130–131	59.95	67.11	0.23	2.0	2.04	1.81	0.19	8.04	1.06	1.70
8H-1, 20–21	62.50	71.48	0.30	2.5	2.13	1.83	0.19	8.41	0.54	3.40
8H-2, 74–75	63.80	72.78	0.36	3.0						
8H-3, 82–83	65.18	74.16	0.38	3.1	2.23	1.85	0.21	7.71	0.98	1.89
8H-4, 74–75	66.61	75.59	0.45	3.7						
8H-5, 20–21	67.53	76.51	0.39	3.3	1.63	1.24	0.14	7.75	0.51	2.44
8H-6, 74–75	69.57	78.55	0.46	3.9						
8H-7, 20–21	70.51	79.49	0.50	4.2	2.73	2.23	0.25	7.76	0.83	2.69
9H-1, 20–21	72.00	84.57	0.51	4.2	2.92	2.41	0.24	8.75	0.77	3.14
9H-2, 74–75	73.21	85.78	0.46	3.8						
9H-3, 74–75	74.72	87.29	0.69	5.8	1.02	0.33	0.08	3.70	0.78	0.42
9H-4, 74–75	76.21	88.78	0.53	4.4						
9H-5, 74–75	77.62	90.19	0.38	3.2	3.33	2.95	0.33	7.62	1.00	2.95
9H-6, 74–75	79.09	91.66	0.29	2.4						
9H-7, 74–76	80.50	93.07	0.26	2.2	0.90	0.64	0.11	5.06	1.11	0.58
10H-1, 20–21	81.50	96.13	0.34	2.9	0.91	0.57	0.10	5.17	0.60	0.95
10H-2, 74–75	82.63	97.26	0.18	1.5						
10H-3, 74–75	84.10	98.73	0.22	1.9	0.94	0.72	0.10	5.96	0.93	0.78
10H-4, 74–75	85.55	100.18	0.13	1.1						
10H-5, 74–75	86.85	101.48	0.17	1.4	1.01	0.84	0.14	5.26	0.98	0.85
10H-6, 74–75	88.07	102.70	0.14	1.2						

Table T14 (continued.)

Core, section, interval (cm)	Depth (mbsf)	Depth (mcd)	IC (wt%)	$CaCO_3$ (wt%)	TC (wt%)	TOC (wt%)	TN (wt%)	TOC/TN (atomic)	TS (wt%)	TOC/TS (atomic)
10H-7, 74–75	89.58	104.21	0.10	0.8	1.31	1.21	0.16	6.58	1.54	0.79
11H-1, 130–131	92.10	108.44	0.36	3.0	0.95	0.59	0.11	4.78	0.73	0.81
11H-2, 130–131	93.61	109.95	0.44	3.6						
11H-3, 130–131	95.08	111.42	0.21	1.7	0.74	0.53	0.09	4.89	0.51	1.03
11H-4, 130–131	96.55	112.89	0.29	2.5						
11H-5, 130–132	97.97	114.31	0.25	2.1	1.04	0.79	0.13	5.40	1.05	0.75
11H-6, 50–51	98.67	115.01	0.20	1.7						
11H-7, 50–51	99.48	115.82	0.15	1.2	0.90	0.75	0.13	5.08	1.02	0.73
12X-1, 20–21	100.50	118.55	0.49	4.1						
12X-1, 74–75	101.04	119.09	0.95	7.9	1.14	0.19	0.11	1.48	0.52	0.37
12X-2, 74–75	102.54	120.59	1.41	11.7	2.89	1.48	0.24	5.37	0.86	1.72
12X-3, 74–75	104.04	122.09	1.10	9.2	2.16	1.06	0.17	5.38	0.47	2.24
12X-4, 74–75	105.54	123.59	0.77	6.4						
12X-5, 74–75	107.05	125.10	0.61	5.1	1.43	0.82	0.13	5.21	0.32	2.52
12X-6, 74–75	108.56	126.61	0.68	5.7						
12X-7, 20–21	109.04	127.09	0.68	5.6						
13X-1, 74–75	109.54	129.12	0.70	5.8	1.36	0.66	0.12	4.74	0.37	1.80
13X-2, 74–75	111.05	130.63	0.58	4.9						
13X-3, 74–75	112.56	132.14	0.65	5.4	1.27	0.62	0.11	4.79	0.21	3.00
13X-4, 74–75	114.05	133.63	0.50	4.1						
13X-5, 74–75	115.56	135.14	0.60	5.0	1.85	1.25	0.18	5.92	0.34	3.70
14X-1, 74–75	119.14	140.45	0.53	4.4						
14X-2, 74–75	120.64	141.95	0.50	4.1	1.42	0.92	0.13	6.09	0.31	3.02
14X-3, 74–75	122.14	143.45	0.49	4.1						
14X-4, 74–75	123.65	144.96	0.81	6.8	1.61	0.80	0.16	4.34	0.50	1.60
14X-5, 74–75	125.15	146.46	0.48	4.0						
14X-6, 20–21	126.00	147.31	0.43	3.5	1.23	0.80	0.12	5.61	0.43	1.87
15X-1, 74–75	128.74	151.78	0.67	5.6	1.26	0.59	0.12	4.39	0.25	2.39
15X-3, 74–75	131.76	154.80	0.69	5.7	1.36	0.67	0.12	4.86	0.17	3.84
15X-5, 50–51	133.18	156.22	0.62	5.1	1.20	0.58	0.12	4.11	0.19	3.02
16X-1, 74–75	138.34	163.11	0.45	3.8	1.23	0.78	0.15	4.59	0.25	3.12
16X-3, 74–75	141.36	166.13	0.56	4.7	1.52	0.96	0.14	5.77	0.39	2.48
16X-5, 74–75	144.37	169.14	0.36	3.0	1.59	1.23	0.16	6.61	0.55	2.23
17X-1, 74–75	147.94	174.44	0.32	2.7	1.20	0.88	0.14	5.29	0.44	2.01
17X-3, 74–75	150.81	177.31	0.16	1.4	1.67	1.51	0.20	6.57	0.81	1.86
18X-1, 74–75	157.64	185.88	0.41	3.4	2.11	1.70	0.21	6.89	0.73	2.33
18X-2, 74–75	159.15	187.39	0.27	2.3						
18X-3, 74–75	160.66	188.90	0.24	2.0	0.93	0.69	0.12	5.07	1.22	0.57
18X-4, 74–75	162.18	190.42	0.22	1.9						
18X-5, 74–75	163.69	191.93	0.11	1.0	0.94	0.83	0.13	5.60	1.12	0.74
19X-1, 70–71	167.20	197.17	0.47	4.0	0.75	0.28	0.09	2.74	0.78	0.36
19X-3, 76–77	170.03	200.00	0.14	1.2	0.97	0.83	0.11	6.27	0.89	0.94
19X-5, 72–73	172.98	202.95	0.24	2.0	0.91	0.67	0.11	5.22	1.14	0.59
20X-1, 138–139	177.58	209.30	0.32	2.7	1.22	0.90	0.11	6.75	1.10	0.81
20X-3, 130–132	180.51	212.23	0.38	3.1	1.29	0.91	0.16	4.92	1.84	0.49
21X-1, 74–75	186.54	219.98	0.19	1.6						
21X-3, 74–75	189.56	223.00	0.22	1.8	2.56	2.34	0.24	8.25	1.39	1.68
21X-5, 20–21	191.54	224.98	1.11	9.3	2.56	1.45	0.24	5.10	0.61	2.36
22X-1, 74–75	196.24	231.43	0.20	1.7						
22X-3, 74–75	199.27	234.46	0.47	3.9	0.72	0.25	0.07	3.09	0.32	0.78
22X-5, 74–75	202.28	237.47	0.31	2.6	0.74	0.43	0.06	5.95	0.38	1.15

Note: IC = inorganic carbon, TC = total carbon, TOC = total organic carbon, TN = total nitrogen, TS = total sulfur.

Table T15. Results of Rock-Eval pyrolysis analyses of selected sediment samples, Hole 1234A.

Core, section, interval (cm)	Depth (mbsf)	Depth (mcd)	TOC (wt%)	S_1 (mg/g)	S_2 (mg/g)	T_{max} (°C)	HI (mg HC/g C)
202-1234A-							
1H-1, 74–75	0.74	0.74	2.36	1.30	7.06	398	299
5H-2, 74–75	34.99	38.21	1.24	0.51	2.62	395	211
5H-4, 74–75	37.95	41.17	0.86	0.30	1.63	421	189
5H-6, 74–75	40.89	44.11	0.79	0.30	1.93	481	246
7H-1, 74–75	53.54	60.70	1.68	0.59	4.06	406	241
7H-3, 74–75	56.56	63.72	1.69	0.57	4.18	404	247
8H-1, 20–21	62.50	71.48	2.18	0.87	5.98	399	274

Notes: TOC = total organic carbon. S_1 = amount of volatile hydrocarbons, S_2 = amounts of hydrocarbons due to thermal cracking of kerogen. T_{max} = peak temperature of kerogen breakdown. HI = hydrogen index ($100 \times S_2$/TOC).